Shape Memory Alloys — Part I: General Properties and Modeling of Single Crystals

Etienne Patoor
LPMM-ISGMP/ENSAM
Ile du Saulcy
57045 Metz Cedex 1
FRANCE

Dimitris C. Lagoudas
Pavlin B. Entchev
Department of Aerospace Engineering
Texas A&M University
College Station, TX 77843-3141
USA

L. Catherine Brinson
Xiujie Gao
Mechanical Engineering Department
Northwestern University
Evanston, IL 60208
USA

October 14, 2004

Abstract

This two-part paper reviews the latest developments in the modeling of Shape Memory Alloys (SMAs) constitutive behavior. The basic properties of SMAs are presented in Part I, including the shape memory effect, pseudoelasticity, as well as other properties such as the acquired and two way shape memory effect, damping capacity and fatigue life. Part I focusses on the modeling at the single crystal level, dealing with the kinematics of the phase transformation and addressing different approaches for the development of the free energy and dissipation in order to derive constitutive equations. Some of the commonly used SMAs are reviewed by chemical composition and thermomechanical properties. The effects that different processing techniques have on their properties are also discussed. The kinematics associated with the martensitic phase transformation in a single crystal is described for a cubic to tetragonal and cubic to monoclinic transformation, and the lattice invariant strain by plastic slip is discussed. The transformation strain in a representative volume element (RVE) and its evolution are then defined. The free energy and dissipative potentials are derived together with the interaction energy for single variant and multivariant formulations in single crystals. A discussion on scale transitions to polycrystalline SMAs is finally presented. Part II deals with the polycrystalline modeling, considering both micromechanical approaches and phenomenological ones. It also includes considerations about the numerical implementation of SMA constitutive models and their integration into finite element codes.

Contents

List of Symbols

A	Austenite
M	Martensite
T	Temperature
S	Entropy
T_0	Critical thermodynamic equilibrium temperature
M_s	Martensitic start temperature (at zero stress level)
M_f	Martensitic finish temperature (at zero stress level)
A_s	Austenitic start temperature (at zero stress level)
A_f	Austenitic finish temperature (at zero stress level)
M_s^σ	Martensitic start temperature at given stress level σ
M_f^σ	Martensitic finish temperature at given stress level σ
A_s^σ	Austenitic start temperature at given stress level σ
A_f^σ	Austenitic finish temperature at given stress level σ
G	Gibbs free energy
M^y	Temperature at phase transformation and plastic yielding occur at the same stress level
$\sigma^{Ms}(T)$	Martensitic phase transformation onset stress at a given temperature T
$\sigma^{Mf}(T)$	Martensitic phase transformation finish stress at a given temperature T
$\sigma^{As}(T)$	Austenitic phase transformation onset stress at a given temperature T
$\sigma^{Af}(T)$	Austenitic phase transformation finish stress at a given temperature T
σ_y	Plastic yield stress
$\mathbf{F}$	Deformation gradient tensor
$\mathbf{F}^M$	Deformation gradient tensor in the martensitic region
$\mathbf{F}^{LIS}$	Lattice invariant shear deformation tensor
γ	plastic slip amplitude
$\mathcal{B}^M$	Martensitic domain
$\mathcal{B}^A$	Austenitic domain
$\mathbf{B}$	Bain deformation tensor
f	Martensitic volume fraction
f^n	Volume fraction of the n-th martensitic variant
ξ	Martensitic volume fraction used in phenomenological models
θ_n	Indicator function for the n-th martensitic variant
$\langle\boldsymbol{\sigma}\rangle$	Macroscopic stress tensor
$\langle\boldsymbol{\varepsilon}\rangle$	Linearized, macroscopic, total strain tensor
$\langle\boldsymbol{\varepsilon}^{th}\rangle$	Macroscopic thermal strain tensor
$\langle\boldsymbol{\varepsilon}^{e}\rangle$	Macroscopic elastic strain tensor
$\langle\boldsymbol{\varepsilon}^{t}\rangle$	Macroscopic transformation strain tensor
$\boldsymbol{\varepsilon}$	Total strain
$\boldsymbol{\varepsilon}^e$	Elastic strain
$\boldsymbol{\varepsilon}^{th}$	Thermal strain
$\boldsymbol{\varepsilon}^t$	Transformation strain
$\boldsymbol{\varepsilon}^{tn}$	Transformation strain in the n-th martensitic variant
$\boldsymbol{\mathcal{C}}$	4-th order elastic stiffness tensor
$\boldsymbol{\mathcal{S}}$	4-th order elastic compliance tensor
$\boldsymbol{\alpha}$	2-nd order thermal dilatations tensor
S_{AM}	Austenite-martensite interface
S_{MM}	Martensite-martensite interface
$w(\mathbf{x})$	Elastic strain energy density
$\varphi(\mathbf{x})$	Crystallographic (chemical) free energy density
$\varphi_A(\mathbf{x})$	Crystallographic (chemical) free energy density of austenite
$\varphi_M(\mathbf{x})$	Crystallographic (chemical) free energy density of martensite
Φ	Helmholtz free energy density
$\mathbf{S}^E$	Eshelby tensor
W^{int}	Interaction energy of the martensitic variants
F^{int}	Interaction force
F^n	Thermodynamic driving force
ζ^n	Volume fraction of the n-th variant inside a single grain
P_{ext}	External power source
$\bar{\boldsymbol{\varepsilon}}^{tn}$	Average transformation strain of n-th variant inside a single grain
$\bar{\boldsymbol{\tau}}^{tn}$	Average stress of n-th variant inside a single grain
λ, μ	Lamé constants
$(\boldsymbol{\sigma})^g$	Average stress of a group of variants
$\langle\boldsymbol{\varepsilon}\rangle^g$	Average transformation strain of a group of variants
$\bar{f}^g$	Volume fraction of group g
N^{nm}	Normal vector of the interface of variants n and m
$\mathbf{Q}^{nm}$	Interface stress transfer operator
$\boldsymbol{\sigma}^A$	Stress tensor inside the austenite region

1 Introduction: Basic Properties of Shape Memory Alloys

Shape Memory Alloys (SMAs) are metallic alloys that can undergo martensitic phase transformations as a result of applied thermomechanical loads and are capable of recovering permanent strains when heated above a certain temperature. At high temperatures the crystal lattice is in a high symmetry, parent austenitic phase. The key characteristic of all SMAs is the occurrence of a martensitic phase transformation between the austenitic phase and the different variants of the low temperature, low symmetry martensitic phase. The martensitic transformation is a shear-dominant diffusionless solid-state phase transformation occurring by nucleation and growth of the martensitic phase from the parent austenitic phase (Olson and Cohen, 1982). What make SMAs remarkably different from other materials are primarily the *Shape Memory Effect* (SME) and *Pseudoelasticity*, which are associated with the specific way the phase transformation occurs.

When a shape memory alloy undergoes a martensitic phase transformation, it transforms from its high-symmetry, usually cubic austenitic phase to a low-symmetry martensitic phase, such as the monoclinic variants of the martensitic phase in a NiTi SMA. In the absence of applied stresses, the variants of the martensitic phase usually arrange themselves in a self-accommodating manner through twinning, resulting in no observable macroscopic shape change. By applying mechanical loading the martensitic variants are forced to reorient (detwin) into a single variant leading to large macroscopic inelastic strains. After heating above certain temperature, the martensitic phase returns to the austenitic phase, and the inelastic strains are recovered. This behavior is known as the SME. Pseudoelasticity is observed when the martensitic

phase transformation is induced by applied thermomechanical loading of the austenitic phase in which case detwinned martensite is directly produced from austenite. The process is associated with large inelastic (transformation) strains which are recovered upon unloading due to the reverse phase transformation (Wayman, 1983). The extensive list of alloys exhibiting SME and pseudoelasticity includes the Ni-Ti alloys, and many copper-, iron-, silver- and gold-based alloys (Nishiyama, 1978).

Martensitic transformations are usually divided into two groups - thermoelastic and nonthermoelastic. The nonthermoelastic transformations occur mainly in ferrous alloys and are associated with non-mobile martensite-parent phase interfaces pinned by permanent defects and proceed by successive nucleation and growth. Due to re-nucleation of austenite during the reverse (martensite to austenite) transformation, these transformations are crystallographically nonreversible in the sense that the martensite cannot revert to the parent phase in the original orientation. The thermoelastic martensitic transformations, on the other hand, are associated with mobile interfaces between the parent and martensitic phases. These interfaces are capable of "backward" movement during the reverse transformation by shrinkage of the martensitic plates rather than nucleation of the parent phase, which leads to a crystallographically reversible transformation (Otsuka and Wayman, 1999). The unique properties of SMAs (i.e. *Shape Memory Effect, Pseudoelasticity*) are the result of thermoelastic martensitic transformation. Summarized below are the main characteristics of martensitic phase transformations that distinguish them among other solid state transformations:

1. It is associated with an inelastic deformation of the crystal lattice with no diffusive process involved. It results from a cooperative and collective motion of atoms over distances smaller than the lattice parameters. The absence of diffusion makes the martensitic phase transformation almost instantaneous (Nishiyama, 1978).

2. Parent and product phases coexist during the phase transformation, since it is a first order transition, and as a result there exists an invariant plane, which separates the parent and product phases. The lattice vectors of the two phases possess well defined mutual orientation relationships (the Bain correspondences, see Bowles and Wayman, 1972), which depend on the nature of the alloy.

3. Transformation of a unit cell element produces a volumetric and a shear strain along well-defined planes. The shear strain is many times larger than the elastic distortion of the unit cell. This transformation is crystallographically reversible (Kaufman and Cohen, 1958).

4. Since the crystal lattice of the martensitic phase has lower symmetry than that of the parent austenitic phase, several variants of martensite can be formed from the same parent phase crystal (De Vos et al., 1978).

5. Stress and temperature have a large influence on the martensitic transformation. Transformation takes place when the free energy difference between the two phases reaches a critical value (Delaey, 1990).

Crystallographic theories of the martensitic transformation developed by Wechsler et al. (1953) and Bowles and MacKenzie (1954) are based on the above characteristics. The interface that separates the martensite from the parent phase is called the *habit plane*. This plane remains unchanged and exhibits neither deformation nor rotation. The crystallographical theory of martensitic phase transformation will be presented in Section 4.1 to 4.3.

In the next Section 2 some general aspects of the martensitic phase transformation in SMAs are reviewed and the complex thermomechanical response of SMAs is described. In Section 3 the most commonly used SMAs, their chemical composition and mechanical properties are briefly summarized. The kinematics of the phase transition from a continuum point of view is described in Section 4. In Section 5, the macroscopic behavior of single crystal SMAs is derived using micromechanical techniques.

2 Characteristics of the Martensitic Transformation in Shape Memory Alloys

The behavior of shape memory alloys is more complex than that of common materials, but this complexity is the basis of their use in many applications. Different effects are observed according to the thermomechanical

loading path and the loading history of the material. The two key effects in SMAs associated with the martensitic transformations are the shape memory effect and pseudoelasticity. In this section they are briefly described and the crystallographic mechanisms behind them presented. In addition, some acquired properties such as the Two-Way Shape Memory Effect (TWSME) are reviewed. The fatigue life and damping capacity of SMAs, which are of great practical interest, are also discussed.

2.1 Phenomenology of the Martensitic Transformation

In SMA materials, the martensitic phase transformation is a rate independent, reversible, crystallographic reorientation process between the two stable phases. The martensitic transformation (austenite-to-martensite) occurs when the free energy of martensite becomes less than the free energy of austenite at a temperature below a critical temperature T_0 at which the free energies of the two phases are equal. However, the transformation does not begin exactly at T_0 but, in the absence of stress, at a temperature M_s (martensite start), which is less than T_0. The free energy necessary for nucleation and growth is responsible for this shift (Delaey, 1990). The transformation continues to evolve as the temperature is lowered until a temperature, denoted by M_f, is reached. When the SMA is heated from the martensitic phase in the absence of stress, the reverse transformation (martensite-to-austenite) begins at the temperature A_s (austenite start), higher than T_0. The transformation continues until a temperature A_f (austenite finish) is reached and the material is entirely in the austenitic phase. The equilibrium temperature T_0 is approximately $(M_s + A_f)/2$ (Tong and Wayman, 1974; Otsuka and Wayman, 1999).

For shape memory alloys, the transformation temperatures M_s, M_f, A_s, A_f, and the difference $M_s - M_f$, $A_f - A_s$ are important factors in characterizing shape memory behavior. The transformation temperatures depend mainly on the alloy's composition and processing. Microstructural defects, degree of order in the parent phase, and grain size of the parent phase can also alter the transformation temperatures by several degrees (MacQueron et al., 1991).

When the martensitic transformation takes place, numerous physical properties are modified. During the transformation, a latent heat associated with the transformation is absorbed or released based on the transformation direction. The forward, austenite-to-martensite ($A \rightarrow M$) transformation is accompanied by the release of heat corresponding to a change in the transformation enthalpy (exothermic phase transformation). The reverse, martensite-to-austenite ($M \rightarrow A$) transformation is an endothermic phase transformation accompanied by absorption of thermal energy. For a given temperature, the amount of heat is proportional to the volume fraction of the transformed material. The two phases also have different resistance due to their different crystallographic structures, so the phase transformation is associated with a change in the electrical resistivity. These changes allow for the measurement of the transformation temperatures. Generally, differential calorimetry and electrical resistance are used for that purpose. In addition, thermoelectrical power, x-ray analysis, acoustic waves, interior friction, and the measure of Young's modulus are also used.

Due to the displacive character of the martensitic transformation, applied stress plays a very important role. Application of a macroscopic stress $\langle \boldsymbol{\sigma} \rangle$ on a volume of austenite provides a mechanical energy contribution [1]. Denoting the entropy by S and the macroscopic strain by $\langle \boldsymbol{\varepsilon} \rangle$ the thermodynamical equilibrium condition between the austenitic and martensitic phases, under certain assumptions, reads (Wollants et al., 1979; Otsuka and Wayman, 1999):

$$-[\Delta S]^{A \rightarrow M} \Delta T - [\Delta \langle \boldsymbol{\varepsilon} \rangle]^{A \rightarrow M} : \Delta \langle \boldsymbol{\sigma} \rangle = 0, \tag{2.1}$$

where $[\Delta S]^{A \rightarrow M}$ and $[\Delta \langle \boldsymbol{\varepsilon} \rangle]^{A \rightarrow M}$ denote the jump in the entropy and total strain between the two phases, respectively. This equilibrium condition gives a Clausius–Clapeyron type equation that relates the applied stress and the temperature. Note that the thermoelastic component of $[\Delta \langle \boldsymbol{\varepsilon} \rangle]^{A \rightarrow M}$ is negligible compared to the transformation strain, which is developed during the phase transformation.

In general, $[\Delta S]^{A \rightarrow M}$ and $[\Delta \langle \boldsymbol{\varepsilon} \rangle]^{A \rightarrow M}$ are assumed to be temperature-independent, and a linear relationship is obtained. More accurate analysis considers the change in $[\Delta \langle \boldsymbol{\varepsilon} \rangle]^{A \rightarrow M}$ under the applied stress (Roytburd and Pankova, 1985). Moreover, there are inhomogeneities in the stress and strain fields inside the material, and thus a transformation stress range is often observed. These parameters are very sensitive to the internal state of the material and to the loading mode (tension, compression, shear).

[1] The notation $\langle \boldsymbol{\sigma} \rangle$ instead of $\boldsymbol{\sigma}$ is used to denote averaging over a representative volume element of the microstructure and will be explained in detail in Section 4.4.

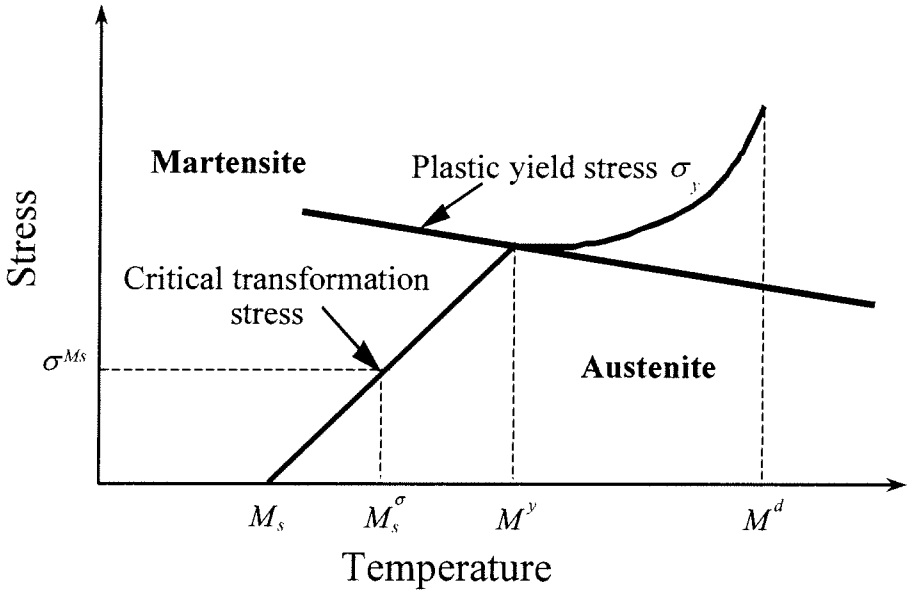

Figure 1: Schematic of the relationship between the critical temperature M_s^σ and critical stress σ^{Ms} required for the onset of the martensitic phase transformation. M_s denotes the martensitic start temperature at zero stress level, M^y is the temperature at which the phase transformation and the plastic yielding of austenite start at the same critical stress level, and M^d is the maximal temperature for which phase transformation is possible. (Gautier and Patoor, 1997, pg. 74).

The total strain jump $[\Delta\langle\varepsilon\rangle]^{A\to M}$ is composed of a shearing component that induces shape change and an expansion component that effects volume change. Accommodating these transformation strains leads to strain energy which plays a very important role. The growth of a martensitic plate within the parent phase matrix produces a significant stress field. If this stress reaches the yield stress of the parent phase (or the martensite phase), plastic accommodation occurs. As a result, the reverse transformation must occur by nucleation of the high-temperature phase in martensite (Olson and Cohen, 1975), leading to non-thermoelastic transformation. If the plastic yield stress level is high enough for the two phases, or if the strain energy is weak, the transformation strain is accommodated in a fully elastic way (Grujicic et al., 1992).

Since the macroscopic properties associated with thermoelastic and nonthermoelastic transformations are very different, it is useful to schematically show the two different ways in which martensitic phase transformations can occur in stress-temperature space. Figure 1 shows the critical uniaxial stress required for initiation of the forward martensitic phase transformation as a function of temperature. The critical temperature for initiation of the stress induced martensitic phase transformation at zero stress level is denoted by M_s. Given a nonzero stress σ, the critical temperature at which the stress induced phase transformation occurs is denoted by M_s^σ. Conversely, for given temperature T, the critical stress for initiation of phase transformation is denoted by $\sigma^{Ms}(T)$. Whenever possible, the argument T will be suppressed to simplify notation. From M_s to a temperature M^y, the martensite is stress-induced and the critical transformation stress $\sigma^{Ms}(T)$ increases linearly with temperature. Plasticity of the martensitic phase does not occur until much higher stress levels. M^y is the temperature at which σ^{Ms} and the austenitic plastic yield stress σ_y are equal, that is, $\sigma^{Ms}(M^y) = \sigma_y(M^y)$ (Olson and Cohen, 1982). As a consequence, at temperatures between M^y and M^d, plastic deformation in the austenitic phase occurs prior to the phase change. The temperature M^d is an upper temperature limit for phase transformations. Above this temperature, plasticity by movement of dislocations becomes the dominant strain mechanism in the parent phase and phase transformation does not occur. The temperature difference $M_s - M^y$ can be maximized by increasing the yield stress of the parent phase, using appropriate thermomechanical treatments (e.g., strengthening or structural hardening), or using alloyed elements (Shimizu, 1985). In most of the work discussed in this paper the load levels do not extend into the plastic region.

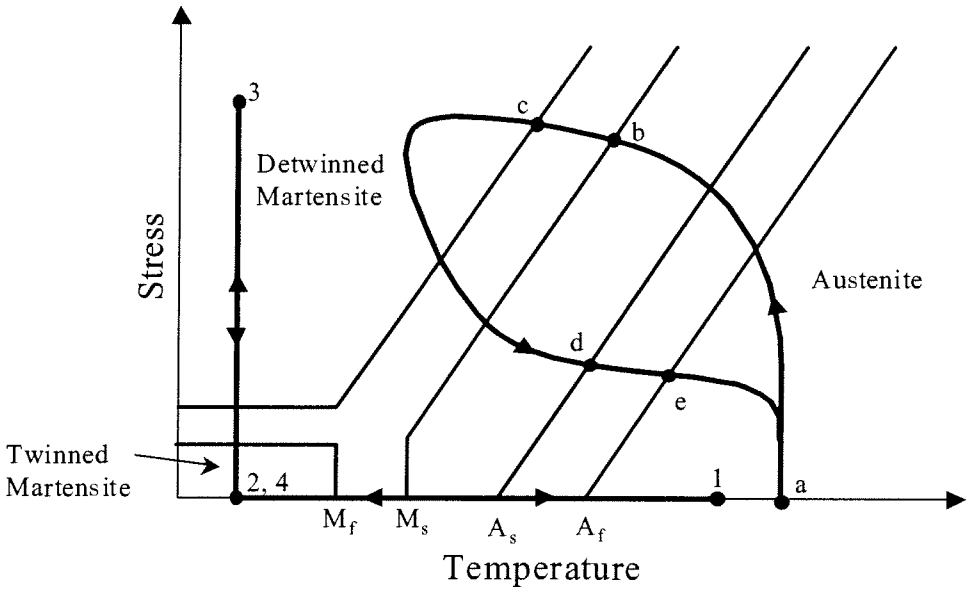

Figure 2: Stress-Temperature diagram showing the relationship of stress and temperature and the austenitic and martensitic domains.

Taking into account the fact that the phase transformation does not always occur instantaneously, but over a certain range of stresses and temperature, considering both forward, and reverse transformations, self-accommodation (twinning) of martensite, reorientation of twinned martensite and restricting the temperature range to include only thermoelastic transformations, the uniaxial thermomechanical response of SMAs can be summarized by the phase diagram shown in Figure 2. The SMA can exist in either austenite and martensite, and the martensite can further be separated in twinned (self-accommodated) and detwinned. There are three regions where the material can be in a pure phase along with the transformation lines (surfaces in multiple dimensions) which separate them. When the material crosses a transformation surface it undergoes phase transformation (austenite-to-martensite) or detwinning (twinned martensite to detwinned martensite). In addition to M_s, the critical temperatures at zero stress level for the completion of the austenite-to-martensite (forward) phase transformation is denoted by M_f. The start and finish of the (reverse) martensite to austenite phase transformation, again at zero stress level, are denoted by A_s and A_f, respectively. The associated effects with the possible thermomechanical loading paths are discussed next.

2.2 Shape Memory Effect

As mentioned earlier, the *Shape Memory Effect* (SME) is a property of SMAs undergoing thermoelastic martensitic transformation. It is exhibited when the SMA is deformed while in the martensitic phase and then unloaded while still at a temperature below M_f. When subsequently heated above A_f it regains its original shape by transforming back into the austenitic phase. A typical loading path $1 \rightarrow 2 \rightarrow 3 \rightarrow 4 \rightarrow 1$, in which the SME is observed is shown in Figure 2. The same path, schematically plotted in Stress-Strain-Temperature space is shown in Figure 3. During the cooling of the parent phase ($1 \rightarrow 2$) it transforms to twinned martensite. The material is then loaded ($2 \rightarrow 3$) causing stress induced detwinning and development of inelastic strains. Upon unloading ($3 \rightarrow 4$) the material remains in detwinned state and the inelastic strains are not recovered. Finally, when it is heated above A_f ($4 \rightarrow 1$), the SMA returns to its cubic parent phase and the inelastic strains are recovered.

The crystallographic changes during this loading path are explained next. The stress-free cooling of austenite produces self-accommodating growth of the martensitic variants ($1 \rightarrow 2$) such that there is no macroscopic transformation strain (Saburi et al., 1980). The self-accommodated morphology is a characteristic of the crystallography of the alloy used. For example, in copper-based alloys, twenty-four variants

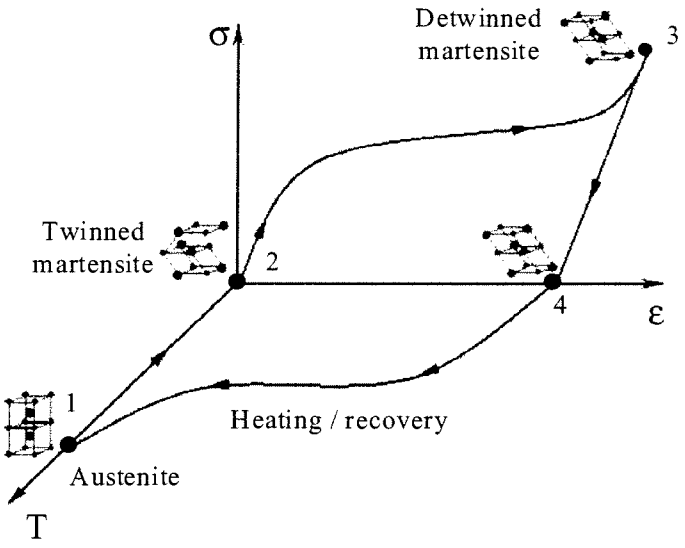

Figure 3: Stress-Strain-Temperature schematic of the crystallographic changes involved in the Shape Memory Effect.

of martensite constitute six self-accommodated groups scattered around the ⟨011⟩ poles of austenite with a typical diamond morphology. The growth of such groups produces no macroscopic transformation strain, but the multiple interfaces present in these structures (boundaries between the martensite variants and twinning interfaces) are very mobile. This great mobility is at the heart of the shape memory effect. Movement of these interfaces accompanied by detwinning is obtained at stress levels far lower than the plastic yield limit of martensite. This mode of deformation, called *reorientation of variants*, dominates at temperatures lower than M_f.

During the second stage ($2 \rightarrow 3$), the mechanical loading in the martensitic phase leads to reorientation of the variants and results in development of large inelastic strains. This inelastic strain is not recovered upon unloading ($3 \rightarrow 4$). During the last step ($4 \rightarrow 1$), heating the sample above A_f induces the reverse transformation and recovers the inelastic strain. When the material approaches A_f, the martensitic phase becomes unstable in the absence of stress. This results in a complete transformation to the parent phase. Since martensite variants have been reoriented by stress, the reversion to austenite produces a large transformation strain having the same amplitude but opposite direction to the inelastic strain. As a result, the SMA returns to the original shape it had in the austenitic phase.

2.3 Two-Way Shape Memory Effect

The term *Shape Memory Effect* in general describes the *one-way shape memory effect* in which an externally applied load is necessary to induce detwinning and/or reorientation and to bring the SMA specimen into a new deformed shape that can be recovered upon heating above A_f. There is no transformation strain induced during the cooling of the material. If transformation strains are generated during both heating and cooling of the material, then this property is known as the *two way shape memory effect* and was observed for the first time by Perkins (1974). In contrast with the SME, discussed earlier, or the *pseudoelasticity*, which will be described in the next section, the two-way shape memory is not an intrinsic but an acquired characteristic. It can be obtained by cyclic repetition of certain thermomechanical loading paths. As an example, the loading path discussed in the previous section can be considered. The full recovery of the inelastic strains generated during the reorientation process after heating ($4 \rightarrow 1$) is an idealization. In practice, only a partial recovery of the inelastic strains is observed and a residual strain remains after completion of each heating. After several cycles this residual strain increases until it saturates. Further cooling of the material, in the absence of applied stress ($1 \rightarrow 2$), now leads to the occurrence of a macroscopic transformation strain contrary to

what is observed in the SMA material before cycling. Different training sequences can be used (Contardo and Guénin, 1990; Miller and Lagoudas, 2001), i.e., by inducing a non-homogeneous plastic strain (torsion, flexion) at a martensitic or austenitic phase; by aging under applied stress in the austenitic phase, in order to stabilize the parent phase, or in the martensitic phase, in order to create a precipitant phase (NiTi alloys); by thermomechanical cycling, either isothermal mechanical loading (Figure 5) or thermal isobaric cycling (Figure 4).

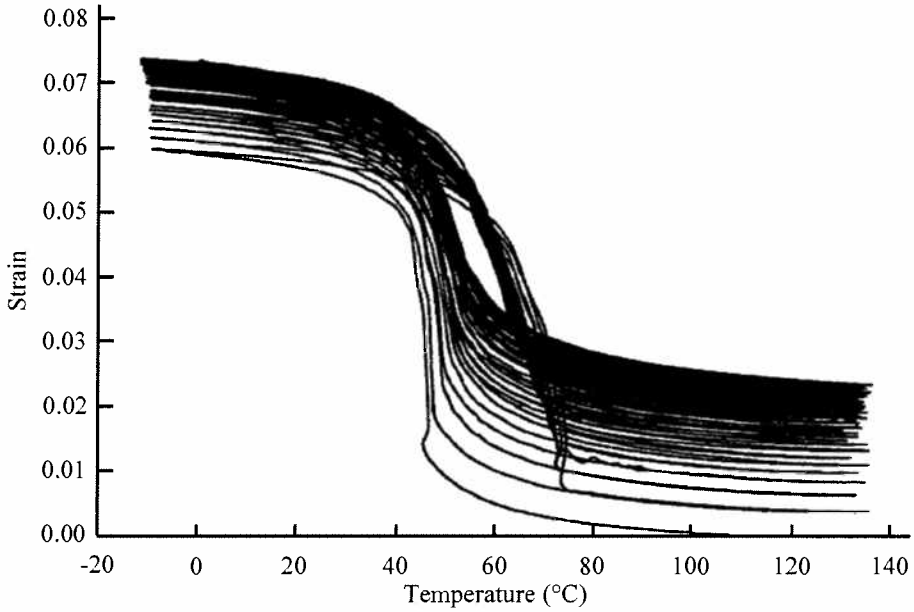

Figure 4: Thermal cyclic loading (50 cycles) of a Ni50Ti50 (%*at.*) SMA wire under constant load of 200 MPa. During the first few cycles the total inelastic (transformation and plastic) strain grows from approx. 6% to 7%, followed by a gradual stabilization at 7.4%. The entire transformation hysteresis also stabilizes as the number of cycles increases (Miller and Lagoudas, 2001).

The fundamental mechanism in all of the above methods consists of introducing a microstructure with oriented defects (e.g., network of dislocations or precipitates). This process leads to the preferential formation and reversal of a particular martensitic variant under the applied load. Generation of permanent defects eventually creates a permanent internal stress state, which allows for further formation of the preferred martensitic variant when cooled in the absence of the external load. In this case the solid exhibits two stable shapes: a high-temperature shape in austenite and a low-temperature shape in martensite and transition between these two shapes is obtained without any applied stress assistance. There is not yet general agreement about the exact nature of this mechanism and the precise way in which it facilitates the two-way memory effect. If, for various reasons (e.g., aging or mechanical overload), these internal stresses are decreased or modified, the two-way memory shape effect is perturbed or even canceled (Rodriguez and Guénin, 1990).

The training cycle leads to secondary effects, like changes in the transformation temperatures, change in the hysteresis size and a decrease in the macroscopic transformation strain. These effects are similar to those observed during thermomechanical fatigue tests performed on this type of alloy explained later in this paper (Lagoudas et al., 2000). It is important to define optimal conditions of training, because an insufficient number of training cycles produces a non-stabilized two-way memory effect and over-training generates unwanted effects that reduce the efficiency of training (Stalmans et al., 1992).

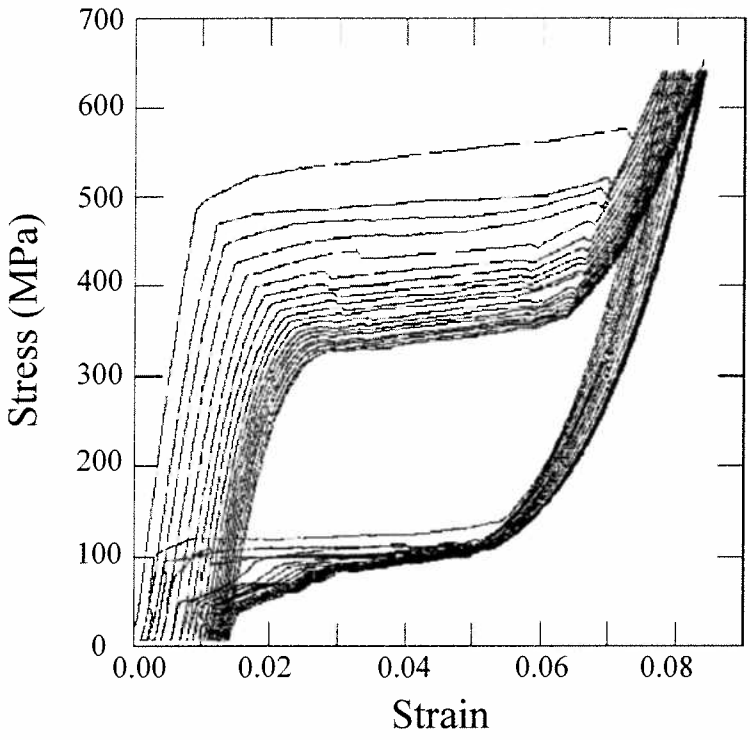

Figure 5: Pseudoelastic response of Ni50Ti50 (%*at.*) wire specimen ($A_f = 65°C$) during the first 20 cycles $T = 70°C$. After the first few cycles the hysteresis of the material stabilizes (Kumar et al., 2003).

2.4 Pseudoelasticity

The *pseudoelastic* behavior of SMAs is associated with stress induced strain recovery upon unloading at temperatures above A_f. Under most general conditions, pseudoelastic thermomechanical loading paths start at zero stress in the austenitic region, then move to the detwinned martensite region and then unload again to the starting point. An example is the path $a \rightarrow b \rightarrow c \rightarrow d \rightarrow e \rightarrow a$ shown on Figure 2. Other examples are the isothermal and isobaric loading paths shown schematically on Figure 6. For clarity, the initial loading from austenite to achieve the required constant stress for the isobaric path is not shown. Note that isothermal condition can be achieved only by quasi-static (small strain increments) loadings, so that the latent heat generated/absorbed during the phase transformation has time to dissipate. For convenience, in this section mostly isobaric or isothermal loading paths will be considered.

Consider the thermomechanical loading path $a \rightarrow b \rightarrow \cdots \rightarrow a$, which starts at zero stress level, above A_f. When the material is loaded at temperatures above A_f, the parent phase (Austenite) undergoes thermoelastic loading up to a critical stress level called the *Transformation stress* ($a \rightarrow b$). At this stress level the material undergoes a stress induced phase transformation ($b \rightarrow c$) from austenite to martensite during which large inelastic strains are developed. Any subsequent loading in the detwinned martensitic region ($c \rightarrow d$) does not produce further phase transformation, although reorientation of the martensitic twins may occur in multi-axial loading conditions. When the point (d) is reached, the reverse transformation begins (martensite-to-austenite), leading to recovery of the inelastic strains. The material fully transforms to austenite at (e) and the final segment of the loading path ($e \rightarrow a$) is characterized by recovery of the thermoelastic strains, leading to zero macroscopic strains upon completion of the path. The transformation process results in a hysteresis which reflects the energy dissipated in the cycle.

In some cases aging of martensite phase can enable reversal of martensitic twins. This phenomenon of reversible detwinning and twinning of the martensitic variants creates a S-S curve similar to the pseudoelastic curve. This phenomenon is called *rubber-like* effect (Otsuka and Wayman, 1999). This effect, first observed

in a Au-Cd alloy (Olander, 1932), constitutes the first studied manifestation of shape memory effect. This type of behavior is a characteristic of the martensitic phase ($T < M_f$). It is observed in specific SMA materials, and unlike the superelastic phenomenon, this involves reorientation within the same phase. Since twin boundaries are very mobile, the critical stress required to move them is very small (a few MPa). Temperature plays only a secondary role in this behavior since there is no phase change. When the motion of twin boundaries is not reversible, the loading/unloading path results in an inelastic strain. However, when the twin boundary motion is reversible during unloading (e.g., in Au-Cd alloys), the macroscopic strain thus obtained is composed of the usual elastic strain and a reversible component associated with the movement of these interfaces. Some authors (Otsuka et al., 1976; Otsuka and Wayman, 1999) use the term *pseudoelasticity* to denote both austenite to detwinned martensite phase transformations and the *rubber-like* effect of reversible detwinning of twinned martensite. In order to distinguish between the two, the term *superelasticity* is used for the first process. In this paper the rubber-like effect is not considered, so the term *pseudoelasticity* will be used throughout in the sense of *superelasticity* as defined by Otsuka et al. (1976); Otsuka and Wayman (1999).

2.4.1 Single Crystal SMAs

The observed stress strain response is different for single- and polycrystalline SMAs. Consider a uniaxial, isothermal loading path in a single crystal. Starting from zero stress level at temperature above A_f, the material response is purely elastic up to the critical stress level σ^{Ms}. As soon as the critical stress is reached, forward transformation (austenite-to-martensite) begins and stress-induced martensite starts forming. During the formation of stress induced martensite large inelastic (transformation) strains are generated, represented by the upper plateau on the stress-strain curves in Figure 7. When the applied stress reaches the value σ^{Mf} the forward transformation is completed and the SMA is in the martensitic phase. For further loading above σ^{Mf}, again only elastic behavior of martensite is observed. Upon unloading, the reverse transformation initiates at the critical stress σ^{As} and completes at a stress σ^{Af}. Due to the difference between σ^{Mf} and σ^{As} and between σ^{Ms} and σ^{Af} a hysteretic loop is obtained in the loading/unloading stress-strain diagram. Although in most single crystal results the stress during the transformation is nearly constant (the plateau on Figure 7), various parameters such as heat treatment, dislocation density, precipitation can introduce hardening.

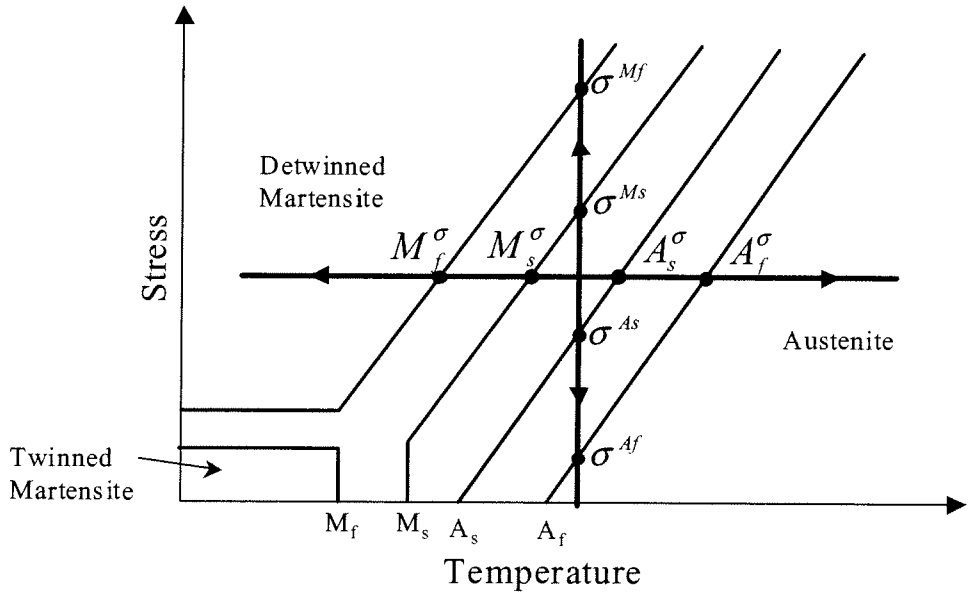

Figure 6: The two loading paths discussed for pseudoelasticity in single crystal SMA. For clarity, the initial loading from austenite to achieve the required constant stress for the isobaric path is not shown.

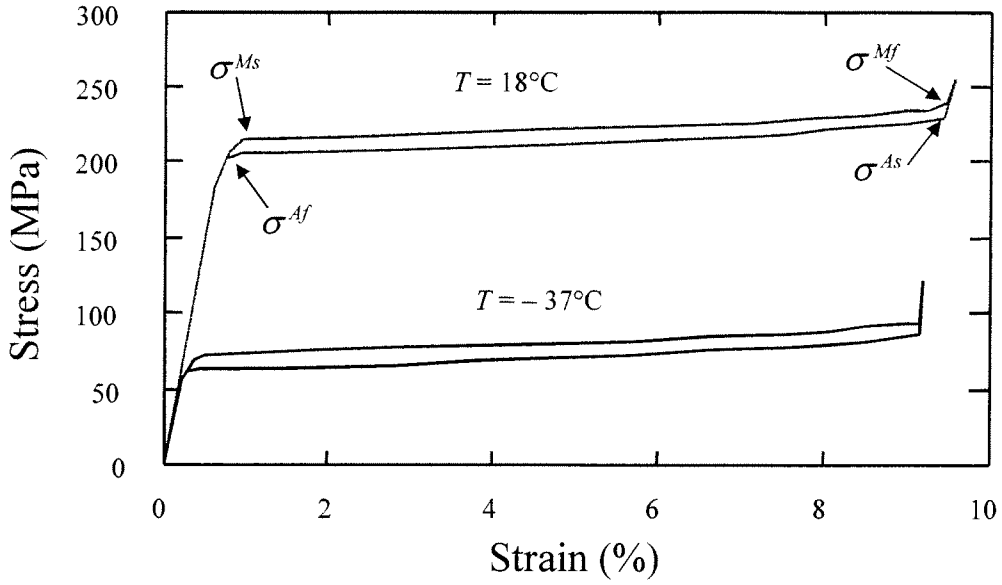

Figure 7: Pseudoelastic behavior observed in a Cu69Zn16Al15 (*%at.*) single crystal. The sample is loaded isothermally at two different temperatures $T = 18°C$ and $T = -37°C$, both above the martensitic start temperature ($M_s = -60°C$). It can be seen that loading at a different temperature results in different stress level for the onset of phase transformation, but the shape of the hysteresis loop is the same (Gautier and Patoor, 1997, pg. 79).

Metallographical observations show that, in single crystal, the pseudoelastic behavior is associated with the growth of a single variant of martensite (Otsuka et al., 1976). This variant possesses the most favorable orientation with respect to the applied stress. Increasing the test temperature results in an increase of the values of critical transformation stresses (Figure 7), while the general shape of the hysteresis loop remains the same.

Consider now an isobaric thermal loading path at some nonzero stress level. Starting from the austenitic region upon cooling it is observed that the transformation is characterized by a martensite start temperature M_s^σ and a martensite finish temperature M_f^σ, which are functions of the applied stress. Macroscopic transformation strain obtained in that way (Figure 8) is a result of formation of detwinned martensite due to the applied load. The transformation is several orders of magnitude greater than the thermal strain corresponding to the same temperature difference required for the phase transformation.

A hysteresis loop is also observed for these isobaric cooling/heating cycles. In a single SMA crystal, the maximum transformation strain observed has the same amplitude as in the pseudoelastic case. Metallographical observations reveal the same kind of microstructure as that for isothermal tests (Patoor et al., 1987). As the applied stress increases, the temperatures M_f^σ, M_s^σ, A_s^σ and A_f^σ increase, but the hysteresis loop characteristics are not affected.

2.4.2 Polycrystalline SMAs

Microstructural aspects have considerable influence on the pseudoelastic behavior. In polycrystals, the differences in crystallographical orientation among grains produce different transformation conditions in each grain. The polycrystalline structure also requires the satisfaction of geometric compatibility conditions at grain boundaries, in addition to compatibility between austenite and the different martensitic variants. Thus, on loading from an initial austenitic state, the martensitic transformation is progressively induced in the different grains and, as opposed to the single crystal case, no well-defined critical transformation stress is observed. In addition, the hysteresis size increases, and the macroscopic transformation strain decreases (Figure 9). In situ optical microscopy observations reveal that several variants of martensite

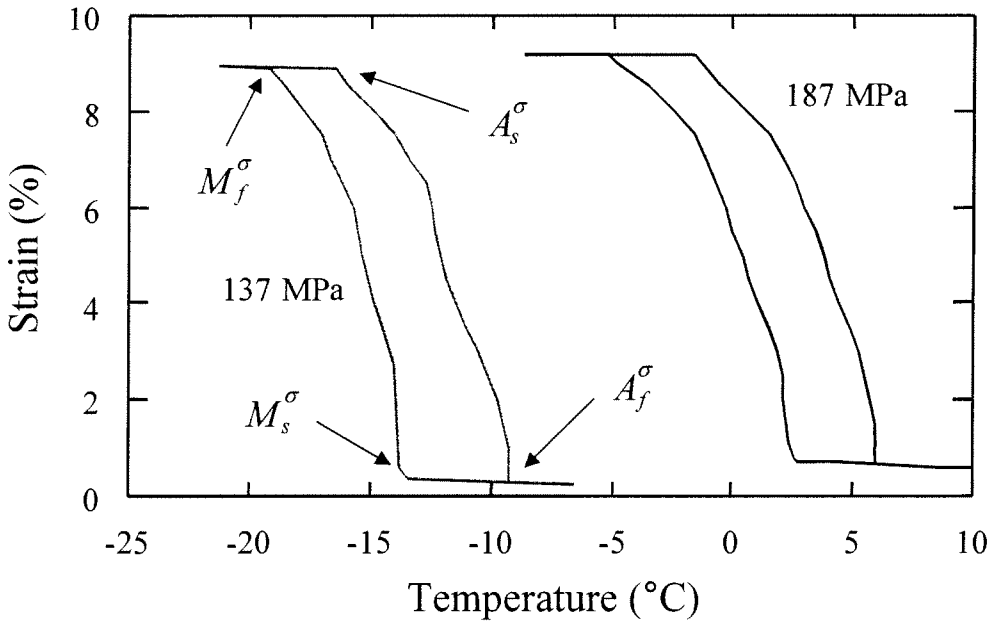

Figure 8: Thermally induced phase transformation of a Cu69Zn16Al15 (%*at.*) single crystal SMA under constant stress levels ($\sigma = 137$ MPa and $\sigma = 187$ MPa). Performing a test at a higher stress level shifts the hysteresis to a higher temperature range, but does not change its shape (Gautier and Patoor, 1997, pg. 80).

are stress-induced inside each grain (Figure 10). The number of these variants with different orientations increases with the progress of the transformation. The macroscopic transformation strain thus obtained is smaller than that for single crystal material as seen from Figure 11. This deformation becomes very sensitive to the applied stress level. At high stress levels, induced variants of martensite are strongly oriented by the applied stress. At low stress levels, the growth of self-accommodated groups becomes dominant.

2.5 Damping Capacity

The damping capacity, which consists of the dissipation of mechanical energy into heat, is not a characteristic behavior that is specific to shape memory alloys only. All materials exhibit this property. However, shape memory alloys exhibit a damping capacity that is far greater than that of standard materials. This is linked to the existence of the numerous interfaces related to the martensitic transformation: those between austenite and martensite, those between the different variants of martensite, and the twin boundaries inside the martensite itself. In spite of the thermoelastic character of the transformation, many irreversible events occur (production of defects, movement of dislocations, etc). Hysteresis observed in pseudoelasticity is one of the energy dissipation manifestations (Stoiber et al., 1990).

During a transformation cycle (or a reorientation one), the damping of an isotropic material is characterized by the ratio of the dissipated energy to the total energy developed. This ratio depends on the excitation frequency, its amplitude and temperature. For shape memory alloys, it also depends on the difference between the operating and transformation temperatures. In general, three damping regimes are distinguished in SMAs:

1. For material initially in the austenitic phase, operating temperatures higher than M_s and weak mechanical excitation the SMA remains in the austenitic phase. The damping capacity is small.

2. For operating temperatures below M_f, the damping capacity increases. This is linked to the large number of interfaces present in the material in the martensitic phase.

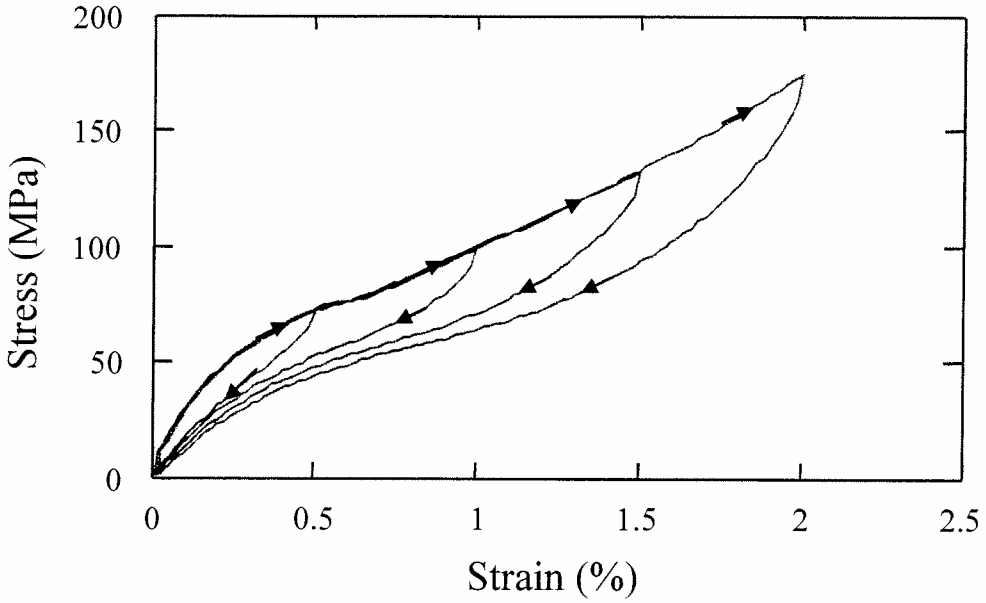

Figure 9: Isothermal loading at room temperature of a polycrystalline Cu66.1Zn24.4Al8.4Ni1.1 (%*at.*) wire. The test is performed above the martensitic start temperature ($M_s = -18°C$) and several minor loops are performed. It can be seen that the hysteresis is bigger compared to a single crystal SMA (Figure 7) and the phase transformation occurs gradually in contrast to the well defined critical transformation stress for single crystals (Gautier and Patoor, 1997, pg. 81).

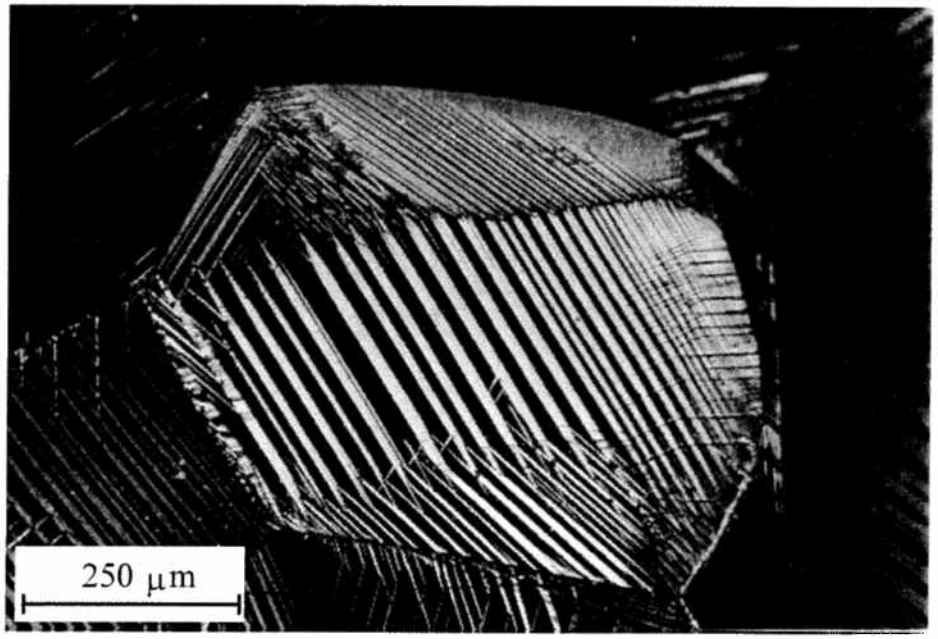

Figure 10: Formation of different martensitic variants in a single grain of a polycrystalline Cu66.9Zn23.7Al9.4(%*at.*) alloy during uniaxial tensile loading (Patoor et al., 1996).

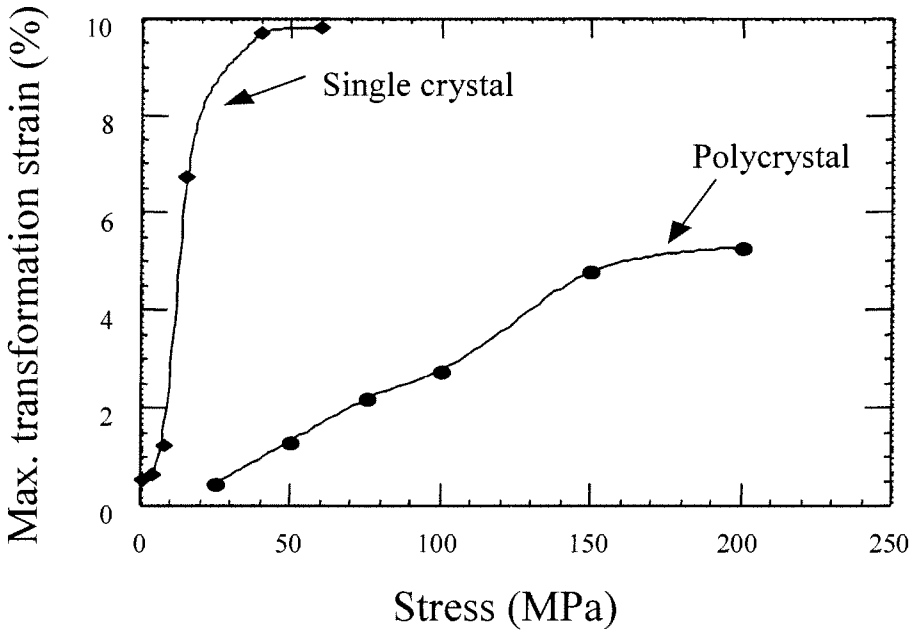

Figure 11: Maximum transformation strain as a function of the applied stress for a single crystal and a polycrystalline Cu73.9Al22.5Be3.6 (%*at.*) SMA.

3. For operating temperatures above A_s and stress levels high enough to induce stress induced martensite, the damping capacity reaches its maximum. Creation and displacement of austenite-martensite interfaces during the loading cycles are accompanied by a strong level of defect production and large thermomechanical coupling.

2.6 Transformation Induced Thermomechanical Fatigue

As shape memory alloys gain popularity for use as large force actuators, knowledge of their thermomechanical fatigue life, in addition to maximum transformation strain and stability of actuation cycles, becomes particularly important. In many applications, a thermomechanical loading path utilizing the pseudoelastic or shape memory effect is repeated, often involving a large number of transformation cycles. Depending on the material history (fabrication process, heat treatments, etc.) and on the type of loading (applied stress, strain, and temperature variations), cyclic martensitic transformations induce microstructural modifications such as defects on grain boundaries due to strain incompatibilities. This leads to low cycle fatigue in comparison to the high cycle fatigue observed for elastic loading. The fatigue life results discussed in this section are summarized in Table 1.

The effect of both mechanical and thermal cyclic loading on the thermomechanical response of NiTi has been investigated by many researchers (Wayman, 1983; Hebda and White, 1995; Lim and McDowell, 1994; Miyazaki et al., 1997; Tanaka et al., 1995; Lagoudas and Bo, 1999; McCormick and Liu, 1994). However, these studies were primarily concerned with the development of two-way SME and the evolution of plastic strain.

One of the early reports on fatigue properties of NiTi SMAs is given by Melton and Mercier (1979b). They present results on crack growth rates and stress-induced transformation fatigue. Constant stress amplitude fatigue results show high fatigue limits for stress levels which do not induce phase transformation whereas the fatigue life for stress-induced phase transformations is significantly reduced. Isothermal cyclic tensile testing has been performed by Miyazaki (1990); Miyazaki et al. (1999), where a constant strain amplitude condition was maintained. This work is similar to that of Melton and Mercier (1979b) but with different test temperatures. Fatigue life of NiTi and NiTiCu alloys are measured using a rotary bending fatigue tester.

Table 1: Transformation induced fatigue life of some common SMAs

Alloy type	and Reference	Fatigue life (number of cycles N_f to failure)	Remarks
NiTi alloys	Melton and Mercier (1979b)	$10^3 \leq N_f \leq 10^4$, $(5\% \geq \varepsilon^t \geq 4\%)$	Ni50.1Ti49.9 and Ni50.3Ti49.7; pseudoelastic cycling under stress control; different alloy compositions and applied heat treatments result in different fatigue life.
	McNichols et al. (1981)	$7 \times 10^3 \leq N_f \leq 2 \times 10^5$ $(8.3\% \geq \varepsilon^t \geq 4.4\%)$	Ni50Ti50; thermal cycling; strong linear correlation between the cycles to failure and the applied cyclic strain amplitude.
	Miyazaki (1990); Miyazaki et al. (1999)	$10^2 \leq N_f \leq 10^5$ $(3.5\% \geq \varepsilon^t \geq 2\%)$	Ni50Ti50 and Ti50Ni40Cu10; pseudoelastic cycling under strain control; maximum recovery strain and stress hysteresis decrease with increasing Cu content; fatigue life for both alloys increases with decreasing testing temperature.
	Bigeon and Morin (1996)	$10 \leq N_f \leq 10^4$, $(50MPa \leq \sigma \leq 800MPa)$	Ti48.8Ni45.2Cu6; thermal cycling; reduction of the applied stress rapidly increases the fatigue life.
	Tobushi et al. (1997, 1998)	$10^2 \leq N_f \leq 10^4$ $(1.4\% \leq \varepsilon^t \leq 3\%)$	Ni50.2Ti49.8; pseudoelastic cycling under strain control; fatigue life increases with decrease of testing temperatures; longer fatigue life: $10^5 \leq N_f \leq 10^7$ $(0.5\% \leq \varepsilon^t \leq 1\%)$ is observed for the R-phase transformation.
	Lagoudas et al. (2000); Bertacchini et al. (2003)	$10^3 \leq N_f \leq 5 \times 10^4$ $(54MPa \leq \sigma \leq 247MPa)$	Ni50Ti40Cu10; thermal cycling; transformation strain is in the range $2\% \leq \varepsilon^t \leq 4\%$; fatigue life increases for smaller transformation strains and stress levels; heat treatments also influence the fatigue life.
Cu based alloys	Melton and Mercier (1979a)	$5 \times 10^4 \leq N_f \leq 10^5$	Cu68.1Zn18.2Al13.7; pseudoelastic cycling under strain control; increasing M_s induces longer fatigue life; stress-induced range used is $30MPa \leq \sigma \leq 100MPa$.
	Sure and Brown (1985)	$3 \times 10^3 \leq N_f \leq 5 \times 10^4$ $(0.8\% \geq \varepsilon^t \geq 0.5\%)$	Cu69.2Al27.6Ni3.2; pseudoelastic cycling under stress control; stress-induced range used is $15MPa \leq \sigma \leq 280MPa$; grain size growth reduces fatigue: for grain size of $\approx 150\mu m$, $3 \times 10^3 \leq N_f \leq 5 \times 10^3$, while for grain size $\approx 20\mu m$ the number of cycles to failure is $N_f \approx 5 \times 10^4$.
	Morin and Trivero (1994)	$N_f \approx 10^4$ $(\sigma \approx 100MPa)$	Cu69.5Al26.8Ni3.7; thermal cycling; $\varepsilon^t \approx 2.5\%$; very low influence of thermal cycling on SME and transformation temperatures; significant creep-like deformation observed during the first 1000 cycles.
	Bigeon and Morin (1996)	$N_f \leq 10^3$ $(10MPa \leq \sigma \leq 200MPa)$	Cu75Zn11Al14; thermal cycling; transformation strain range is $\varepsilon^t \leq 7\%$; reduction of the applied stress rapidly increases the fatigue life.
	Lu et al. (1996)	$4 \times 10^3 \leq N_f \leq 2.1 \times 10^4$	Cu77.5Zn17.5Al5; pseudoelastic cycling under strain control; fatigue life decreases for higher annealing temperatures, while slower cooling rates increase it; pre-straining structural elements impacts the fatigue life.

Two types of strain amplitude vs. fatigue life curves are observed: one composed of two straight lines with one turning point and another composed of three straight lines with two turning points. Due to the lower percentage of martensitic transformation associated with elevated test temperatures, a higher fatigue life is observed.

The above studies of NiTi SMA fatigue life are primarily focused on the stress-induced phase transformation fatigue. One of the first published studies of thermally induced transformation fatigue in NiTi SMA coil springs has been performed by McNichols et al. (1981). The test data shows that the cycles to failure for NiTi are related exponentially to the cyclic strain amplitude (the difference between maximum and minimum cyclic strain). It is difficult, however, to compare these results to those where specimens are subjected to uniform axial stress. Suzuki and Tamura (1990) also presented results on thermal transformation fatigue of NiTi coil spring specimens. Of primary interest during these tests, however, is the number of cycles required for the recovery stress to drop below 70% of the initial value, and the number of cycles to failure is not reported. Thermally induced transformation fatigue experiments under constant uniform stress have also been recently performed on NiTiCu (Lagoudas et al., 2000; Bertacchini et al., 2003). Some selected results of this work are shown in Figure 12 and Figure 13.

Both pseudoelastic transformation fatigue and thermally induced fatigue modify the microstructure of the alloy. Early studies by Melton and Mercier (1979b) on stress induced transformation fatigue in NiTi alloys show that different compositions and heat treatments result in different fatigue life. In a more recent work Tobushi et al. (1997, 1998) report longer fatigue limits for decreasing testing temperatures. Within the range of small transformation strains ($0.5\% < \varepsilon^t < 1\%$), Tobushi et al. (1997, 1998) demonstrated an extended fatigue life ($10^5 < N_f < 10^7$) due to the R-phase transformation, which occurs at lower strains and develops due to certain heat treatment conditions. Miyazaki (1990); Miyazaki et al. (1999) have shown that adding copper as a ternary element in NiTiCu alloys reduces the maximum recovery strain and the stress hysteresis. In addition, fatigue life is increased with the reduction of testing temperatures. These results are confirmed by Tobushi et al. (1997, 1998). The study of the thermally induced transformation fatigue of NiTi alloys establishes a strong linear correlation between the applied cyclic strain amplitude and the number of cycles to failure (McNichols et al., 1981). Thermally induced transformation fatigue life is dictated by the temperature range, and therefore, by the amount of strain applied to the SMA. In fact, a partial transformation where less martensite is created extends significantly the fatigue life of the alloy (Bertacchini et al., 2003). Heat treatments have also been identified to improve the fatigue properties (Lagoudas et al., 2000). Another key parameter is the stress level applied to assist the transformation; lower stresses lead to better fatigue life (Bigeon and Morin, 1996; Bertacchini et al., 2003). However, due to elevated annealing temperatures and depending on the environment where the alloy is cycled, oxidation and corrosion may occur, creating brittleness and discontinuities responsible for crack nucleation and growth (Bertacchini et al., 2003). Figure 12 illustrates the evolutions of the low temperature total strain (a), the high temperature total strain (b) and the difference between them, i.e. the transformation strain (c). The first hundred cycles show the stabilization of the shape memory effect and then the stability of the transformation strain (c). Figure 13 shows the influence of the heat treatments on the number of cycles to failure as a function of the unrecoverable strain.

Other alloys, such as Cu-based SMAs, have also been studied. Melton and Mercier (1979a) compare their results with NiTi alloys to CuZnAl. They find that martensitic alloys have the longest fatigue life and their fatigue properties are controlled by intergranular cracking resulting from strain incompatibilities across the grain boundaries. Stress induced transformation fatigue properties in Cu-based SMAs are very sensitive to the applied stress. As in NiTi alloys, Cu-based SMAs have an increased fatigue life for smaller stresses (Bigeon and Morin, 1996). However, the stress range is much smaller than in NiTi alloys for equivalent maximum transformation strain (Bigeon and Morin, 1996). These alloys are also very sensitive to heat treatments: temperatures that are too high can induce detrimental grain size growth (Sure and Brown, 1985). Cooling rates can also affect the fatigue life. Methods such as step quenching (Lu et al., 1996) have been shown to increase the fatigue life. Thermally induced transformation fatigue life can be increased by lowering the applied stress level (Bigeon and Morin, 1996). Alloys like CuAlNi show a creep-like deformation throughout cycling, especially during the first 1000 cycles (Sure and Brown, 1985). Figure 14 indicates the different attainable stresses for equivalent cycles to failure in a CuAlNi SMA. Results for both single crystal and polycrystal are presented.

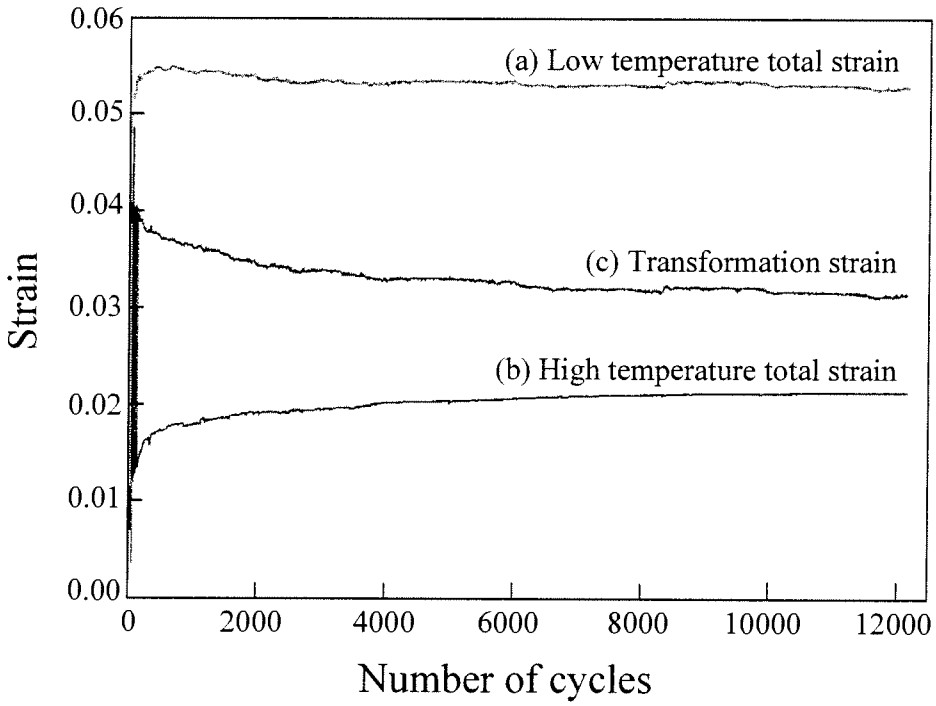

Figure 12: Fatigue life results for Ni50Ti40Cu10 (%*at.*) SMA wires undergoing isobaric transformation at 54 MPa heat treated at 550°C during 15 minutes. After the first few cycles, the low temperature total strain (a) and high temperature total strain (b) slowly increase with the number of cycles. The transformation strain (c) however reaches a saturation point and does not exhibit long term variations. The specimen failed after approximately 12200 cycles (Bertacchini et al., 2003).

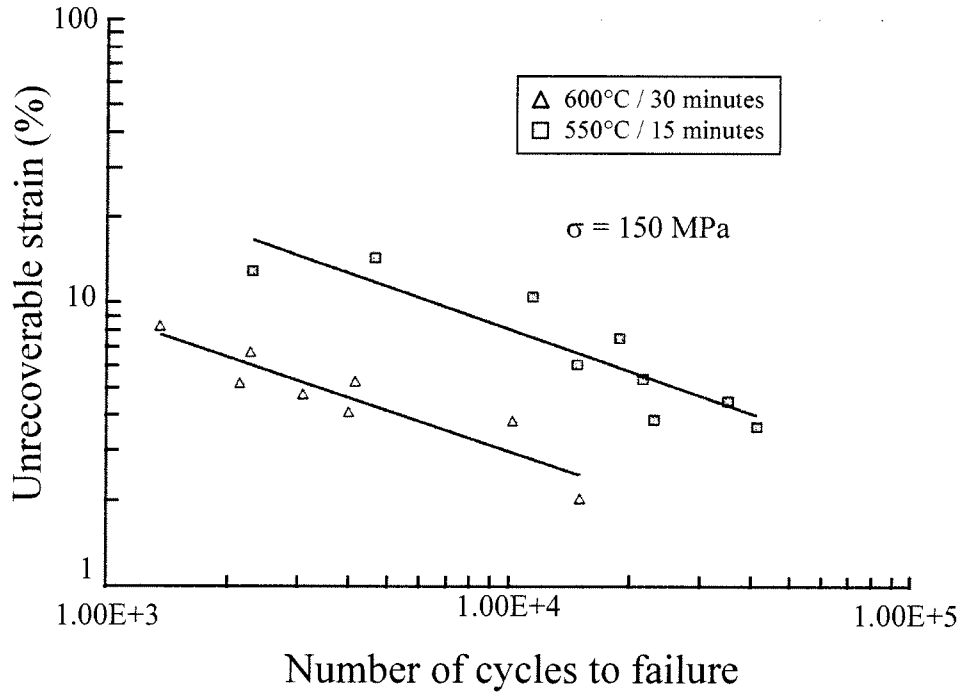

Figure 13: Fatigue life results for Ni50Ti40Cu10 (%*at.*) SMA wires undergoing thermal cycles: influence of two heat treatments on the fatigue life. The test are performed at constant stress level (Lagoudas et al., 2000).

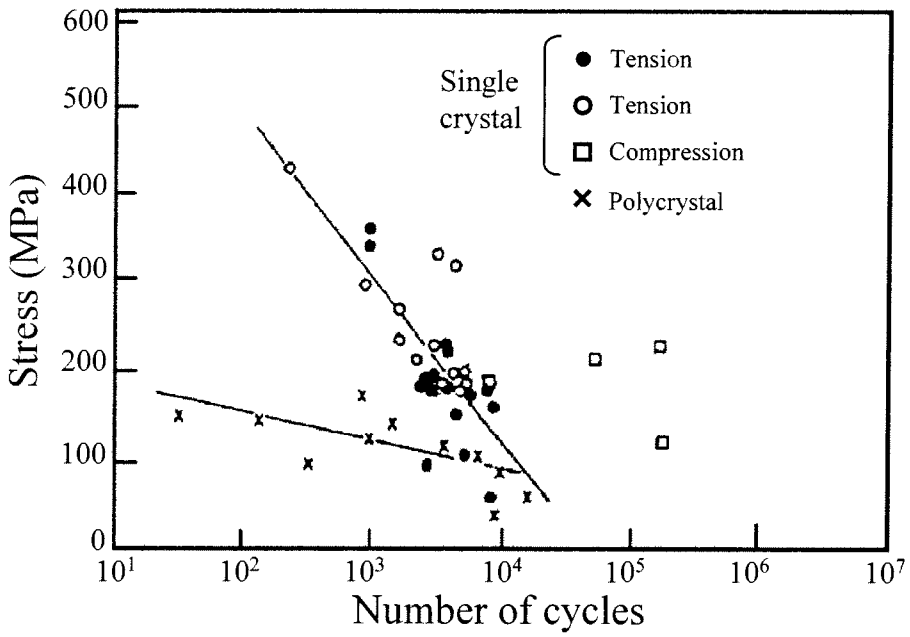

Figure 14: Comparison between the pseudoelastic fatigue life of a polycrystal and a single crystal Cu68.8Al27.6Ni3.8 (*%at.*) alloy. The single crystal SMA has significantly better fatigue life compared to a polycrystal one (Sakamoto, 1983).

3 Commonly Used Shape Memory Alloys

The thermomechanical properties of SMAs depend crucially on their chemical composition, cold work, heat treatment, and thermomechanical cycling. In this section the properties of common SMAs of different chemical compositions are summarized.

3.1 NiTi

In the early 1960s, Buehler and co-workers first explored the shape memory effect in an equiatomic NiTi alloy (Buehler et al., 1963; Buehler and Wiley, 1965). This material, commonly referred to as "Nitinol", has been investigated extensively. One of the first rigorous characterizations of NiTi has been performed in the early 1970s by Jackson et al. (1972). Although its cost is still high, it is popular due to its strong SME behavior with transformation strains of approximately 8% (Melton, 1990). TWSME can also be observed with transformation strains of approximately 5% (Tautzenberger, 1990). A wide range of transformation temperatures for typical NiTi alloys have been reported in the literature with $M_f = 288 \pm 40K$ and $A_f = 362 \pm 80K$ (Lindquist and Wayman, 1990; Strnadel et al., 1995; Xu et al., 1996). The variation in the transformation temperatures is due to different methods of cold work and thermomechanical treatment. Its fine-grained structure and its low elastic anisotropy allow the production of thin wires ($30\,\mu m$), sheets ($50\,\mu m$) and tubes ($0.2\ mm$ in diameter). It also exhibits very good resistance to corrosion and is biocompatible, which promotes its use in biomedical applications (Miyazaki, 1999).

Ti-rich NiTi differs from equiatomic NiTi in that the additional Ti increases the transformation temperatures. Transformation finish temperatures for a representative alloy have been observed at $M_f = 313K$ and $A_f = 358K$ (Todoroki and Tamura, 1986).

Ni-rich NiTi differs from equiatomic NiTi in that increasing Ni content decreases the transformation temperatures. These materials exhibit pseudoelasticity over a wide range due to the effect of precipitation which hardens the matrix. Typical pseudoelastic strain for this material recorded by Saburi et al. (1986) is approximately 8% (Saburi, 1999; Strnadel et al., 1995; Funakubo, 1987).

The commonly used NiTi SMAs often have close to equiatomic composition, but adding a third element may result in an improvement of some of the properties.

NiTiCu is formed by substituting Cu for Ti in binary NiTi. This decreases and stabilizes the hysteresis and reduces aging effects by suppressing precipitate formation. It also reduces the sensitivity of the material to small composition differences in Ni and Ti. In the Ni50Ti50, M_s drops significantly when the composition of Ni increases from 50 to 51 at%. Addition of Cu suppresses this behavior, making the material more suitable for commercial use (Moberly and Melton, 1990). Representative transformation finish temperatures are $M_f = 243K$ and $A_f = 340K$ for Ti50Ni40Cu10 (Strnadel et al., 1995). Temperature ranges of $M_f \approx \pm 20K$ and $A_f \approx \pm 10K$ are observed throughout the literature and are due to varying the ratio of Ni to Ti while holding at% of Cu constant as well as varying levels of cold work and thermomechanical treatment. However, these ranges are much smaller than those observed in an NiTi SMA. The addition of Cu beyond at% ≥ 10 causes the material to become brittle (Otsuka and Wayman, 1999). SME transformation strains of 3% have been observed for Ti50Ni40Cu10 (Moberly and Melton, 1990). Fatigue results for Ti50Ni40Cu10 and Ti40Ni50Cu10 are presented in Table 1.

TiNiZr is formed when zirconium is substituted for Ti in binary NiTi. This high temperature alloy was explored by Eckelmeyer (1976) who showed that a small amount of Ti replaced by Zr could increase the M_s temperature of NiTi SMA. With the Zr content above 10 at% and Ni $\geq$ 49.5 at%, the M_s temperature can be raised above 393K. Increase in the composition of Zr results in an increase in the transformation temperature (Hsieh and Wu, 1998). In this alloy the transformation temperature increases rapidly up to 10% composition of Zr followed by a gradual increase with further addition of Zr (Angst and Kao, 1995). Representative transformation temperatures for TiNiZr are $M_f = 373K$, and $A_f = 503K$ for Ni47Ti38Zr15. It is also observed that for Ni47Ti53-xZrx, where x is the at% of Zr, transformation temperatures increase by $13K$ for every at% of Zr substituted (Hsieh and Wu, 1998).

TiNiHf is formed when hafnium is substituted for Ti in binary NiTi. Over the past decade extensive investigation in this material has been performed. Among ternary alloys developed for high temperature applications, TiNiHf shows some of the most promise. Compared to other ternary alloys like TiNiZr or TiNiPd, the percentage of Hf required to obtain similar transformation temperatures is much smaller. A

typical transformation temperature set is $M_f = 421K$ and $A_f = 504K$ for Ti36Ni49Hf15 (Wang et al., 1999). However, the reported transformation finish temperature range is significant. Specifically, M_f ranges from $323K$ for Ti42.2Ni49.8Hf8 (Potapov et al., 1997) to $460K$ for Ti35.95Ni49.42Hf14.63 (Firstov et al., 2004). Additionally, A_f ranges from $415K$ for Ti42.2Ni49.8Hf8 to $549K$ for Ti30.2Ni49.8Hf20 (Potapov et al., 1997). On average, if the percentage of Ni is held near 49 at%, A_f increases $12K$ for every atomic percentage of Hf substituted for Ti assuming that the at% of Hf is greater than 3%. The material transformation temperatures are also affected by the percentage of Ni. While the transformation temperatures remain relatively constant for Ni compositions varying from 40 to 50 at%, Ni exceeding 50 at% results in a steep fall in the transformation temperatures (Angst and Kao, 1995; Thoma and Boehm, 1999). The mechanical properties of the material are also dependent on the composition of the material. Low Ni (<40 at%) causes brittleness (Besseghini et al., 1999). The material exhibits SME at various test temperatures and ε^t of 3% has been observed. However, the material exhibits poor pseudoelastic properties due to plastic deformation coupled with transformation leading to partial recovery on unloading above A_f (Wang et al., 1999). Addition of Cu to TiNiHf results in small decrease in the transformation temperature (Meng et al., 2002).

TiNiPd alloys are formed when Pd is substituted for Ni in binary NiTi. Early investigations of Ti-Pd materials generated interests in their high transformation temperatures and thermal hysteresis due to transformation behavior (Donkersloot and Van Vucht, 1970). The addition of Pd to NiTi as a ternary element was studied in the early 1990's (Lindquist and Wayman, 1990). Ti50Pd30Ni20 exhibits the typical transformation temperatures of $M_f = 488K$ and $A_f = 542K$ (Goldberg et al., 1995). Published M_f values range from $234K$ for Ti50Pd10Ni40 to $823K$ for Ti50Pd50. Additionally, A_f ranges from $266K$ for Ti50Pd10Ni40 to $864K$ for Ti50Pd50 (Lindquist and Wayman, 1990). Assuming that Ti is held at 50 at% and Pd>10 at%, this yields an average increase in A_f of $13K$ for every at% of Pd substituted for Ni. These transformation temperatures can be further varied by altering the composition of Ti. As the composition of Ti increases from 50 to 51 at% (where Pd is kept constant and Ni reduced) the transformation temperatures gradually decrease with increasing Ti (Tian and Wu, 2002). An ε^t of up to 2.8 to 3% has been observed assuming a total applied strain of 7 to 7.2% (Goldberg et al., 1995; Wu and Tian, 2003). Pseudoelasticity has also been observed in this material with a recoverable strain of up to 7% at high temperature (Wu and Tian, 2003). Addition of a small quantity of Boron greatly helps in increasing the critical stress for slip.

NiTiPt is formed when platinum is substituted for Ni in binary NiTi. In the early 1960's and 1970's, researchers investigated the Ti-Pt phase diagram and the variation of transformation temperatures with composition (Donkersloot and Van Vucht, 1970). During the 1990's Liddquist and Wayman investigated the NiTiPt alloys, including the variation of transformation temperature with composition and SME properties (Lindquist and Wayman, 1990). Representative transformation temperatures include $M_f = 514K$ and $A_f = 573K$ for Ti50Pt20Ni30 (Lindquist and Wayman, 1990). Alloys with more than 30 at% Pt become brittle. Recoverable strain of NiTiPt is approximately 2% for an applied strain of 3.5%.

Other elements which can be alloyed with NiTi include niobium and iron. Niobium ($\sim 9\%at$), in the form of precipitates, stabilizes the martensite by shifting the transformation points to higher temperatures. Fe (1-3%at) promotes a transformation to an intermediate phase (R phase) with very low hysteresis and good fatigue performance.

3.2 Cu-Based Alloys

The main copper-based alloys are found in the Cu-Zn and Cu-Al systems β-domain. The presence of a third element allows the adjustment of the transformation temperatures by a wide margin (about 370°C). The transformation temperatures are highly dependent on the composition. A precision from 10^{-3} to 10^{-4}%at is sometimes necessary to get a reproducibility better than 5°C.

Copper-based alloys generally exhibit less hysteresis than NiTi. The Cu-Zn-Al alloy is easy to create and rather cheap. However, it exhibits a high tendency of decomposing into its equilibrium phases when overheated, thus bringing about a stabilization of the martensite. The presence of additives, such as Co, Zr, B or Ti, is necessary to produce grains from 50 to 100 nm in size. Addition of boron is also used to improve the ductility of the material.

Cu-Al-Ni is less sensitive to stabilization and aging phenomena. This alloy exhibits less hysteresis than NiTi and is known to become brittle as Ni increases much beyond 4 at% (Tadaki, 1999). It is common for Ni to be held at a constant 4 at% such that the alloy has composition Cu96-xAlxNi4 (Miyazaki et al., 1982:

Horikawa et al., 1988). Generally the alloy has a higher Al content as this increases the stability of martensite (Wu, 1990). The substitution of Al for Cu can be seen to decrease the transformation temperatures. This variation is almost perfectly linear, ranging from $M_f = 203K$ and $A_f = 250K$ for an at% Al of 14.4 to $M_f = 308K$ and $A_f = 348K$ for an at% Al of 13.6 (Tadaki, 1999). Although the temperatures can be manipulated over a wide range, the practical upper limit for transformation is 473K. Above this temperature there is a rapid degradation in the transformation due to aging effects. The pseudoelastic strain for a typical Cu based SMA is 4 to 6%. However, with successive martensite-to-martensite transformation (Wu, 1990), very high pseudoelastic strain levels can be obtained. A single crystal formed from a Cu81.8Al14Ni4.2 alloy of this material has been shown to exhibit 18% pseudoelastic strain with 100% recovery (Otsuka et al., 1979). Addition of other elements to the alloy has been explored by Wu (1990).

CuZnSn is a low temperature SMA which exhibits an M_f of $208K$ and an A_f of $235K$ for Cu62.3Zn34.7Sn3 (Eisenwasser and Brown, 1972). The material also exhibits $\varepsilon^t \approx 2\%$ with an applied strain of 2.5% and a pseudoelastic strain of approximately 8% with full recovery (Eisenwasser and Brown, 1972).

Developed in 1982, the Cu-Al-Be alloy has been studied much during the last few years. Its nearly eutectoid composition gives it a good thermal stability. Beryllium, in small amounts (about 0.6%wt), enables adjustment the transformation temperatures from -200°C to 150°C.

Copper based alloys are also used in single crystalline form to improve their properties in some industrial applications.

3.3 Other Shape Memory Alloys

Iron based alloys are known to exhibit less SME than many other alloys types. FeMnSi alloy is a widely studied example of a Fe based SMA. The martensitic transformation, considered non-thermoelastic, leads to an incomplete one-way shape memory effect. Pseudoelasticity is weak or nonexistent. The performance of these alloys is very sensitive to thermomechanical treatments. To avoid corrosion, Cr and Ni are sometimes added, diminishing the memory effect (Maki, 1999).

NiAl alloys have attracted attention due to their very good high temperature strength and resistance to corrosion. Chakravorty and Wayman (1976) performed early crystallographic studies on the thermoelastic martensitic behavior of this material. NiAl materials exhibit good SME but are extremely brittle and exhibit a high sensitivity of the transformation temperatures due to varying Al content. Ishida et al. (1991) have explored the effect of alloying elements to improve the ductility of the material. Addition of Fe to the alloy greatly increases the ductile properties of the material. The martensitic transformation of the alloy is identical to the binary NiAl and M_s is easier to control by annealing at appropriate temperatures. The addition of Fe lowers the transformation temperatures of the alloy but this effect can be compensated by adding Mn or by lowering the Al content. As an example, Ni59Al11Mn30 displays an M_f of $736K$ and an A_f of $833K$. The effect of adding Fe can be seen in Ni60Al19Mn16Fe5 which exhibits an M_f of $598K$ and an A_f of $773K$ (He and Zhou, 2003). The ductility of this material can also be improved by the addition of B or Cr.

Tiβ alloys have high transformation temperatures. For example, TiAu has exhibited transformation temperatures of $M_f = 858K$ and $A_f = 963K$ for Ti57.5Au42.5 (Donkersloot and Van Vucht, 1970).

4 Kinematics of Martensitic Phase Transformation in Shape Memory Alloys

Compared with other classes of materials, phase transition problems in SMAs exhibit more complex microstructure at different length scales as well as coupling between different strain mechanisms (elasticity, plasticity by movement of dislocations, thermal dilatation, phase transition). The complexity of the microstructure and its strong influence on the different types of behavior observed in SMA necessitate a recall of the phenomenological crystallographic theory developed in the late 1950's to describe martensitic transformation mechanisms. The transformation strain observed and its evolution in a Representative Volume Element where several variants of martensite can coexist are then defined. The short overview of the inelastic behavior related to shape memory alloys of the first section showed that plastic flow usually has a negligible effect, except for phenomena such as the Two-Way Shape Memory Effect (TWSME) or the fatigue behavior

during thermomechanical cycling. In the following, these aspect will not be addressed and the modeling will consider only the pseudoelastic and one-way shape memory effects.

This section describes the kinematics of the phase transition adopting a continuum stand point. We assume the existence of a Representative Volume Element (RVE) inside the material, whose characteristic size is larger than the martensite plates and small compared to the size of the considered sample. The RVE is subjected to homogeneous boundary conditions and macroscopic stress and strain for this element are defined from standard definitions in micromechanics. As a first approximation, neglecting the TWSME and cyclic effect, we assume that the only inelastic mechanism apparent in SMAs is related to the transformation strain.

4.1 Transformation Strain Mechanisms

Martensitic phase transformations are non-diffusive first-order phase transitions (Delaey, 1990; Cohen, 1988; Guénin, 1986; Khachaturyan, 1983), which means that the chemical composition remains constant, but the atoms are organized in a new crystallographic lattice. This leads to the formation of martensitic phase "islands" within the parent phase crystal lattice. Morphologically, the martensitic phase is formed as thin platelets, needles, or laths with well-defined crystallographical orientations with respect to the parent phase crystal. Based on these observations, consistent crystallographic theories of martensitic transformations were proposed by Wechsler et al. (1953) and Bowles and MacKenzie (1954). Both theories have been shown to be mathematically identical by Christian (1956) and have been summarized by Khachaturyan (1983). The discussion below closely follows the presentation given by Khachaturyan (1983). These descriptions start with the observation that the austenitic and martensitic phases fit together along planes called *Invariant Planes* or *Habit Planes*. The connectivity of the parent with the martensitic phase occurs without the requirement of an elastic strain.

When a crystal undergoes a homogeneous deformation, like in martensitic transformation, each initial crystal lattice site vector $\mathbf{r}$ transforms into $\mathbf{r}'$. The initial and transformed lattice sites are related by

$$\mathbf{r}' = \mathbf{F}\mathbf{r}, \tag{4.1}$$

where $\mathbf{F}$ is the deformation gradient tensor. In a stress-free martensitic phase transformation, $\mathbf{F}$ incurs a jump across the invariant plane and is defined as

$$\mathbf{F}(\mathbf{x}) = \begin{cases} \mathbf{F}^M & \text{if} \quad \mathbf{x} \in \mathcal{B}^M \\ \mathbf{I} & \text{if} \quad \mathbf{x} \in \mathcal{B}^A. \end{cases} \tag{4.2}$$

In the equation above, region $\mathcal{B}^M$ corresponds to the martensite region and $\mathcal{B}^A$ corresponds to the untransformed austenite region.

The continuity of displacement across the invariant plane is expressed by the Hadamard condition in the form of

$$\mathbf{F}^M = \mathbf{I} + \mathbf{m} \otimes \mathbf{n}, \tag{4.3}$$

where $\mathbf{n}$ is the unit vector normal to the invariant plane, $\mathbf{m}$ is a vector pointing in the direction of the transformation (see Figure 15(a)).

The linearized transformation strain in the martensitic region in terms of the deformation gradient $\mathbf{F}^M$ is given by

$$\varepsilon^{tM} = \frac{1}{2}\left(\mathbf{F}^M + (\mathbf{F}^M)^T\right) - \mathbf{I}. \tag{4.4}$$

Substituting equation (4.3) into the equation above results in

$$\varepsilon^{tM} = \frac{1}{2}\left(\mathbf{m} \otimes \mathbf{n} + \mathbf{n} \otimes \mathbf{m}\right). \tag{4.5}$$

Note that the presence of stresses will not change the above result, provided both martensite and austenite have identical elastic properties. Recalling that the transformation strain in the austenitic region is zero, ε^{tM} will be referred to simply as ε^t.

Often the deformation associated with the martensitic phase deformation results in a gap between the parent phase and the martensite along the habit plane. Therefore, a rigid body rotation of the martensite

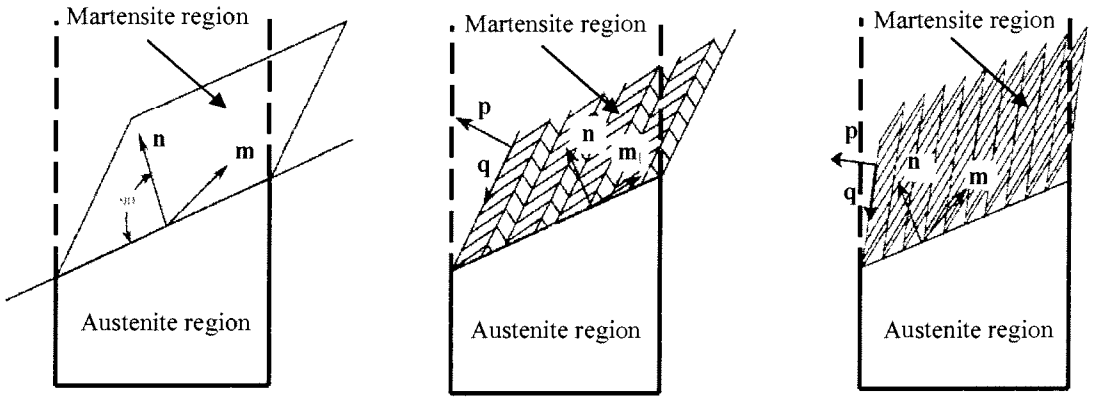

(a) Invariant plane strain (b) Twin formation (c) Plastic slip

Figure 15: Different mechanisms for martensitic phase transformation: homogeneous plane invariant strain (a), macroscopic shape deformation produced by a heterogeneous martensitic transformation (b) and by lattice invariant plastic slip (c).

may be necessary to enforce the continuity between the phases. In this case the deformation gradient $\mathbf{F}^M$ can be written as

$$\mathbf{F}^M = \hat{\mathbf{R}}\mathbf{F}, \tag{4.6}$$

where $\hat{\mathbf{R}}$ is a rotation and $\mathbf{F}$ can be found from crystallography.

The vectors $\mathbf{n}$ and $\mathbf{m}$ can be expressed in terms of the eigenvalues of $(\mathbf{F}^M)^T\mathbf{F}^M$, which correspond to the principal stretches, associated with the lattice distortion. Note that $(\mathbf{F}^M)^T\mathbf{F}^M = (\mathbf{F})^T\mathbf{F}$.

Let λ_1^2, λ_2^2 and λ_3^2 be the eigenvalues and $\mathbf{e}_1$, $\mathbf{e}_2$, $\mathbf{e}_3$ be the eigenvectors of $(\mathbf{F})^T\mathbf{F}$. As shown by Khachaturyan (1983), one of the eigenvalues is less than 1, the other is equal to 1 and the third eigenvalue is greater than 1. Let

$$\lambda_1^2 < 1, \quad \lambda_2^2 = 1, \quad \lambda_3^2 > 1. \tag{4.7}$$

Then $\mathbf{n}$ and $\mathbf{m}$ are given in terms of the above eigenvalues by:

$$\mathbf{n} = \sqrt{\frac{\lambda_3^2 - 1}{\lambda_3^2 - \lambda_1^2}}\mathbf{e}_3 + \sqrt{\frac{1 - \lambda_1^2}{\lambda_3^2 - \lambda_1^2}}\mathbf{e}_1, \tag{4.8}$$

$$\mathbf{m} = (\lambda_3 - \lambda_1)\left(\lambda_1\sqrt{\frac{\lambda_3^2 - 1}{\lambda_3^2 - \lambda_1^2}}\mathbf{e}_3 - \lambda_3\sqrt{\frac{1 - \lambda_1^2}{\lambda_3^2 - \lambda_1^2}}\mathbf{e}_1\right), \tag{4.9}$$

The transformation strain in the martensitic phase can be calculated by considering different mechanisms. The next two sections describe two of the possible mechanisms: twin formation and plastic slip. These mechanisms have been observed in different alloys undergoing martensitic transformation as the means of relaxing incompatibilities developed during the lattice distortion.

4.2 Transformation Strain by Twin Formation

Consider an austenitic region which transforms into thermally-induced martensite by twin formation as shown in Figure 15(b). The two alternating martensitic domains are produced by two different crystal rearrangements with deformation gradients $\mathbf{F}_1$ and $\mathbf{F}_2$. Both $\mathbf{F}_1$ and $\mathbf{F}_2$ do not necessarily result in an invariant plane strain, i.e., they do not satisfy the relationship (4.3), even though their combination will result in an invariant plane strain. Now consider a material vector inside the twin structure, which in the reference domain (before the transformation) is equal to $\mathbf{X}$. This vector $\mathbf{X}$ is transformed into vector $\mathbf{X}'$ as:

$$\mathbf{X}' = (x\mathbf{F}_1 + (1 - x)\mathbf{F}_2)\,\mathbf{X}. \tag{4.10}$$

where the parameter x is the fraction of the martensitic crystal occupied by domains of the first variant ($\mathbf{F}_1$) and $(1-x)$ is the fraction of martensite occupied by domains of second variant ($\mathbf{F}_2$). Thus the macroscopic deformation associated with the martensitic phase transformation is described by the deformation gradient

$$\mathbf{F} = x\mathbf{F}_1 + (1-x)\mathbf{F}_2. \tag{4.11}$$

One could choose the parameter x in such a way that the deformation described by $\mathbf{F}$ results in an invariant plane strain, i.e., it satisfies the relationship (4.3). Therefore, it is possible that a certain combination of $\mathbf{F}_1$ and $\mathbf{F}_2$ may describe an invariant plane strain, despite the fact that none of the deformations described by $\mathbf{F}_1$ and $\mathbf{F}_2$, taken separately, are associated with invariant plane strains.

The martensitic transformation results in different crystallographic orientations for the different variants of the martensitic phase. Let the transformation of the crystallographic vectors of the austenitic phase to the crystallographic vectors of the different martensitic variants be given by the following *Bain deformation tensors*

$$\mathbf{B}_1, \mathbf{B}_2, \mathbf{B}_3, \ldots, \mathbf{B}_n, \tag{4.12}$$

where n corresponds to the possible number of martensitic variants. These tensors are related to each other by certain rotations and reflections. Transformation to martensitic variants of adjacent regions, corresponding to tensors $\mathbf{B}_1$, $\mathbf{B}_2$, etc, may lead to incompatibilities among the crystal lattices of the resulting martensitic variants. Thus, to enforce the continuity of the resulting crystal structure, the domains of the martensitic variants must be rotated as rigid bodies. Therefore, combining the tensors (4.12) with rigid body rotations leads to the following lattice rearrangement tensors

$$\mathbf{F}_1 = \mathbf{R}_1\mathbf{B}_1, \quad \mathbf{F}_2 = \mathbf{R}_2\mathbf{B}_2, \quad \mathbf{F}_3 = \mathbf{R}_3\mathbf{B}_3, \ldots, \quad \mathbf{F}_n = \mathbf{R}_n\mathbf{B}_n, \tag{4.13}$$

where $\mathbf{R}_1$, $\mathbf{R}_2$, $\mathbf{R}_3$,..., $\mathbf{R}_n$ are orthogonal tensors, corresponding to rigid body rotations of the martensitic variants *lattice invariant deformation tensors.* This formulation can be applied to different cases such as cubic-to-tetragonal or cubic-to-monoclinic martensitic phase transformations.

4.3 Transformation Strain by Plastic Slip

The inelastic lattice Bain deformation resulting from the lattice distortion during martensitic phase transformation [cf. equation (4.12)] describes the geometrical transformation from the parent lattice (austenite) to the product lattice (martensite). The strain field induced by the lattice distortion is usually strongly incompatible. These incompatibilities lead to high internal stresses which can be relaxed (at least partially) by lattice-invariant shear deformation inducing $\mathbf{F}^{LIS}$ appearing simultaneously with and inside the martensite. Thus, the deformation during martensitic transformation is obtained as

$$\mathbf{F} = \mathbf{F}^{LIS}\mathbf{B}. \tag{4.14}$$

In the theory presented by Wechsler et al. (1953), the Bain deformation is assumed to be known from crystallography, and the lattice invariant shear deformation $\mathbf{F}^{LIS}$ is assumed to be realized from plastic slip having amplitude γ and slip direction $\mathbf{q}$ acting on a plane with unit normal $\mathbf{p}$ (see Figure 15(c)). Thus, $\mathbf{F}^{LIS}$ is given by

$$\mathbf{F}^{LIS} = \mathbf{I} + \gamma\mathbf{q} \otimes \mathbf{p}. \tag{4.15}$$

The unknown value of γ may be calculated from the requirement that one of the eigenvalues of $(\mathbf{F})^T\mathbf{F}$ is equal to 1. Then, the vectors $\mathbf{n}$ and $\mathbf{m}$ can be found using the other two eigenvalues and the eigenvectors, as shown by equations (4.8), (4.9).

To demonstrate the above approach, consider FCC→BCC in Fe-31 wt%Ni alloy. The Bain deformation is given by

$$\mathbf{B} = \begin{pmatrix} \eta_1 & 0 & 0 \\ 0 & \eta_1 & 0 \\ 0 & 0 & \eta_3 \end{pmatrix} \tag{4.16}$$

where the $\eta_1 = 1.1322$ and $\eta_3 = 0.8006$. The lattice invariant strain is assumed to occur by slip on the (101) $[\bar{1}01]$ system. Thus, the unit vectors $\mathbf{p}$ and $\mathbf{q}$ (cf. equation (4.15)) are given by $\mathbf{p} = (1/\sqrt{2}, 0, 1/\sqrt{2})$ and

$\mathbf{q} = (-1/\sqrt{2}, 0, 1/\sqrt{2})$. Equation (4.15) leads to

$$\mathbf{F}^{LIS} = \begin{pmatrix} 1-\gamma/2 & 0 & -\gamma/2 \\ 0 & 1 & 0 \\ \gamma/2 & 0 & 1+\gamma/2 \end{pmatrix}. \tag{4.17}$$

Using equation (4.14), $\mathbf{F}$ is given by

$$\mathbf{F} = \begin{pmatrix} (1-\gamma/2)\eta_1 & 0 & -\gamma/2 \\ 0 & \eta_1 & 0 \\ \gamma/2 & 0 & (1+\gamma/2)\eta_3 \end{pmatrix}. \tag{4.18}$$

The condition of $\lambda_2^2 = 1$ leads to the following two values: $\gamma_1 = 0.2569$ and $\gamma_2 = 0.4097$. Keeping only the lowest value $\gamma = 0.2569$, the eigenvalues λ_1^2 and λ_3^2 of $(\mathbf{F})^T\mathbf{F}$ and the corresponding eigenvectors $\mathbf{e}_1$ and $\mathbf{e}_3$ are given by

$$\lambda_1^2 = 0.8216, \quad \mathbf{e}_1 = (-0.2971, 0, -0.9548) \tag{4.19a}$$

$$\lambda_3^2 = 1.2819, \quad \mathbf{e}_3 = (0, 1, 0) \tag{4.19b}$$

The normal $\mathbf{n}$ to the habit plane and the transformation direction $\mathbf{m}$ are calculated using equations (4.8), (4.9):

$$\mathbf{n} = (-0.1850, 0.7826, -0.5944), \tag{4.20a}$$

$$\mathbf{m} = (0.0473, 0.1601, 0.1519). \tag{4.20b}$$

Finally, the macroscopic deformation gradient is calculated using equation (4.3) as

$$\mathbf{F}^M = \begin{pmatrix} 1.0087 & -0.0370 & 0.0281 \\ 0.0296 & 0.8747 & 0.0952 \\ 0.0281 & -0.1189 & 1.0903 \end{pmatrix}. \tag{4.21}$$

These theories were successful for transformations in which the lattice distortion associated with the transformation is small. However, the predictions show deviations for materials whose transformation strains are larger (Otsuka, 1990; Bhattacharya, 1993). Over the years, several modifications to the initial theories have been proposed (Roytburd and Pankova, 1985; Ball and James, 1987).

4.4 Definitions of the Macroscopic Transformation Strain

Phenomenological crystallographical theories like the one proposed by Wechsler et al. (1953) allow determination of the transformation strain related to the growth of a single variant of martensite in stress-free conditions. In the current section this result will be extended to describe a stress-induced multivariant transformation.

4.4.1 Transformation Strain of a Representative Volume Element

Let the reference configuration of the representative volume element (RVE) be the austenite grain of a polycrystal in its natural state (stress-free, $\boldsymbol{\sigma} = \mathbf{0}$) at a temperature $T > A_f$. Due to a thermomechanical loading, some part V^M of this RVE of volume V is transformed into martensite. The formation of several variants of martensite of volume V_n, having different crystallographical orientations is considered. Each part V_n of V^M undergoes a uniform transformation strain $\boldsymbol{\varepsilon}^{tn}$. The total strain $\boldsymbol{\varepsilon}$ so obtained results from several contributions: an elastic part denoted $\boldsymbol{\varepsilon}^e$, a thermal part denoted $\boldsymbol{\varepsilon}^{th}$, and a transformation part $\boldsymbol{\varepsilon}^t$, which is determined from the phenomenological crystallographic theory. Thus for the displacement field $\mathbf{u}$ one obtains for infinitesimal deformation (linearized strain) the following total strain that satisfies the compatibility conditions:

$$\frac{1}{2}\left(\nabla\mathbf{u} + (\nabla\mathbf{u})^T\right) = \boldsymbol{\varepsilon} = \boldsymbol{\varepsilon}^e + \boldsymbol{\varepsilon}^{th} + \boldsymbol{\varepsilon}^t. \tag{4.22}$$

By averaging over the volume V and the assumption that $\mathbf{u} = \langle\boldsymbol{\varepsilon}\rangle\mathbf{x}$, the macroscopic total strain $\langle\boldsymbol{\varepsilon}\rangle$ is given by:

$$\langle\boldsymbol{\varepsilon}\rangle = \frac{1}{V}\int_V \boldsymbol{\varepsilon} dV = \frac{1}{V}\int_V (\boldsymbol{\varepsilon}^e + \boldsymbol{\varepsilon}^{th} + \boldsymbol{\varepsilon}^t) dV. \tag{4.23}$$

The macroscopic strain $\langle\boldsymbol{\varepsilon}\rangle$ may also be decomposed into elastic $\langle\boldsymbol{\varepsilon}^e\rangle$ thermal $\langle\boldsymbol{\varepsilon}^{th}\rangle$ and transformation $\langle\boldsymbol{\varepsilon}^t\rangle$ parts. Assuming the 4-th order elastic compliance tensor $\boldsymbol{\mathcal{S}}$ and the 2-nd order thermal dilatations tensor $\boldsymbol{\alpha}$ to be homogeneous, the overall strains $\langle\boldsymbol{\varepsilon}^e\rangle$ and $\langle\boldsymbol{\varepsilon}^{th}\rangle$ can be identified with the corresponding mean values of the local parts.

$$\langle\boldsymbol{\varepsilon}\rangle = \frac{1}{V}\int_V \boldsymbol{\mathcal{S}}\boldsymbol{\sigma} dV + \frac{1}{V}\int_V \boldsymbol{\alpha} T dV + \frac{1}{V}\int_V \boldsymbol{\varepsilon}^t dV, \tag{4.24}$$

The uniformity of $\boldsymbol{\mathcal{S}}$ and $\boldsymbol{\alpha}$ leads to

$$\langle\boldsymbol{\varepsilon}\rangle = \boldsymbol{\mathcal{S}}\frac{1}{V}\int_V \boldsymbol{\sigma} dV + \boldsymbol{\alpha}\frac{1}{V}\int_V T dV + \frac{1}{V}\int_V \boldsymbol{\varepsilon}^t dV. \tag{4.25}$$

From the property $\langle\boldsymbol{\sigma}\rangle = \frac{1}{V}\int_V \boldsymbol{\sigma} dV$ and the uniformity of the temperature T over the RVE, one gets

$$\langle\boldsymbol{\varepsilon}^e\rangle = \boldsymbol{\mathcal{S}}\langle\boldsymbol{\sigma}\rangle, \quad \text{and} \quad \langle\boldsymbol{\varepsilon}^{th}\rangle = \boldsymbol{\alpha} T. \tag{4.26}$$

and the macroscopic transformation strain $\langle\boldsymbol{\varepsilon}^t\rangle$ is defined by

$$\langle\boldsymbol{\varepsilon}^t\rangle = \frac{1}{V}\int_V \boldsymbol{\varepsilon}^t dV. \tag{4.27}$$

Since the field $\boldsymbol{\varepsilon}^t$ is piecewise uniform, considering it keeps a uniform value inside each variant of martensite, it can be represented by a set of indicator functions θ_n so that

$$\boldsymbol{\varepsilon}^t = \sum_{n=1}^{N} \boldsymbol{\varepsilon}^{tn}\theta_n, \tag{4.28}$$

where $\boldsymbol{\varepsilon}^{tn}$ is the (uniform) transformation strain inside V_n, and

$$\theta_n(\mathbf{x}) = \begin{cases} 1 & \text{if} \quad \mathbf{x} \in V_n \\ 0 & \text{if} \quad \mathbf{x} \notin V_n. \end{cases} \tag{4.29}$$

From equations (4.27) and (4.28), one gets

$$\langle\boldsymbol{\varepsilon}^t\rangle = \frac{1}{V}\sum_{n=1}^{N}\int_{V_n} \boldsymbol{\varepsilon}^{tn} dV \quad = \sum_{n=1}^{N} f^n \boldsymbol{\varepsilon}^{tn}, \tag{4.30}$$

where the parameter $f^n = V_n/V$ represents the volume fraction of variant n.

In that case, the overall transformation strain is described by (known) transformation strains $\boldsymbol{\varepsilon}^{tn}$ and the corresponding (unknown) volume fractions f^n.

4.4.2 Evolution of the Transformation Inside the RVE

When the loading conditions change, the progress of the transformation can result from the growth of variants from the parent phase or from the motion of interfaces between the different variants of martensite. In the small strain approximation, the time derivative of equation (4.27) is given by

$$\frac{d\langle\boldsymbol{\varepsilon}^t\rangle}{dt} = \frac{1}{V}\int_V \frac{\partial\boldsymbol{\varepsilon}^t}{\partial t} dV - \frac{1}{V}\int_S [\boldsymbol{\varepsilon}^t]\mathbf{w}\cdot\mathbf{n} dS, \tag{4.31}$$

where $\frac{\partial\boldsymbol{\varepsilon}^t}{\partial t}$ denotes the variation of the transformation strain with respect to time, $[\boldsymbol{\varepsilon}^t] = \boldsymbol{\varepsilon}^{t+} - \boldsymbol{\varepsilon}^{t-}$ is the jump of $\boldsymbol{\varepsilon}^t$ across the interface S. Unit normal $\mathbf{n}$ is oriented pointing from the minus side to the plus side, and $\mathbf{w}\cdot\mathbf{n}$ is the normal velocity of the boundary S (Figure 16).

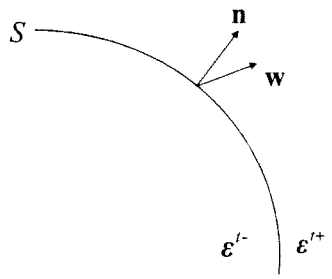

Figure 16: Definition of jumps of strain across a moving interface.

Considering the internal interface S is composed of austenite-martensite interfaces S_{AM} and martensite-martensite interfaces S_{MM}, and taking into account that $\frac{\partial \varepsilon^t}{\partial t} = \mathbf{0}$, the overall transformation strain rate is given by

$$\frac{d\langle \boldsymbol{\varepsilon}^t \rangle}{dt} = \frac{1}{V} \int_{S_{AM}} \boldsymbol{\varepsilon}^{t-} \mathbf{w} \cdot \mathbf{n} dS - \frac{1}{V} \int_{S_{MM}} [\boldsymbol{\varepsilon}^t] \mathbf{w} \cdot \mathbf{n} dS, \tag{4.32}$$

where the following two mechanisms involved in the behavior of the shape memory alloys appear:

- the first integral in equation (4.32) corresponds to transformation with deformation,
- the second integral corresponds to deformation without phase transformation ($\dot{f} = 0$) and describes the mechanism of reorientation of the martensite variants.

Similar conclusions may be obtained using a crystallographical approach. Evolution of $\langle \boldsymbol{\varepsilon}^t \rangle$ with respect to time is related to changes in the f^n parameters. From equation (4.30) we have

$$\frac{d\langle \boldsymbol{\varepsilon}^t \rangle}{dt} = \sum_{n=1}^{N} \boldsymbol{\varepsilon}^{tn} \frac{df^n}{dt} = \sum_{n=1}^{N} \boldsymbol{\varepsilon}^{tn} \dot{f}^n. \tag{4.33}$$

Since $\dot{f}^n$ may be either positive or negative, equation (4.33) includes both the transformation and the reorientation mechanism.

5 Free Energy and Dissipation

The derivation of the macroscopic (overall) behavior of the austenite-martensite representative volume element requires the calculation of the free energy of the RVE in which the elastic and the chemical parts have to be taken into account, as described in Section 5.1. The dissipation, which is deduced from the comparison of external power and the change in free energy, defines the driving force for the evolution of the phase transformation.

5.1 Free Energy Related to a Martensitic Transformation in the RVE

Let us consider an RVE in a two-phase state (austenite and martensite). The total potential energy of this system is composed of the following components:

- the elastic strain energy with density $w(\mathbf{x}) = \frac{1}{2}\boldsymbol{\sigma}(\mathbf{x})\boldsymbol{\varepsilon}^e(\mathbf{x})$, where local stresses $\boldsymbol{\sigma}(\mathbf{x})$ are related to internal and applied stresses;
- the crystallographic (usually called chemical) free energy with density $\varphi(\mathbf{x})$;
- the interfacial energy between all the constituents. Due to the oblate shape of martensite plates or needles, this last term is generally neglected in martensitic transformations.

Other sources of energy (dislocations, points, defects), which are neglected in this approach, influence some specific effects in the behavior of shape memory alloys (training effect or cyclic behavior). The reference configuration of the RVE is considered to be in a stress-free austenitic state. It is assumed that the thermomechanical loading rate is slow enough to keep the temperature uniform over the RVE. For a unit volume V, the Helmholtz free energy Φ is given by

$$\Phi = \frac{1}{V}\int_V \varphi(\mathbf{x})dV + \frac{1}{V}\int_V w(\mathbf{x})dV. \tag{5.1}$$

Since $\varphi(\mathbf{x})$ is equal to $\varphi_A(T)$ in the austenite phase of volume V_A and $\varphi_M(T)$ in the martensite of volume V_M, the first term in equation (5.1) may be written as

$$\frac{1}{V}\int_V \varphi(\mathbf{x})dV = \frac{V_A}{V}\varphi_A(T) + \frac{V_M}{V}\varphi_M(T) = f\varphi_M + (1-f)\varphi_A = \varphi_A + (\varphi_M - \varphi_A)f. \tag{5.2}$$

Since austenite is stable at high temperatures and martensite at low temperature, a temperature $T = T_0$ for which $\varphi_M = \varphi_A$ does exist. This temperature T_0 is called the *thermodynamical equilibrium temperature*. In the vicinity of T_0, the chemical part of the free energy may be linearized by

$$\frac{1}{V}\int_V \varphi(\mathbf{x})dV = B(T - T_0)f, \tag{5.3}$$

where B can be treated as a material constant. In terms of the phase diagram description of Section 2.1, B is responsible for the slope of the austenite to detwinned martensite transformation lines.

The elastic part of the free energy

$$W = \frac{1}{V}\int_V w(\mathbf{x})dV = \frac{1}{2V}\int_V \boldsymbol{\sigma} : \boldsymbol{\varepsilon}^e dV \tag{5.4}$$

may be transformed using equation (4.22) from the kinematics

$$\boldsymbol{\varepsilon}^e = \frac{1}{2}\left(\nabla\mathbf{u} + (\nabla\mathbf{u})^T\right) - \boldsymbol{\varepsilon}^t \quad \text{inside} \quad V \quad \text{and} \quad \mathbf{u} = \langle\boldsymbol{\varepsilon}\rangle\mathbf{x} \quad \text{at} \quad \partial V, \tag{5.5}$$

so that

$$W = \frac{1}{2V}\int_V \boldsymbol{\sigma}(\nabla\mathbf{u} - \boldsymbol{\varepsilon}^t)dV. \tag{5.6}$$

By partial integration, and by taking into account the boundary conditions, equation (5.6) is reduced to

$$W = \frac{1}{2}\langle\boldsymbol{\sigma}\rangle : \langle\boldsymbol{\varepsilon}\rangle - \frac{1}{2V}\int_V \boldsymbol{\sigma} : \boldsymbol{\varepsilon}^t dV, \tag{5.7}$$

where

$$\langle\boldsymbol{\sigma}\rangle = \frac{1}{V}\int_V \boldsymbol{\sigma}dV$$

are the overall stresses.

Decomposing the stresses $\boldsymbol{\sigma}$ into macroscopic stresses $\langle\boldsymbol{\sigma}\rangle$ and internal stresses $\boldsymbol{\tau}$ (with properties $\mathrm{div}\boldsymbol{\tau} = \mathbf{0}$ and $(1/V)\int_V \boldsymbol{\tau}dV = \mathbf{0}$) and using the Hooke's law $\langle\boldsymbol{\sigma}\rangle = \boldsymbol{\mathcal{C}}(\langle\boldsymbol{\varepsilon}\rangle - \langle\boldsymbol{\varepsilon}^t\rangle)$, equation (5.7) can be written as

$$W = \frac{1}{2}(\langle\boldsymbol{\varepsilon}\rangle - \langle\boldsymbol{\varepsilon}^t\rangle) : \boldsymbol{\mathcal{C}}(\langle\boldsymbol{\varepsilon}\rangle - \langle\boldsymbol{\varepsilon}^t\rangle) - \frac{1}{2V}\int_V \boldsymbol{\tau} : \boldsymbol{\varepsilon}^t dV, \tag{5.8}$$

where the internal stresses $\boldsymbol{\tau}$ depend only on the incompatibilities of the transformation strain field $\boldsymbol{\varepsilon}^t$. Thus, W depends on boundary conditions $\langle\boldsymbol{\varepsilon}\rangle$, transformation strain field $\boldsymbol{\varepsilon}^t$ and elastic properties $\boldsymbol{\mathcal{C}}$. Calculation of the internal stress field $\boldsymbol{\tau}$ may be performed using Green function techniques (Kröner, 1989; Berveiller and Zaoui, 1984). The classical equations of the problem

$$\begin{aligned} \boldsymbol{\sigma} &= \boldsymbol{\mathcal{C}}(\boldsymbol{\varepsilon} - \boldsymbol{\varepsilon}^t) \\ \mathrm{div}\boldsymbol{\sigma} &= \mathbf{0} \\ \mathbf{u} &= \langle\boldsymbol{\varepsilon}\rangle\mathbf{x} \quad \text{on} \quad \partial V \end{aligned} \tag{5.9}$$

are solved by

$$\boldsymbol{\varepsilon}(\mathbf{x}) = \langle \boldsymbol{\varepsilon} \rangle + \int_V \boldsymbol{\Gamma}(\mathbf{x} - \mathbf{x}') \boldsymbol{\mathcal{C}} (\boldsymbol{\varepsilon}^t(\mathbf{x}') - \langle \boldsymbol{\varepsilon}^t \rangle) dV, \tag{5.10}$$

where the modified, 4th order tensor, Green's function $\boldsymbol{\Gamma}$ is related to the displacement Green function tensor $\mathbf{G}$ by

$$\boldsymbol{\Gamma} = \frac{1}{2}(\nabla(\nabla \mathbf{G}) + \nabla(\nabla \mathbf{G}^T)), \tag{5.11}$$

The application of equation (4.23) to elementary inclusion-matrix problems leads to the famous Eshelby (1961) and Kröner (1961) solutions. For a single martensitic ellipsoidal domain, the transformation strain field $\boldsymbol{\varepsilon}^t$ is given by

$$\boldsymbol{\varepsilon}^t(\mathbf{x}) = \boldsymbol{\varepsilon}^{tn} \theta_n(\mathbf{x}), \tag{5.12}$$

where $\boldsymbol{\varepsilon}^{tn}$ is the uniform stress-free strain inside V_n, and $\theta_n(\mathbf{x})$ is the indicator function of V_n. In that case, $\boldsymbol{\varepsilon} = \boldsymbol{\varepsilon}^n$ is uniform inside the inclusion and given by

$$\boldsymbol{\varepsilon}^n = \langle \boldsymbol{\varepsilon} \rangle + \mathbf{S}^E \boldsymbol{\varepsilon}^{tn}, \tag{5.13}$$

and

$$\boldsymbol{\sigma}^n = \langle \boldsymbol{\sigma} \rangle - \boldsymbol{\mathcal{C}}(\mathbf{I} - \mathbf{S}^E) \boldsymbol{\varepsilon}^{tn}, \tag{5.14}$$

where $\mathbf{S}^E$ is the Eshelby tensor. Elastic energy W is given by

$$W = \frac{1}{2}(\langle \boldsymbol{\varepsilon} \rangle - \langle \boldsymbol{\varepsilon}^t \rangle) : \boldsymbol{\mathcal{C}}(\langle \boldsymbol{\varepsilon} \rangle - \langle \boldsymbol{\varepsilon}^t \rangle) + \frac{1}{2} \frac{V_n}{V} \boldsymbol{\varepsilon}^{tn} : \boldsymbol{\mathcal{C}}(\mathbf{I} - \mathbf{S}^E) \boldsymbol{\varepsilon}^{tn}. \tag{5.15}$$

Here we note that W depends on $\langle \boldsymbol{\varepsilon} \rangle$ and $\boldsymbol{\varepsilon}^{tn}$, but also on the volume V_n and the morphology of the transformed region. For a non-dilute concentration of transformed domains ($n = 1, \ldots, N$) with volume V_n and transformation strain $\boldsymbol{\varepsilon}^{tn}$, elastic interactions between domains contribute also to the elastic energy W. To illustrate this points, the method initially proposed by Kröner (1961) and developed by Mori and Tanaka (1973) is used to model these interactions. A single domain with Eshelby tensor $\mathbf{S}^E$ and transformation strain $\boldsymbol{\varepsilon}^{tn}$ can be considered an Eshelby inclusion with the stresses $\boldsymbol{\sigma}^A$ inside the matrix (austenite) as long-range stresses. Thus

$$\boldsymbol{\sigma}^n = \boldsymbol{\sigma}^A - \boldsymbol{\mathcal{C}}(\mathbf{I} - \mathbf{S}^E) \boldsymbol{\varepsilon}^{tn}. \tag{5.16}$$

From the equilibrium conditions

$$\langle \boldsymbol{\sigma} \rangle = (1 - f) \boldsymbol{\sigma}^A + \sum_{n=1}^{N} f^n \boldsymbol{\sigma}^n, \tag{5.17}$$

one gets

$$\boldsymbol{\sigma}^n = \langle \boldsymbol{\sigma} \rangle - \boldsymbol{\mathcal{C}}(\mathbf{I} - \mathbf{S}^E) \boldsymbol{\varepsilon}^{tn} + \sum_{m=1}^{N} f^m (\mathbf{I} - \mathbf{S}^{Em}) \boldsymbol{\varepsilon}^{tm}. \tag{5.18}$$

Considering the internal stresses $\boldsymbol{\tau}^n = \boldsymbol{\sigma}^n - \langle \boldsymbol{\sigma} \rangle$, the elastic energy is given by

$$\begin{aligned} W = & \frac{1}{2}(\langle \boldsymbol{\varepsilon} \rangle - \langle \boldsymbol{\varepsilon}^t \rangle) : \boldsymbol{\mathcal{C}}(\langle \boldsymbol{\varepsilon} \rangle - \langle \boldsymbol{\varepsilon}^t \rangle) + \frac{1}{2} \sum_{n=1}^{N} \boldsymbol{\varepsilon}^{tn} : \boldsymbol{\mathcal{C}}(\mathbf{I} - \mathbf{S}^{En}) \boldsymbol{\varepsilon}^{tn} f^n \\ & - \frac{1}{2} \sum_{n=1}^{N} \sum_{m=1}^{N} \boldsymbol{\varepsilon}^{tn} \boldsymbol{\mathcal{C}}(\mathbf{I} - \mathbf{S}^{Em}) \boldsymbol{\varepsilon}^{tm} f^n f^m \end{aligned} \tag{5.19}$$

and the interaction energy is defined as

$$\begin{aligned} W^{int} = & \frac{1}{2} \sum_{n=1}^{N} \boldsymbol{\varepsilon}^{tn} : \boldsymbol{\mathcal{C}}(\mathbf{I} - \mathbf{S}^{En}) \boldsymbol{\varepsilon}^{tn} f^n \\ & - \frac{1}{2} \sum_{n=1}^{N} \sum_{m=1}^{N} \boldsymbol{\varepsilon}^{tn} : \boldsymbol{\mathcal{C}}(\mathbf{I} - \mathbf{S}^{Em}) \boldsymbol{\varepsilon}^{tm} f^n f^m. \end{aligned} \tag{5.20}$$

The first term (proportional to f^n) is usually small compared with the second one (proportional to $f^n f^m$), which describes the interaction between the variants. We note that this description assumes some disorder for the spatial position in the variant, which is not necessarily observed in single crystals or in grains inside a polycrystal.

A more precise but rather complex estimation may be obtained using the discrete interactions tensor between two inclusions (Fehri et al., 1987). The internal stresses can be expressed by:

$$\boldsymbol{\tau}(\mathbf{x}) = \int_{V'} \boldsymbol{\Gamma}^{\sigma}(\mathbf{x}-\mathbf{x}')\boldsymbol{\varepsilon}^{t}(\mathbf{x}')dV', \tag{5.21}$$

where $\boldsymbol{\Gamma}^{\sigma}$ represents a modified stress Green function which can be easily derived from $\boldsymbol{\Gamma}$ and $\boldsymbol{\mathcal{C}}$ (Dederichs and Zeller, 1972). The internal stress part of the free energy (5.8)

$$W^{int} = -\frac{1}{2V}\int_{V} \boldsymbol{\tau}(\mathbf{x}) : \boldsymbol{\varepsilon}^{t}(\mathbf{x})dV \tag{5.22}$$

is now

$$W^{int} = -\frac{1}{2V}\int_{V}\int_{V'} \boldsymbol{\varepsilon}^{t}(\mathbf{x}) : \boldsymbol{\Gamma}^{\sigma}(\mathbf{x}-\mathbf{x}')\boldsymbol{\varepsilon}^{t}(\mathbf{x}')dV'dV. \tag{5.23}$$

Since $\boldsymbol{\varepsilon}^t$ is piecewise uniform, we get

$$\begin{aligned} W^{int} &= -\frac{1}{2V}\sum_{n=1}^{N}\sum_{m=1}^{N}\int_{V'}\int_{V} \boldsymbol{\varepsilon}^{tn}\theta_n(\mathbf{x}) : \boldsymbol{\Gamma}^{\sigma}(\mathbf{x}-\mathbf{x}')\boldsymbol{\varepsilon}^{tm}\theta_m(\mathbf{x}')dV'dV \\ &= \frac{1}{2}\sum_{n=1}^{N}\sum_{m=1}^{N} \boldsymbol{\varepsilon}^{tn} : \mathbf{T}^{nm}\boldsymbol{\varepsilon}^{tm}, \end{aligned} \tag{5.24}$$

where the interaction tensors $\mathbf{T}^{nm}$ given by

$$\mathbf{T}^{nm} = -\frac{1}{2V}\int_{V_n}\int_{V_m} \boldsymbol{\Gamma}^{\sigma}(\mathbf{x}-\mathbf{x}')dV'dV \tag{5.25}$$

depend on the volume, the shape and the orientation of V_n and V_m and on their relative position. This exact calculation of the interaction term W^{int} requires the spatial description of the transformation field, which greatly complicates the problem. Several approaches have been used for explicit calculation of this interaction energy term. Some researchers consider only one martensite variant (Lu and Weng, 1997; Vivet and Lexcellent, 1998). Patoor et al. (1994) and Siredey et al. (1999) have developed an interaction matrix technique. Huang and Brinson (1998) have derived the analytical solution for the case where several self-accommodating variants tend to decrease the free energy. As a general treatment in this section, the interaction energy will be denoted by W^{int}. Different explicit treatments from different groups will be given in detail in Section 5.5. In order to present the different approaches in a unified form we write the elastic energy as

$$W = \frac{1}{2}(\langle\boldsymbol{\varepsilon}\rangle - \langle\boldsymbol{\varepsilon}^{t}\rangle) : \boldsymbol{\mathcal{C}}(\langle\boldsymbol{\varepsilon}\rangle - \langle\boldsymbol{\varepsilon}^{t}\rangle) + W^{int}. \tag{5.26}$$

From equations (5.3) and (5.26), the Helmholtz free energy is defined to be

$$\Phi(\langle\boldsymbol{\varepsilon}\rangle, T, f^n) = \frac{1}{2}(\langle\boldsymbol{\varepsilon}\rangle - \langle\boldsymbol{\varepsilon}^{t}\rangle) : \boldsymbol{\mathcal{C}}(\langle\boldsymbol{\varepsilon}\rangle - \langle\boldsymbol{\varepsilon}^{t}\rangle) + W^{int} + B(T-T_0)f, \tag{5.27}$$

where $\langle\boldsymbol{\varepsilon}\rangle$ and T are the control variables and f^n are the internal variables describing the evolution of the microstructure for the RVE, assuming that the shape of the domains is given and B is a material constant. From kinematic equation (4.30) determined in Section 4.4.1, the mesoscopic (i.e., at the grain level) transformation strain $\langle\boldsymbol{\varepsilon}^t\rangle$ and the global amount of martensite f can be related to the volume fraction of each variant of martensite formed inside a grain:

$$\langle\boldsymbol{\varepsilon}^{t}\rangle = \sum_{n=1}^{N} \boldsymbol{\varepsilon}^{tn} f^n \quad \text{and} \quad f = \sum_{n=1}^{N} f^n. \tag{5.28}$$

The variables f^n must satisfy the natural physical constraints

$$f^n \geq 0 \quad \text{for each } n; \quad \sum_{n=1}^{N} f^n = f \leq 1. \tag{5.29}$$

Using the Legendre transformation $G = \Phi - \langle\boldsymbol{\sigma}\rangle : \langle\boldsymbol{\varepsilon}\rangle$, the complementary Gibbs free energy $G(\langle\boldsymbol{\sigma}\rangle, T, \boldsymbol{\varepsilon}^t)$ is given by

$$G(\langle\boldsymbol{\sigma}\rangle, T, \boldsymbol{\varepsilon}^t) = -\frac{1}{2}\langle\boldsymbol{\sigma}\rangle : \boldsymbol{\mathcal{S}}\langle\boldsymbol{\sigma}\rangle - \langle\boldsymbol{\sigma}\rangle : \langle\boldsymbol{\varepsilon}^t\rangle + W^{int} + B(T - T_0)f, \tag{5.30}$$

The physical constraints (5.29) are taken into account using the Kuhn-Tucker conditions in order to define the thermodynamical forces F^n (Kröner, 1989). From the $n+1$ conditions (5.29), additional $n+1$ Lagrange multipliers are associated. The multiplier associated to condition $f \leq 1$ is denoted by λ_0. This nonnegative quantity must satisfy the following property:

$$\lambda_0 \left(\sum_{n=1}^{N} f^n - 1 \right) = 0. \tag{5.31}$$

In the same way, the n multipliers λ_n associated with the n inequalities $f^n \geq 0$ must satisfy

$$\lambda_n \left(-f^n - 0\right) = 0 \quad \text{for each } n. \tag{5.32}$$

The Lagrangian L of the Gibbs free energy G is defined using conditions (5.31) and (5.32) as follows:

$$L(\langle\boldsymbol{\sigma}\rangle, T, f^n) = G(\langle\boldsymbol{\sigma}\rangle, T, f^n) + \lambda_0 \left(\sum_{n=1}^{N} f^n - 1 \right) + \lambda_n(-f^n - 0). \tag{5.33}$$

Partial derivatives of the Lagrangian (5.33) give the thermodynamical forces F^n acting on internal variables f^n:

$$F^n = -\frac{\partial L}{\partial f^n} = -\frac{\partial G}{\partial f^n} - \lambda_0 + \lambda_n. \tag{5.34}$$

Expression (5.30) for the complementary free energy leads to

$$F^n = \langle\boldsymbol{\sigma}\rangle\boldsymbol{\varepsilon}^{tn} - F_n^{int} - B(T - T_0) - \lambda_0 + \lambda_n, \tag{5.35}$$

where the interaction force F_n^{int} is determined from the partial derivative of W^{int} with respect to f^n.

Due to the existence of hysteresis phenomena, the knowledge of thermodynamical forces (cf. equation (5.35)) is not sufficient to derive the thermodynamical behavior associated with a stress-induced martensitic transformation. This study must be completed by the definition of a dissipative potential, which will be presented in Section 5.3.

5.2 Driving Forces for Martensitic Transformation and Reorientation

We find the intrinsic dissipation D of a system of volume V by comparing its free energy change $\dot{\Phi} = \frac{d\Phi}{dt}$ with the external power P_{ext}. For quasi-static evolutions and isothermal approximation, D is given by

$$D = P_{ext} - \dot{\Phi}. \tag{5.36}$$

Since the fields w and φ are discontinuous across the moving internal boundaries, the time derivative of Φ is given by

$$\dot{\Phi} = \frac{1}{V}\int_V \frac{\partial(w+\varphi)}{\partial t} dV - \frac{1}{V}\int_S [w+\varphi]\mathbf{w}\cdot\mathbf{n} dS, \tag{5.37}$$

where the same notations as in Section 4.4.2 are used. Since $\frac{\partial\varphi}{\partial t} = 0$ and $\frac{\partial\boldsymbol{\varepsilon}^t}{\partial t} = 0$, the first integral reduces to

$$\frac{1}{V}\int_V \frac{\partial(w+\varphi)}{\partial t} dV = \frac{1}{V}\int_V \boldsymbol{\sigma}\dot{\boldsymbol{\varepsilon}} dV. \tag{5.38}$$

From the results concerning φ, its jumps $[\varphi]$ across the moving boundaries are zero for martensite-martensite interfaces and equal to $\varphi_A - \varphi_M$ across martensite-austenite interfaces. This gives

$$\frac{1}{V}\int_S [\varphi]\mathbf{w}\cdot\mathbf{n}dS = \frac{1}{V}\int_S (\varphi_A - \varphi_M)\mathbf{w}\cdot\mathbf{n}dS, \tag{5.39}$$

and since $\varphi_A - \varphi_M$ is uniform along S,

$$\frac{1}{V}\int_S (\varphi_A - \varphi_M)\mathbf{w}\cdot\mathbf{n}dS = (\varphi_A - \varphi_M)\frac{1}{V}\int_S \mathbf{w}\cdot\mathbf{n}dS = (\varphi_A - \varphi_M)\dot{f}. \tag{5.40}$$

The jump $[w]$, defined by

$$[w] = \frac{1}{2}(\boldsymbol{\sigma}^+(\boldsymbol{\varepsilon}^+ - \boldsymbol{\varepsilon}^{t+}) - \boldsymbol{\sigma}^-(\boldsymbol{\varepsilon}^- - \boldsymbol{\varepsilon}^{t-})), \tag{5.41}$$

can be simplified assuming uniform elasticity and using the properties $\mathcal{C}_{ijkl} = \mathcal{C}_{klij}$. We then have

$$[w^e] = \frac{1}{2}(\boldsymbol{\sigma}^+ + \boldsymbol{\sigma}^-)[\boldsymbol{\varepsilon} - \boldsymbol{\varepsilon}^t]. \tag{5.42}$$

The change in free energy is now

$$\begin{aligned}\frac{d\Phi}{dt} =& \frac{1}{V}\int_V \boldsymbol{\sigma}\dot{\boldsymbol{\varepsilon}}dV - \frac{1}{V}\int_S \frac{1}{2}(\boldsymbol{\sigma}^+ + \boldsymbol{\sigma}^-)[\boldsymbol{\varepsilon} - \boldsymbol{\varepsilon}^t]\mathbf{w}\cdot\mathbf{n}dS \\ & - \frac{1}{V}\int_S (\varphi_A - \varphi_M)\mathbf{w}\cdot\mathbf{n}dS.\end{aligned} \tag{5.43}$$

The external power P_{ext} results from the boundary condition $\mathbf{t} = \boldsymbol{\sigma}\mathbf{n}$ on ∂V and the hypothesis of zero volume forces

$$VP_{ext} = \int_{\partial V} \boldsymbol{\sigma}\mathbf{n}\cdot\mathbf{v}dS, \tag{5.44}$$

where $\mathbf{v}$ is the velocity of particles at ∂V. Using the divergence theorem applied on a volume V containing moving discontinuity surfaces S, we get

$$VP_{ext} = \int_V \mathrm{div}(\boldsymbol{\sigma}\mathbf{v})dV + \int_S [\boldsymbol{\sigma}\mathbf{n}\cdot\mathbf{v}]dS. \tag{5.45}$$

At the moving surfaces S, the following relations result from the continuity conditions of $\boldsymbol{\sigma}$ and the displacement $\mathbf{u}$:

$$[\boldsymbol{\sigma}]\mathbf{n} = 0 \quad \text{and} \quad [\mathbf{u}] = 0, \tag{5.46}$$

and the Hadamard (1903) conditions on the jump of the particle velocity across the interface $[\mathbf{v}]$

$$[\mathbf{v}] = -[\nabla\mathbf{u}]\mathbf{n}(\mathbf{w}\cdot\mathbf{n}). \tag{5.47}$$

From equations (5.45), (5.46), and (5.47) the external power is given by

$$VP_{ext} = \int_V \boldsymbol{\sigma}\dot{\boldsymbol{\varepsilon}}dV - \frac{1}{2}\int_S (\boldsymbol{\sigma}^+ + \boldsymbol{\sigma}^-)[\boldsymbol{\varepsilon}]\mathbf{w}\cdot\mathbf{n}dS. \tag{5.48}$$

Finally, the dissipation follows from equations (5.36), (5.43) and (5.48):

$$D = \frac{1}{V}\int_S \left(-\frac{1}{2}(\boldsymbol{\sigma}^+ + \boldsymbol{\sigma}^-)[\boldsymbol{\varepsilon}^t] + [\varphi]\right)\mathbf{w}\cdot\mathbf{n}dS. \tag{5.49}$$

The term

$$F \equiv -\frac{1}{2}(\boldsymbol{\sigma}^+ + \boldsymbol{\sigma}^-)[\boldsymbol{\varepsilon}^t] + [\varphi] \tag{5.50}$$

is defined as the driving force for interface motion (Eshelby, 1961).

In the case of a thermodynamically reversible system, one has to find the transformation field (active variant, position of interfaces) for which $F = 0$ on each part of S. If internal stresses are neglected and a single variant with transformation strain $\boldsymbol{\varepsilon}^t$ is assumed, the driving force reduces to

$$F = -\langle\boldsymbol{\sigma}\rangle\boldsymbol{\varepsilon}^t + (\varphi_A - \varphi_M). \tag{5.51}$$

At equilibrium, the condition

$$\langle\boldsymbol{\sigma}\rangle\boldsymbol{\varepsilon}^t = B(T - T_0) \tag{5.52}$$

gives the relation between applied stress $\langle\boldsymbol{\sigma}\rangle$ and temperature T for which austenite and martensite are in equilibrium. Equation (5.52) generalizes the famous uniaxial criterion of Patel and Cohen (1953).

5.3 Dissipative Potential and Local Transformation Criteria

Hysteresis is an important phenomenon in shape memory alloys. It is linked to dissipation processes occurring during the martensitic transformation, which can be described by a dissipative potential W^d.

Evolution of this potential must obey the second law of thermodynamics. Combined use of this fundamental law with the energy balance gives

$$\dot{G}\Big|_{\langle\boldsymbol{\sigma}\rangle T} = W^d \geq 0. \tag{5.53}$$

As for the case of plasticity, we suppose that the thermodynamical driving force F^n must reach a critical value denoted by F_c^n to produce growth (or shrinkage) of a variant. This critical value is a function of the microstructural state of the material. As for the thermodynamical potential, it is assumed that these aspects can be described using internal variables f^n only. We then write

$$F_c^n = F_c^n(f^m). \tag{5.54}$$

This gives the following transformation conditions:

$$\text{if } F^n < F_c^n \text{ then } \dot{f}^n = 0 \text{ for all } \dot{F}_c^n \tag{5.55a}$$

$$\text{if } F^n = F_c^n \text{ and } \dot{F}_c^n = 0 \text{ then } \dot{f}^n = 0 \tag{5.55b}$$

$$\text{if } F^n = F_c^n \text{ and } \dot{F}_c^n = \dot{F}^n \text{ then } \dot{f}^n \neq 0 \tag{5.55c}$$

This problem is simplified if we assume that the resistive forces F_c^n are positive material constants and are identical for all variants. In this case, F_c^n reduces to F_c for each n. This hypothesis implicitly considers the dissipative potential to be a function that is proportional to the cumulative martensitic volume fraction f_{cu} (Sun et al., 1991):

$$W^d = F_c \int_0^t |df| = F_c f_{cu}. \tag{5.56}$$

Application of inequality (5.53) produces different transformation conditions for forward and reverse transitions. Austenite-to-martensite transition occurs when

$$\sum_n F^n \dot{f}^n = F_c \dot{f}, \tag{5.57}$$

and the reverse transformation occurs when

$$\sum_n F^n \dot{f}^n = -F_c \dot{f}. \tag{5.58}$$

Assuming that the dissipation occurs without coupling effects between variants, equations (5.57) and (5.58) give

$$\begin{aligned} F^n \dot{f}^n &= F_c \dot{f}^n \quad \text{for the forward transformation,} \\ F^n \dot{f}^n &= -F_c \dot{f}^n \quad \text{for the reverse transformation.} \end{aligned} \tag{5.59}$$

This analysis lets us define local criteria. A volume of austenite transforms to a given variant of martensite when

$$\langle \boldsymbol{\sigma} \rangle \boldsymbol{\varepsilon}^{tn} - F^{int} - B(T - T_0) - \lambda_0 + \lambda_n = F_c. \tag{5.60}$$

Nevertheless, this transformation will only be possible if conditions (5.31) and (5.32) are satisfied, which forces the Lagrange multipliers to satisfy

$$\lambda_n = -\langle \boldsymbol{\sigma} \rangle \boldsymbol{\varepsilon}^{tn} + F^{int} + B(T - T_0) + \lambda_0 + F_c \geq 0 \tag{5.61a}$$

$$\lambda_0 = \langle \boldsymbol{\sigma} \rangle \boldsymbol{\varepsilon}^{tn} - F^{int} - B(T - T_0) + \lambda_0 - F_c \geq 0. \tag{5.61b}$$

If the volume fraction for a variant reaches one or if the global volume fraction reaches this threshold value, applying constraints (5.61) limits the transformation, even when condition (5.60) is satisfied. These restrictions constitute a major difference from the modeling of plastic behavior by movement of dislocations.

The reverse transformation happens when the following condition is satisfied:

$$\langle \boldsymbol{\sigma} \rangle \boldsymbol{\varepsilon}^{tn} - F^{int} - B(T - T_0) - \lambda_0 + \lambda_n = -F_c. \tag{5.62}$$

In this case, the Lagrange multipliers λ_0 and λ_n must satisfy

$$\lambda_n = -\langle \boldsymbol{\sigma} \rangle \boldsymbol{\varepsilon}^{tn} + F^{int} + B(T - T_0) + \lambda_0 - F_c \geq 0 \tag{5.63a}$$

$$\lambda_0 = \langle \boldsymbol{\sigma} \rangle \boldsymbol{\varepsilon}^{tn} - F^{int} - B(T - T_0) + \lambda_0 + F_c \geq 0. \tag{5.63b}$$

Constraints (5.63) verify that enough martensite remains for the reverse transformation to occur. Conditions (5.60)–(5.63) constitute the local criteria for thermoelastic martensitic transformation.

5.4 Constitutive Equations

If conditions (5.60) and (5.61) (respectively, (5.62) and (5.63)) are satisfied, using the coherency relationship (5.55c) lets us determine the evolution of the transformation rates $\dot{f}^n$ for each variant:

$$\dot{F}^n = \frac{\partial \dot{F}^n}{\partial \langle \boldsymbol{\sigma} \rangle} : \langle \dot{\boldsymbol{\sigma}} \rangle - \frac{\partial \dot{F}^n}{\partial T} \dot{T} + \sum_{m=1}^{N} \frac{\partial \dot{F}^n}{\partial f^m} \dot{f}^m = \dot{F}_c = 0. \tag{5.64}$$

Substituting driving force (5.35) in equation (5.64) gives

$$\boldsymbol{\varepsilon}^{tn} : \langle \dot{\boldsymbol{\sigma}} \rangle - B\dot{T} - \sum F_n^{int} \dot{f}_n = 0. \tag{5.65}$$

Resolution of equation (5.65) gives the evolution of $\dot{f}^n$ with the loading parameters $\langle \dot{\boldsymbol{\sigma}} \rangle$ and $\dot{T}$. This result and the kinematics equation (5.28) define the constitutive equation that describes the monocrystalline behavior:

$$\langle \dot{\boldsymbol{\varepsilon}} \rangle = \sum \boldsymbol{\varepsilon}^{tn} \dot{f}_n. \tag{5.66}$$

This equation characterizes the behavior of a unit volume crystal of parent phase undergoing a stress-induced martensitic transformation. Production of several variants of martensite is taken into account. This polyvariant transformation, though difficult to produce in monocrystals, really happens in the grains of polycrystalline materials. From this consideration, relationship (5.66) appears well-suited to describe the local behavior at the grain level in a scale transition approach.

The different material parameters included in relationship (5.65) can be determined. The coefficient B related to the chemical energy can be evaluated for monocrystals from tensile tests performed at different temperatures (Patoor et al., 1988). If we denote the applied stress by $\langle \sigma_{33} \rangle$, condition (5.62) gives us the following for a purely austenitic state:

$$\varepsilon_{33}^{tn} \langle \sigma_{33} \rangle = B(T - T_0) + F_c. \tag{5.67}$$

This result is similar to that obtained using the well-known Patel and Cohen (1953) criterion. For characteristic temperatures M_s and A_f, the material is in a fully parent-phase state ($f^m = 0$ for each variant m). Consequently, the Lagrange multipliers λ_n and λ_0 both equal zero, which lets us write

$$M_s = T_0 - \frac{F_c}{B} \quad \text{and} \quad A_f = T_0 + \frac{F_c}{B}. \tag{5.68}$$

As a result, these two temperatures are intrinsic parameters. They can be used to obtain an evaluation of the T_0 temperature and to determine the critical force F_c.

5.5 Interaction Energy in Single Crystals

In this section we will survey several different ways in which to estimate the interaction energy in single crystals. Consider a reference austenitic crystal of volume V bounded by a surface ∂V. For a temperature T larger than T_0, a transformation strain field $\boldsymbol{\varepsilon}^t(\mathbf{x})$ is induced by applying surface forces $\mathbf{T} = \langle\boldsymbol{\sigma}\rangle\mathbf{n}$ on the boundary ∂V. From the thermodynamical study presented in the previous section, complementary free energy G per unit volume is expressed as (cf. equation (5.30)):

$$G(\langle\boldsymbol{\sigma}\rangle, T, \boldsymbol{\varepsilon}^t) = \frac{1}{2}\langle\boldsymbol{\sigma}\rangle : \boldsymbol{\mathcal{S}}\langle\boldsymbol{\sigma}\rangle + \langle\boldsymbol{\sigma}\rangle\langle\boldsymbol{\varepsilon}^t\rangle + \frac{1}{2V}\int_V \boldsymbol{\tau} : \boldsymbol{\varepsilon}^t dV - B(T - T_0)f. \tag{5.69}$$

As shown in the Section 5.1, the free energy plays a fundamental role in the behavior. Energy W^{int} is a complex function of the transformation strain field $\boldsymbol{\varepsilon}^t(\mathbf{x})$. Its contribution is closely linked to the microstructure of the martensitic phase and cannot be reduced easily to a simple expression of f^n. According to equation (5.22), this contribution is defined as

$$W^{int} = -\frac{1}{2V}\int_V \boldsymbol{\tau} : \boldsymbol{\varepsilon}^t dV. \tag{5.70}$$

It is from this point that many different micromechanical models will diverge. The divergence stems from two fundamental issues. One is how many active variants are considered in a single grain, i.e., a single active variant vs. multiple active variants. The other is how many variants are considered in one inclusion. The models by Lu and Weng (1997) and Vivet and Lexcellent (1998) consider only one active variant and are described in Section 5.5.2. Other models such as (Huang and Brinson, 1998; Gao and Brinson, 2002) consider several self-accommodating variants together as an inclusion and are presented in Sections 5.5.1 and 5.5.4. The last group of models considered is by Patoor et al. (1994, 1996) who treat the martensitic variants inside a domain in a different way. The details of the last two works are given in Section 5.5.3.

5.5.1 Simplified Multivariant Formulation

In the simplified multivariant model Gao and Brinson (2002) simply remove the micromechanics calculation of the interaction energy entirely, lumping any energy barrier due to incompatibilities of the transformation strain with respect to the surrounding material into a constant resistance force F^C. The simplification is justified by experiments showing that martensite variants tend to form large plates most of which have an invariant plane interface with the austenite and reach the grain boundary (Figure 17). Consider Figure 17(a) which shows several thermally induced martensitic habit plane variants in a CuAlNi single crystal. The martensite plates are not only large in size but also often span the specimen. This phenomenon is also common for stress induced martensite plates and Figures 17(b)–(c) show typical examples. Since the habit plane is an invariant plane, the stress and strain fields of the austenitic phase around the martensite plate are not disturbed by the transformation strain of the martensite plate. In most cases, the stress-induced martensite forms with a sharp habit plane with no distortion due to a finely twinned substructure in the habit plane variant. Hence the incompatibility of the stress-induced variant is indeed quite small and the assumption may be justified. An examples is the formation of CuAlNi$\gamma_1'(2H)$ phase from austenite.

Removing the interaction energy simplify the calculations and therefore significantly decrease computational time. Eliminating the interaction energy removes much of the explicit grouping structure from the model but the transformation strains are still calculated based on crystallographic parameters for habit plane

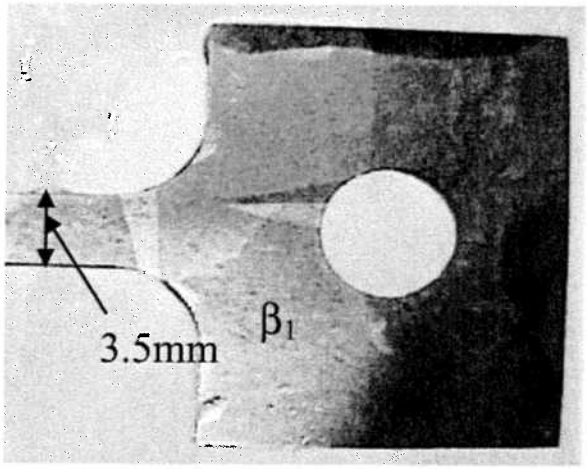

(a)

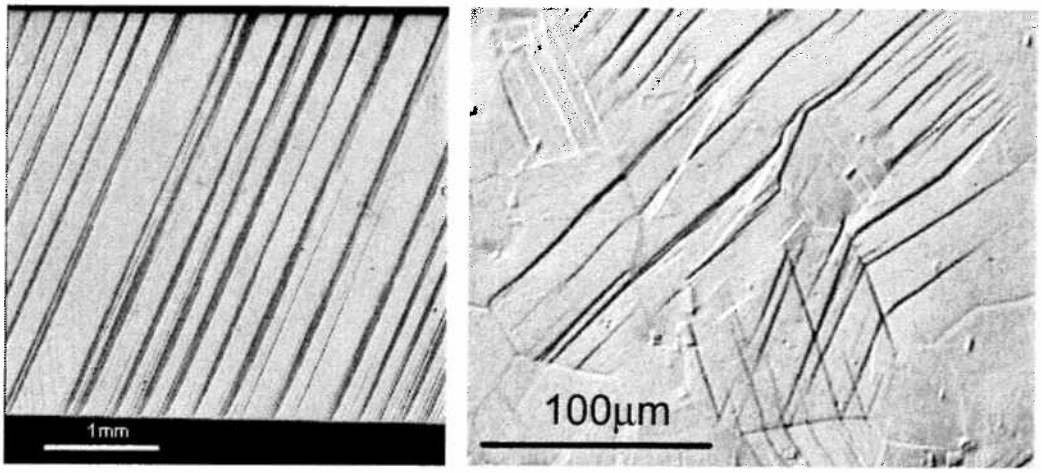

(b) (c)

Figure 17: Temperature-induced martensite (a) and stress-induced martensite (b)–(c). (a) In a single CuAlNi crystal: two martensite plates are seen, one toward the end of the narrow section and the other near the hole. Each martensite plate is composed of two HPVs; (b) single CuAlNi crystal (3.5 mm wide) under uniaxial tension showing evenly spaced martensitic plates spanning the specimen, strain rate 10^{-4} s^{-1} used, and (c) NiTi polycrystal under uniaxial tension, where martensitic plates are seen to typically span the entire width of the grains.

variants [cf. equation (4.5)]. This equation is appropriate for materials such as CuZnAl with stacking faults acting as the invariant plane shear prior to de-faulting (Miyazaki et al., 1984). It is also appropriate for materials such as γ_1' CuAlNi, and B19' NiTi with internally twinned structure before detwinning of correspondence variants occurs. With further increases in load, reorientation or conversion among correspondence variants can happen for the thermally induced case). Ongoing work to address these issues includes examining the stress induced detwinning/de-faulting and conversion process both experimentally by *in situ* SEM and numerically by including a subgrouping scheme for correspondence variants and direct calculation of their transformation strains, using an approach similar to that pursued recently by Govindjee and Miehe (2001). However, some recent results have shown that a non-invariant plane relative to the austenite (Sun et al., 1997, 1999) is possible, accompanied by a finite amount of distortion of the material around the interface. In such cases, (for example, β to β_1' in CuAlNi alloy) a different calculation of the interaction energy due to the distorted region around the interface would be appropriate. Future work should investigate this possibility and its influence on SMA models. For results the reader is referred to the work of Gao (2002)

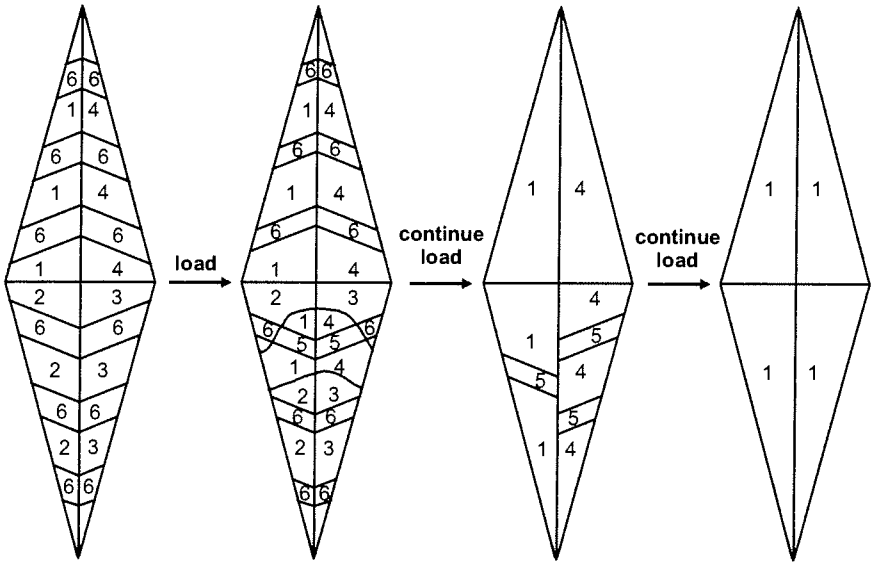

Figure 18: Conversion process during loading of a thermally induced 2H (γ_1') SMA material at low temperature. Note that the final product after loading is not a single habit plane variant, but a correspondence variant (a detwinned habit plane variant). After work by Saburi and Nenno (1981) where some information about the intermediate products are known, however the details of the loading and specimen orientation are not given.

5.5.2 Single Variant Formulation

Although there are many (usually 24) crystallographically equivalent habit plane variants in a shape memory alloy, it is experimentally reasonable to consider only one active variant for approximation. This also leads to simpler implementation. It is quite often observed that during a single crystal tensile experiment, only one variant forms (see Figures 17(b)). This is also true for polycrystal tensile test, i.e., only one variant inside a grain activates (see Figure 17(c)). Based on this observation and considering the complexity of equation (5.20), some researchers begin modeling by assuming only one active martensite variant per grain and using the therefore much simplified version of equation (5.20):

$$W^{int} = \frac{1}{2}\boldsymbol{\varepsilon}^t : \boldsymbol{\mathcal{C}}(\mathbf{I} - \mathbf{S}^E)\boldsymbol{\varepsilon}^t f - \frac{1}{2}\boldsymbol{\varepsilon}^t : \boldsymbol{\mathcal{C}}(\mathbf{I} - \mathbf{S}^E)\boldsymbol{\varepsilon}^t f^2, \tag{5.71}$$

where f is the volume fraction of the martensite plate. After collecting terms the interaction energy becomes

$$W^{int} = \frac{1}{2}f(1-f)\boldsymbol{\varepsilon}^t : \boldsymbol{\mathcal{C}}(\mathbf{I} - \mathbf{S}^E)\boldsymbol{\varepsilon}^t. \tag{5.72}$$

The interaction force, defined as the gradient of the interaction energy with respect to f is given by (see Table 2):

$$F^{int} = -\frac{1}{2}(1-2f)\boldsymbol{\varepsilon}^t : \mathcal{C}(\mathbf{I} - \mathbf{S}^E)\boldsymbol{\varepsilon}^t. \tag{5.73}$$

Lu and Weng (1997) used equation (5.72) to represent the interaction energy. In addition, instead of using a constant transformation resistance (as seen in Patoor's and Brinson's works, shown in later sections), they considered the surface energy created by the parent-martensite interface as well as a non-linear energy dissipation (associated with interfacial friction and twinning motion) that depends on the volume fraction of martensite. A linear dependence of entropy on temperature was also used during phase transformation instead of assuming constant entropy.

Vivet and Lexcellent (1998) also used equation (5.72) for their interaction energy between a single martensite variant and the parent phase although they also presented a general expression considering all variants. Similar to Lu and Weng (1997), they considered surface energy as well as a non-linear energy dissipation depending on two volume fractions, i.e., the current and the one just before the sign change of the loading rate.

5.5.3 Interfacial Operator Technique

In this section an alternate approach to develop the interaction energy (5.70) is developed that does not rely on an inclusion approach. Here both topological and morphological considerations in the growth process of martensite inside grains of a polycrystal are used to evaluate W^{int}. It is observed that the increase of the volume fraction for a given variant is mainly produced by the growth of new plates in a limited region of the grain (see Figure 10). From this observation, and considering that internal stresses arise mainly from the martensite/martensite interactions, a "cluster" description (Patoor et al., 1996) is used for the microstructure (Figure 19). Denote by V_n the domain partially filled by a variant n, and by v_n^M the volume constituted by the plates of martensite. The volume fraction f^n for a variant n is then defined by

$$f^n = \frac{v_n^M}{V} \quad \text{with} \quad \boldsymbol{\varepsilon}^t(\mathbf{x}) = \boldsymbol{\varepsilon}^{tn} \quad \text{when} \quad \mathbf{x} \in v_n^M. \tag{5.74}$$

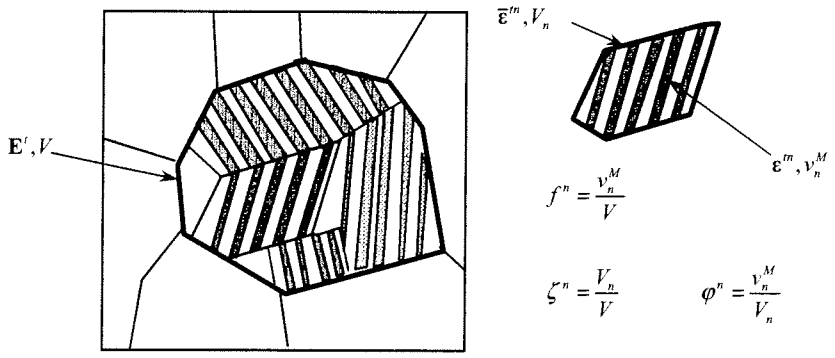

Figure 19: Application of a cluster type description to represent the microstructural aspects inside a grain of the polycrystalline material (Patoor et al., 1996).

Note that $\zeta^n = \frac{V_n}{V}$ is the volume fraction of the domain filled by variant n inside the grain. The amount of martensite inside V_n is characterized by the parameter $\varphi^n = \frac{v_n^M}{V_n}$. The quantities f^n, φ^n and ζ^n are linked by

$$f^n = \frac{v_n^M}{V} = \frac{v_n^M}{V_n}\frac{V_n}{V} = \varphi^n \zeta^n. \tag{5.75}$$

The mean transformation strain $\bar{\boldsymbol{\varepsilon}}^{tn}$ over a domain V_n is defined as

$$\bar{\boldsymbol{\varepsilon}}^{tn} = \frac{1}{V_n}\int_{V_n} \boldsymbol{\varepsilon}^t dV = \boldsymbol{\varepsilon}^{tn}\frac{v_M^n}{V_n} = \boldsymbol{\varepsilon}^{tn}\varphi^n. \tag{5.76}$$

The transformation strain field $\boldsymbol{\varepsilon}^t(\mathbf{x})$ is considered to be piecewise uniform. Inside each volume V_n, a uniform transformation strain $\bar{\boldsymbol{\varepsilon}}^{tn}$ is defined. Interaction energy (5.70) is then expressed as

$$W^{int} = -\frac{1}{2V}\int_V \boldsymbol{\tau} : \boldsymbol{\varepsilon}^t dV = -\frac{1}{2V}\sum_{n=1}^{N} \bar{\boldsymbol{\tau}}^n : \bar{\boldsymbol{\varepsilon}}^{tn} V_n, \tag{5.77}$$

where $\bar{\boldsymbol{\tau}}^n$ denotes the internal stress over domain V_n. Siredey et al. (1999) proposed to evaluate this energy using interface operator techniques because the stress field fluctuates weakly inside domains but suffers jumps across domain interfaces. These interfaces are very mobile, so neglecting the dissipation associated with this motion, an adequate set of internal variables should be determined to minimize this energy.

The internal stress $\bar{\boldsymbol{\tau}}^n$ is related to the jump of the transformation strain across the interface between domains labeled n and m with a normal N^{nm} using the following interface operator $\mathbf{Q}^{nm}$:

$$\bar{\boldsymbol{\tau}}^n = \bar{\boldsymbol{\tau}}^m - \mathbf{Q}^{nm} : \left(\bar{\boldsymbol{\varepsilon}}^{tn} - \bar{\boldsymbol{\varepsilon}}^{tm}\right), \tag{5.78}$$

where the operator $\mathbf{Q}^{nm}$ has the following properties:

$$\mathbf{Q}^{nm}(\mathbf{N}) = \mathbf{Q}^{nm}(-\mathbf{N}), \quad Q^{nm}_{ijkl} = Q^{nm}_{klij}. \tag{5.79}$$

An explicit form of interface operator for an isotropic elastic material behavior is given by

$$Q_{ijkl} = 2\mu\left(F_{ijkl} + \frac{\lambda}{\lambda + 2\mu}\left(\delta_{ij} - N_i N_j\right)\left(\delta_{kl} - N_k N_l\right)\right), \tag{5.80}$$

where F_{ijkl} is given by

$$F_{ijkl} = \frac{1}{2}\left(\delta_{ik} - N_i N_k\right)\left(\delta_{jl} - N_j N_l\right) + \frac{1}{2}\left(\delta_{jk} - N_j N_k\right)\left(\delta_{il} - N_i N_l\right), \tag{5.81}$$

and μ and λ are the Lamé constants.

Using equation (5.78) the expression for the interaction energy for two variants n and m becomes

$$W^{int} = \frac{1}{2} f^n f^m \frac{1}{a_n a_m}\left(a_m \bar{\boldsymbol{\varepsilon}}^{tn} - a_n \bar{\boldsymbol{\varepsilon}}^{tm}\right) : \mathbf{Q}^{nm} : \left(a_m \bar{\boldsymbol{\varepsilon}}^{tn} - a_n \bar{\boldsymbol{\varepsilon}}^{tm}\right) = \frac{1}{2} f^n f^m H^{mn}, \tag{5.82}$$

where the interaction matrix H^{mn} is defined as

$$H^{mn} = \frac{1}{a_n a_m}\left(a_m \bar{\boldsymbol{\varepsilon}}^{tn} - a_n \bar{\boldsymbol{\varepsilon}}^{tm}\right) : \mathbf{Q}^{nm} : \left(a_m \bar{\boldsymbol{\varepsilon}}^{tn} - a_n \bar{\boldsymbol{\varepsilon}}^{tm}\right), \tag{5.83}$$

and the quantity a_n is defined as

$$a_n = \sqrt{\bar{\boldsymbol{\varepsilon}}^{tn} : \mathbf{Q}^{nm} : \bar{\boldsymbol{\varepsilon}}^{tn}}. \tag{5.84}$$

The interaction energy given by equation (5.82) depends only on the following material parameters: elastic constants μ and λ, transformation strains $\bar{\boldsymbol{\varepsilon}}^{tn}$ and $\bar{\boldsymbol{\varepsilon}}^{tm}$ and the normal vector $\mathbf{N}^{nm}$ of the interface between the domains n and m. The interaction energy has to be minimized with respect to the orientation of the interface for two given variants n and m.

In the case where more than two variants are activated it is assumed that the interaction energy can still be described by the same type of relation so that

$$W^{int} = \frac{1}{2}\sum_{n,m} H^{nm} f^n f^m. \tag{5.85}$$

It is necessary to note that the different assumptions used to determine the interaction matrix limit its utilization to stress-induced transformations (superelasticity and two-way shape memory). Among these limitations, the number of variants present in a grain has to remain weak. By consequence, in a fully thermally-induced martensitic state where different self-accommodated groups coexist the use of this matrix gives a considerable overestimation of the elastic energy associated to this configuration. An extension of this work for the martensitic state was recently proposed by Niclaeys et al. (2002).

5.5.4 Multivariant Formulation

From a micromechanical perspective, a straightforward formulation to consider interactions between all variants, i.e., a multivariant model, is to treat every martensite variant as an inclusion. The simplest calculations with this assumption is one where all martensite variants in a single crystal experience the same averaged stress. If there are N crystallographically equivalent martensite variants then the interaction energy is the same as equation (5.20). One can derive interaction forces and perform simulations very easily starting from here. However, not much usage of this approach is found in the literature because the resulting interaction energy (therefore the interaction forces) is too high, preventing reasonable simulations. In what follows, we will first summarize the treatment by Huang and Brinson (1998) in which each inclusion is considered as a self-accommodating group of variants. Therefore treating each variant as an inclusion is only a special case, i.e., there is only one variant in a self-accommodating group. At the end of this section, we will verify that equation (5.20) can be derived from Huang and Brinson (1998) general treatment.

The work by Huang and Brinson (1998) considered that the martensitic variants tend to form in self-accommodated groups of compatible variants in order to minimize the energy of their formation. In Figure 20, a self-accommodating group is depicted with a diamond shape (Saburi and Wayman, 1979); it is noted that parallelogram (Murakami et al., 1994) and triangular shapes (Miyazaki et al., 1989a,b) have also been proposed for various SMAs. Using this key concept, the interaction energy is approximated as a sum over G groups of V self-accommodating variants each ($G \cdot V = N$). Equation (5.22) turns:

$$W^{int} = -\frac{1}{2}\sum_{g=1}^{G} \langle \boldsymbol{\sigma} \rangle^g : \bar{\boldsymbol{\varepsilon}}^g \bar{f}^g, \tag{5.86}$$

where $\langle \boldsymbol{\sigma} \rangle^g$ is the average stress in an inclusion of group g and $\bar{\boldsymbol{\varepsilon}}^g$ and $\bar{f}^g$ are the average transformation strain of group g and the total volume fraction of group g respectively:

$$\bar{\boldsymbol{\varepsilon}}^g = \frac{1}{\bar{f}^g}\left(\sum_{n=1}^{V} f^{(g,n)} \boldsymbol{\varepsilon}^{(g,n)}\right), \tag{5.87}$$

$$\bar{f}^g = \sum_{n=1}^{V} f^{(g,n)}. \tag{5.88}$$

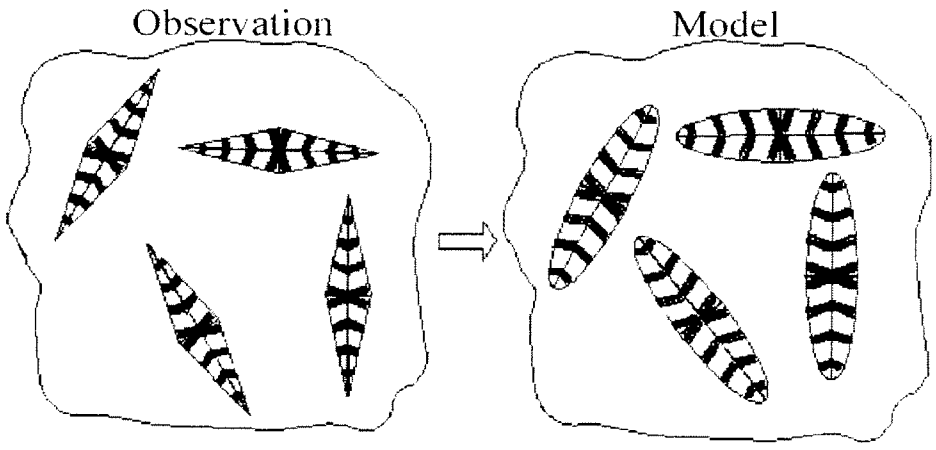

Figure 20: Growth of self accommodated martensitic variants in the parent phase: the experimentally observed (Saburi and Wayman, 1979) diamond shaped variants (left) are modeled by penny shaped inclusions (right) for which analytical results are available (Gao et al., 2000).

Here the superscript (g,n) represents the nth variant in the gth self-accommodating group. Equation (5.86) can be shown (see, for example, Huang and Brinson (1998)) to reduce to

$$W^{int} = -\frac{1}{2}\sum_{g=1}^{G} \bar{\boldsymbol{\varepsilon}}^g : \left[\hat{\boldsymbol{\sigma}}^g - \sum_{m=1}^{G} \bar{f}^m \hat{\boldsymbol{\sigma}}^m\right] \bar{f}^g, \tag{5.89}$$

where

$$\hat{\boldsymbol{\sigma}}^g = \mathbf{C}(\mathbf{S}^g \bar{\boldsymbol{\varepsilon}}^g - \bar{\boldsymbol{\varepsilon}}^g) \tag{5.90}$$

and $\mathbf{S}^g$ is the Eshelby tensor of group g. The equivalence of equations (5.89) or (5.86) to equation (5.20) in absence of self-accommodating groups will be shown at the end of this section. Equation (5.90) can be rewritten as

$$\hat{\boldsymbol{\sigma}}^g = \mathbf{C}(\mathbf{S}^g - \mathbf{I})\bar{\boldsymbol{\varepsilon}}^g = \mathbf{M}^g \bar{\boldsymbol{\varepsilon}}^g, \tag{5.91}$$

where

$$\mathbf{M}^g = \mathbf{C}(\mathbf{S}^g - \mathbf{I}). \tag{5.92}$$

The interaction energy (5.89) can now be rewritten as

$$W^{int} = -\frac{1}{2}\sum_{g=1}^{G} \bar{\boldsymbol{\varepsilon}}^g : \left[\mathbf{M}^g \bar{\boldsymbol{\varepsilon}}^g - \sum_{m=1}^{G} \bar{f}^m \mathbf{M}^m \bar{\boldsymbol{\varepsilon}}^m\right] \bar{f}^g. \tag{5.93}$$

Note that $\mathbf{M}^g$ is a material property of group g depending only on the elastic constant and Eshelby tensor of group g. Using equation (5.87), the interaction energy (5.93) can be rewritten as

$$\begin{aligned} W^{int} = -\frac{1}{2}\sum_{g=1}^{G} \Bigg[& \frac{1}{\bar{f}^g} \sum_{u=1}^{V}\sum_{v=1}^{V} f^{(g,v)} f^{(g,u)} \boldsymbol{\varepsilon}^{(g,u)} : \mathbf{M}^g \boldsymbol{\varepsilon}^{(g,v)} \\ & - \sum_{m=1}^{G}\sum_{u=1}^{V}\sum_{v=1}^{V} f^{(g,u)} f^{(m,v)} \boldsymbol{\varepsilon}^{(g,u)} : \mathbf{M}^m \boldsymbol{\varepsilon}^{(m,v)} \Bigg]. \end{aligned} \tag{5.94}$$

For computational efficiency, it is useful to define another material property, $J^{(g,u,m,v)}$, as

$$J^{(g,u,m,v)} = \boldsymbol{\varepsilon}^{(g,u)} : \mathbf{M}^m \boldsymbol{\varepsilon}^{(m,v)} \tag{5.95}$$

which depends on two sets of group and variant numbers, i.e. group g and variant u in group g as well as group m and variant v in group m. Note, $J^{(g,u,m,v)}$ is not equal to $J^{(m,v,g,u)}$ since the former uses the Eshelby tensor of group m only. With this notation the material properties are extracted into the J array, therefore accelerating the calculation of the interaction energy and interaction forces during numerical implementation.

As shown in (Huang and Brinson, 1998), the interaction force equation (5.35) can be shown to be

$$F^{int}_{(g,n)} = \frac{1}{2}\left[\boldsymbol{\varepsilon}^{(g,n)} : \left(\mathbf{M}^g + (\mathbf{M}^g)^T\right) - \bar{\boldsymbol{\varepsilon}}^g : \mathbf{M}^g\right] \bar{\boldsymbol{\varepsilon}}^g - \frac{1}{2}\boldsymbol{\varepsilon}^{(g,n)} : \sum_{p=1}^{G} \left[\left(\mathbf{M}^p + (\mathbf{M}^g)^T\right) \bar{\boldsymbol{\varepsilon}}^p \bar{f}^p\right] \tag{5.96}$$

and further as

$$\begin{aligned} F^{int}_{(g,n)} = & \frac{1}{2}\left[\boldsymbol{\varepsilon}^{(g,n)} : \left(\mathbf{M}^g + (\mathbf{M}^g)^T\right) - \frac{1}{\bar{f}^g}\left(\sum_{v=1}^{V} f^{(g,v)} \boldsymbol{\varepsilon}^{(g,v)}\right) : \mathbf{M}^g\right] \frac{1}{\bar{f}^g}\left(\sum_{u=1}^{V} f^{(g,u)} \boldsymbol{\varepsilon}^{(g,u)}\right) \\ & - \frac{1}{2}\boldsymbol{\varepsilon}^{(g,n)} : \sum_{m=1}^{G}\left[\left(\mathbf{M}^m + (\mathbf{M}^g)^T\right)\left(\sum_{v=1}^{V} f^{(m,v)} \boldsymbol{\varepsilon}^{(m,v)}\right)\right]. \end{aligned} \tag{5.97}$$

After rearrangements, the interaction force becomes

$$\begin{aligned} F^{int}_{(g,n)} = & \frac{1}{2}\sum_{u=1}^{V} \frac{f^{(g,u)}}{\bar{f}^g}\left[\boldsymbol{\varepsilon}^{(g,u)} : \left(\mathbf{M}^g + (\mathbf{M}^g)^T\right) \boldsymbol{\varepsilon}^{(g,n)} - \sum_{v=1}^{V} \frac{f^{(g,v)}}{\bar{f}^g} \boldsymbol{\varepsilon}^{(g,v)} : \mathbf{M}^g \boldsymbol{\varepsilon}^{(g,u)}\right] \\ & - \frac{1}{2}\sum_{m=1}^{G}\sum_{v=1}^{V} f^{(m,v)} \boldsymbol{\varepsilon}^{(g,n)} : \left(\mathbf{M}^m + (\mathbf{M}^g)^T\right) \boldsymbol{\varepsilon}^{(m,v)}. \end{aligned} \tag{5.98}$$

Using the definition of J (equation (5.95)), the interaction force is finally simplified as

$$\begin{aligned} F^{int}_{(g,n)} =& \frac{1}{2}\sum_{u=1}^{V}\frac{f^{(g,u)}}{\bar{f}^g}\left[J^{(g,n,g,u)} + J^{(g,u,g,n)} - \sum_{v=1}^{V}\frac{f^{(g,v)}}{\bar{f}^g}J^{(g,v,g,u)}\right] \\ & - \frac{1}{2}\sum_{m=1}^{G}\sum_{v=1}^{V} f^{(m,v)}\left[J^{(g,n,m,v)} + J^{(m,v,g,n)}\right]. \end{aligned} \tag{5.99}$$

With the interaction force defined, the system of equations (5.60) can be solved numerically, as will be shown later. Note that the formulation of the interaction energy imposes that an "inclusion" is a group of variants; at the same time, however, the volume fractions for each individual variant are tracked so that a final product of a single variant is possible.

With the grouping structure as represented by equations (5.94) and (5.98), the final product that forms can be either a single variant or a single group or variants from several groups, depending on the thermo-mechanical forces applied to the system. Since there is only one level to the grouping structure, the model is appropriately configured for representation of cases in which the applied stress is less than the threshold for defaulting or detwinning to a single correspondence variant (CV) to happen. In particular, to enable deformation products of a single CV (as opposed to a single HPV) to be accurately achieved, the modeling would require both the existing HPV grouping system and an additional sub-grouping structure for the CVs (correspondence variants) that comprise each HPV. The modification to the grouping structure to account for the difference between HPVs and CVs is to be presented in the two-tier multivariant model Gao (2002).

In above equations the Eshelby tensor for group g, $\mathbf{S}^g$ was extensively used. The shape of an inclusion has a large impact on the Eshelby Tensor. In a previous work by Gao et al. (2000), different inclusion shapes and crystallographically defined directions for a penny shape inclusion have been considered. In that paper, the impact of specific crystallographic details on the overall stress-strain response as predicted by the multivariant model are explored. The key findings are summarized below:

1. Inclusion shape has a significant impact on model predictions and a direction selection scheme is proposed for penny shaped inclusions based on the fact that several HPVs tend to cluster about one of the 011 or 001 poles.

2. Differences between type I and type II twinning are examined and it is shown that choice of the proper twinning type is essential to capture experimental data.

3. Using HPVs as the minimum units, the grouping structure is examined and several different options published for a NiTi alloy are implemented and results compared (see also Gao (2002)).

4. It is shown that the level of anisotropy exhibited by SMA single crystal would impact not only initial slopes of stress-strain response, magnitude of transformation stress, orientation dependence, but also would have great impact on polycrystalline response (see also Gao (2002)). These results indicate that proper representation of the crystallographic microstructure is crucial to obtaining accurate macroscopic stress-strain predictions.

To conclude this section, we show the equivalence of the interaction energy defined by equations (5.20) and (5.89) in the absence of self-accommodating groups. Starting from equation (5.89) and substituting the first equality of equation (5.91) for $\dot{\boldsymbol{\sigma}}^g$ one obtains

$$W^{int} = -\frac{1}{2}\sum_{g=1}^{G}\bar{\boldsymbol{\varepsilon}}^g : \left[\mathbf{C}(\mathbf{S}^g - \mathbf{I})\bar{\boldsymbol{\varepsilon}}^g - \sum_{m=1}^{G}\bar{f}^m\mathbf{C}(\mathbf{S}^m - \mathbf{I})\bar{\boldsymbol{\varepsilon}}^m\right]\bar{f}^g. \tag{5.100}$$

If no self-accommodation is considered, the total number of groups is N, i.e., $G = N$, which is the total number of crystallographically equivalent variants. In each group, there is only one variant ($V = 1$) and therefore $\bar{\boldsymbol{\varepsilon}}^g = \boldsymbol{\varepsilon}^{tn}$ and $\bar{f}^g = f^n$. Equation (5.100) can be reduced to

$$W^{int} = -\frac{1}{2}\sum_{n=1}^{N}\boldsymbol{\varepsilon}^{tn} : \left[\mathbf{C}(\mathbf{S}^{En} - \mathbf{I})\boldsymbol{\varepsilon}^{tn} - \sum_{m=1}^{N} f^m\mathbf{C}(\mathbf{S}^{Em} - \mathbf{I})\boldsymbol{\varepsilon}^{tm}\right] f^n. \tag{5.101}$$

Note here $\mathbf{S}^{En}$ is the Eshelby tensor for a single variant. One can still choose penny shape, although a reasonable assumption is required to define its direction for each variant. Equation (5.101) can be rewritten as

$$\begin{aligned} W^{int} =& \frac{1}{2}\sum_{n=1}^{N} \boldsymbol{\epsilon}^{tn} : \mathbf{C}(\mathbf{I} - \mathbf{S}^{En})\boldsymbol{\epsilon}^{tn} f^n \\ & - \frac{1}{2}\sum_{n=1}^{N}\sum_{m=1}^{N} \boldsymbol{\epsilon}^{tn} : \mathbf{C}(\mathbf{I} - \mathbf{S}^{Em})\boldsymbol{\epsilon}^{tm} f^n f^m. \end{aligned} \tag{5.102}$$

Notice that $\mathbf{I}$ is the fourth order identity tensor. One can verify easily that above equation is identical to equation (5.20).

Since the case in which no self-accommodation is considered is a special case of the general treatment in Huang and Brinson (1998), the simulation for the former case is done using the same general code with appropriate assignment of G, V and Eshelby tensor $\mathbf{S}^{En}$ for each variant.

Temperature induced transformations, shape memory effect, pseudoelasticity and ferroelasticity are all accounted for properly by the multivariant model summarized in this section. In addition, multiaxial loading cases were also simulated and the results are in good qualitative agreement with the experimental data. The reader is referred to previous papers showing these results (Huang and Brinson, 1998; Gao et al., 2000; Huang et al., 2000). However, close examination of results reveals a few difficulties in the multivariant model:

1. Experimental data indicate that stress induced martensite in a single crystal is formed by a single habit plane variant spanning the specimen, in contrast to the Eshelby inclusion approach which assumes many inclusions in a matrix.

2. The transformation stresses remain a factor of two higher than experiments.

3. Anisotropy of austenite and martensite phases were not accounted for due to added computational complexity.

4. For polycrystalline materials, the iterations involved in solving the system of equations for each grain become computationally expensive.

5. The self-accommodated grouping structure currently used is based on an 18R structure and habit plane variants; it is oversimplified for B19' (NiTi), 3R and 2H (CuAlNi).

6 Discussion and Conclusions

In the first part of this paper a detailed summary of the basic properties of Shape Memory Alloys was given. The kinematics of the martensitic transformations were reviewed and several micromechanical based models, which attempt to predict the thermomechanical response of SMAs, were presented.

The thermomechanical properties of SMAs were discussed in terms of their chemical composition and processing techniques. A large amount of experimental data published in the literature over the past decades on the dependence of the transformation temperatures on the chemical composition of different alloys was summarized. Along with traditional description of different processing techniques on pseudoelasticity and detwinning, some recently studied aspects of SMA behavior were also addressed. In particular, several new studies on thermomechanical fatigue and cyclic loading and damping capacity of polycrystalline SMAs were discussed.

On the topic of modeling, several micromechanical models describing the response of single crystal SMAs were discussed. Both single variant and multi-variant models were considered and they were presented in a unified way, with the Helmholtz free energy and dissipative potentials being derived in an RVE. The differences in the models were described by an interaction energy term. While some of the multivariant models included the interaction between many possible martensitic variants, experimental observations as well as difficulties with the implementation typically lead to the consideration of only a single variant. Some authors (Huang and Brinson, 1998) have also proposed a two level homogenization, by first homogenizing groups of clustered variants and averaging over the groups of variants.

A careful look at the derivation of the micromechanical models considered reveals that the different models can be presented using a generalized framework involving the interaction energy. The models considered here are summarized in Table 2, with references and expressions for the interaction energy and interaction force used in the model. The last column lists pertinent features of each model. Note that all of these models originally start with an integral expression for interaction energy that is identical to that shown in equation (5.22) of this paper. From that common starting point, different assumptions are made to enable realistic calculations. The interaction force F^{int}, the gradient of the interaction energy, is ultimately what is used in calculating the transformation kinetics (c.f. equation (5.35)).

Referring to Table 2, the model by Lexcellent and co-workers (Raniecki et al., 1992; Goo and Lexcellent, 1997; Vivet and Lexcellent, 1998) and the model by Lu and Weng (1997) start with the same form for the interaction energy (the integral in equation (5.22)) and both approximate the integral as a sum by considering the martensitic plates to be transforming inclusions. The energy between martensitic plates and the austenitic matrix for the two models is identical. Lexcellent and co-workers have an additional term accounting for interaction between martensitic variants in the general expression, but in application they assume only a single active variant such that this second term drops out. Lu and Weng (1997) also assume only a single active variant in the application of the model and then perform the calculations based on that variant alone. The multivariant model in the previous section has a very similar expression for the interaction energy, being also based on the transforming inclusion concept, but the exact form differs due to the grouping of variants into self-accommodated clusters in the calculation.

Table 2 illustrates how the grouping of self-accommodated variants dramatically decreased the interaction energy over what was calculated when considering each inclusion to be a single variant. The numerical values of F^{int} for the Lexcellent and Weng models are at least an order of magnitude smaller due to the plate aspect ratio chosen, which determines the Eshelby tensor $\mathbf{S}$. In the multivariant model of the previous section, the aspect ratio of the inclusion/variant was selected to be approximately 0.01, based on experimental observations (Saburi and Wayman, 1979). The images in Figures 17(b)–17(c) also support this ratio for width to length of the martensitic plates formed. Lu and Weng (1997), however, explicitly take $\alpha \rightarrow 0$ which enables a much smaller final interaction force; while not stated in the paper, the aspect ratio for Vivet and Lexcellent (1998) can be calculated[2] to be approximately 0.001 in order to obtain the value for W_s cited, given the other material constants provided.

The second part of this two-part paper will summarize the work on the micromechanical modeling of polycrystalline Shape Memory Alloys (SMAs). Averaging micromechanics methods based on the self-consistent approximation will be reviewed for the modeling of polycrystalline SMAs. Rate independent phenomenological models, which are based on characterizing the inelastic fields associated with the phase transformation, will also be discussed. A typical numerical implementation of an SMA constitutive model using return-mapping algorithms will also be presented.

[2]Input parameters include $\mu = 12Gpa$, $\nu = 0.3$, $\varepsilon^t_{11} = -0.1174\%$, and $\varepsilon^t_{12} = \varepsilon^t_{21} = 6.646\%$, where the remaining transformation strain components are set to zero. Using these, the authors calculated the value for $\boldsymbol{\varepsilon}^t \mathbf{C}(\mathbf{I} - \mathbf{S}^E)\boldsymbol{\varepsilon}^t$ to be 4.16 and 0.416 MPa for aspect ratios 0.01 and 0.001 respectively.

Model	**Interaction energy** $W^{int} = \frac{1}{2V}\int_V \tau\varepsilon^t dV$	**Interaction force** $F_n^{int} = -\frac{\partial W^{int}}{\partial f^n}$	**Magnitude (unit volume)** F_n^{int} **(MPa)**	Features
Patoor et al. (1996)	$\frac{1}{2}\sum_n^N\sum_m^N H^{nm} f^n f^m$	$-\sum_m^N H^{nm} f^m$	$H^1 = \frac{\mu}{1000} \approx 40$ $H^2 = \frac{\mu}{150} \approx 270$	A multivariant model; Interaction matrix H as approximation: H^1 for self-accommodating variants, H^2 for non-self-accommodating ones; Resistance force of F^{int} increases with increased volume fraction, causing a continuous strain hardening effect; Good qualitative agreement to uniaxial experimental results.
Lu and Weng (1997)	$\frac{1}{2}f(1-f)\boldsymbol{\varepsilon}^t : \boldsymbol{\mathcal{C}}(\mathbf{I}-\mathbf{S}^E)\boldsymbol{\varepsilon}^t$ (only 1 variant considered)	$-\frac{1}{2}(1-2f)\boldsymbol{\varepsilon}^t : \boldsymbol{\mathcal{C}}(\mathbf{I}-\mathbf{S}^E)\boldsymbol{\varepsilon}^t$	< 1	A single variant model; analytical solution just for one variant; The elastic tensor $\boldsymbol{\mathcal{C}}$ is assumed the same for austenite and martensite; resistance force of F^{int} decreases with increased volume fraction, becoming actually a driving force for $f > 0.5$; aspect ratio of thin oblate was taken to be 0, reducing the magnitude of F^{int}; non-linear dependence on f of dissipation; good agreement to uniaxial experimental results for plates of aspect ratio 0.
Vivet and Lexcellent (1998)	$\sum_{n=1}^N f^n(1-f^n)W^n$ $-\sum_{n=1}^N\sum_{m=1,m\neq n}^N f^n f^m W^{nm}$, $W^n = \frac{1}{2}\boldsymbol{\varepsilon}^{tn} : \boldsymbol{\mathcal{C}}(\mathbf{I}-\mathbf{S}^{En})\boldsymbol{\varepsilon}^{tn}$ (same as equation (5.20)	$-(1-2f)W$ (simplified form when only one variant is considered; same as in (Lu and Weng, 1997))	$W \approx 0.468$ (Interaction between austenite and martensite)	A single variant model; analytical solution just for one variant; resistance force of F^{int} decreases with increased volume fraction, becoming actually a driving force for $f > 0.5$; very thin oblate ($a_3/a_1 \approx 0.001$) $\rightarrow$ lower W_s; very good agreement to uniaxial experimental results
Huang and Brinson (1998)	$-\frac{1}{2}\sum_{g=1}^G \langle\sigma_{ij}\rangle^g \bar{\varepsilon}_{ij}^g \bar{f}^g =$ $\frac{1}{2}\sum_{g=1}^G \bar{\varepsilon}_{ij}^g[\mathbf{C}(\mathbf{I}-\mathbf{S}^g)\bar{\varepsilon}_{ij}^g$ $-\sum_{m=1}^G \bar{f}^m\mathbf{C}(\mathbf{I}-\mathbf{S}^g)\bar{\varepsilon}_{ij}^m]\bar{f}^g$	$-\frac{\partial W^{int}}{\partial f^n}$	-40 to 60 when $\mu = 40$ GPa -12 to 18 when $\mu = 12$ GPa	A multivariant model; analytical solution without additional approximation; self-accommodating groups of variants without interaction among themselves; plate aspect ratio: $a_3/a_1 = 0.01$; long time of calculation; good qualitative agreement to uni- or multi- axial experimental results
Gao and Brinson (2002)	Constant	0	0 (note, typically $F^C = 4$)	A multivariant model; based on invariant plane nature of martensitic transformation; accounts for anisotropy in single crystal case; very fast calculation; excellent agreement to uni- or multi- axial experimental results

Table 2: Interaction energy and force comparison between the Helmholtz free energy for different models: $\Psi = \Delta G^{chem} + W^{surf} + W^{int} + \cdots$

Acknowledgements

The authors would like to acknowledge the support of the Air Force of Scientific Research (AFOSR), Army Research Office (ARO), the Texas Higher Education Coordinating Board, the National Air and Space Administration (NASA), and the Centre National de la Recherche Scientifique (CNRS). We would also like to express our gratitude to Bjoern Kiefer, Christophe Niclaeys, Denis Entemeyer, Parikshith Kumar, Yves Gillet, Luciano Machado, Mohammed El Amrani, Olivier Bertacchini, and Darren Hartl, who spent a significant amount of time and effort on the manuscript of this paper. E. Patoor would also like to thank Marcel Berveiller and André Eberhardt for the many fruitful discussions which led to this paper.

References

Angst, D. R., T. P. E., Kao, M. Y., 1995. The effect of hafnium content on the transformation temperatures of Ni49Ti51-xHfx shape memory alloys. Journal De Physique IV C8, 747.

Ball, J. M., James, R. D., 1987. Fine phase mixture as minimizers of energy. Arch. Ration. Mech. Anal. 100, 13–52.

Bertacchini, O., Lagoudas, D., Patoor, E., 2003. Transformation fatigue life characterization of shape memory alloy actuators. In: Proceedings of SPIE. Vol. 5053.

Berveiller, M., Zaoui, A., 1984. Modelling of the plastic behavior of inhomogeneous media. Journal of Engineering Materials and Technology (106), 295–299.

Besseghini, S., Villa, E., Tuissi, 1999. Ni-Ti-Hf shape memory alloy: effect of aging and thermal cycling. Material Science and Engineering A273-275, 390–394.

Bhattacharya, K., 1993. Comparison of the geometrically nonlinear and linear theories of martensitic transformation. Continuum Mech. Thermodyn. 5, 205–242.

Bigeon, M., Morin, M., 1996. Thermomechanical study of the stress assisted two way memory effect fatigue in TiNi and CuZnAl wires. Scripta Materialia 35 (12), 1373–1378.

Bowles, J. S., MacKenzie, J. K., 1954. The crystallography of martensite transformations I and II. Acta Metallurgica 2, 129–137 and 138–147.

Bowles, J. S., Wayman, C. M., 1972. The Bain strain, lattice correspondances and deformations related to martensitic transformations. Metall. Trans. 3, 1113–1121.

Buehler, W. J., Gilfrich, J. V., Wiley, R. C., 1963. Effects of low-temperature phase changes on the mechanical properties of alloys near composition TiNi. J. Appl. Phys. 34, 1475.

Buehler, W. J., Wiley, R. C., 1965. Nickel-base alloys. U.S. Patent 3,174,851.

Chakravorty, S., Wayman, C., 1976. Thermoelastic martensitic transformation in ni-al alloys: 1. crystallography and morphology .

Christian, J. W., 1956. J. Inst. Metals 84, 386.

Cohen, M., 1988. Martensitic transformations in material science and engineering. Transactions of the Japan Institute of Metals 39 (8), 609–624.

Contardo, L., Guénin, G., 1990. Training and two way memory effect in Cu-Zn-Al alloy. Acta Metall. Mater. 38 (7), 1267–1272.

De Vos, J., Aernoudt, E., Delaey, L., 1978. The crystallography of the martensitic transformation of BCC into 9R: A generalized mathematical model. Z. Metallkde 69 (H7), 438–444.

Dederichs, P. H., Zeller, R., 1972. Elastische konstanten vor vielkristallen. Tech. Rep. 877-FF, KFA.

Delaey, L., 1990. Diffusionless transformations. In: Cahn, R. W., Haasen, P., Kramen, E. J. (Eds.), Phase Transformations in Materials. Vol. 5 of Material Science and Technologies. VCH Publishers, New York, Ch. 6, pp. 339–404.

Donkersloot, H. C., Van Vucht, J., 1970. Martensitic transformations in gold-titanium, palladium-titanium alloys near the equiatomic composition. J. Less Common Metals 20, 83–91.

Eckelmeyer, K., 1976. The effect of alloying on the shape memory phenomenon in nitinol. Scripta Metallurgica 10, 671–672.

Eisenwasser, J., Brown, L., 1972. Pseudoelasticity and strain-memory effect in Cu-Zn-Sn alloys. Matall. Trans. , 1359.

Eshelby, J. D., 1961. Elastic inclusions and inhomogeneities. In: Sneddon, I. N., Hill, R. (Eds.), Progress in Solid Mechanics. Vol. 2. North-Holland, Amsterdam, pp. 87–140.

Fehri, O., Fassi, H., Berveiller, M., 1987. Elastic interactions between variants in pseudoelastic single crystals. Scripta Met. 21, 771.

Firstov, G., Van Humbeeck, J., Koval, Y., 2004. Comparison of high temperature shape meory behaviour for ZrCu-based , TiNiZr and TiNiHf alloys. Scripta materialia 50, 243–248.

Funakubo, H., 1987. Shape Memory Alloys. Gordon and Bleach, New York.

Gao, X., 2002. Multivariant modeling and characterization of SMAs based on hierarchical characteristics of martensite crystallography. Ph.D. thesis, Northwestern University, Evanston, IL.

Gao, X., Brinson, L. C., 2002. A simplified multivariant SMA model based on invariant plane nature of martensitic transformation. J. Intell. Mater. Systems Struct. 13 (12), 795–810.

Gao, X., Huang, M., Brinson, L. C., 2000. A multivariant micromechanical model for SMAs. Part 1. Crystallographic issues for single crystal model. Int. J. Plasticity 16 (10–11), 1345–1369.

Gautier, E., Patoor, E., 1997. Mechanics of Solids with Phase Changes. Vol. 7 of CISM International Centre for Mechanical Sciences. Courses and Lectures. Springer, Ch. Experimental Observations for Shape Memory Alloys and Transformation Induced Plasticity Phenomena, pp. 69–103.

Goldberg, D., Xu, Y., Murakami, Y., Otsuka, K., Ueki, T., Horikawa, H., 1995. High-temperature shape memory effect in Ti50Pd50-xNix (x=10,15,20) alloys. Journal Materials letters 22, 241–248.

Goo, B. C., Lexcellent, C., 1997. Micromechanics-based modeling of two-way shape memory effect of a single crystalline shape memory alloy. Acta Metall. Mater. 45 (2), 727–737.

Govindjee, S., Miehe, C., 2001. A multi-variant martensitic phase transformation model: Formulation and numerical implementation. Computer Methods in Applied Mechanics and Engineering 191, 215–238.

Grujicic, M., Ling, H. C., Haezebrouck, D. M., Owen, W. S., 1992. The growth of martensite. In: Olson, G. B., Owen, W. S. (Eds.), Martensite. ASM International, Ch. 10, pp. 175–196.

Guénin, G., 1986. Alliages à mémoire de forme. In: Techniques de l'ingénieur. Vol. M530.

Hadamard, J., 1903. Leçons sur la propagation des ondes et les équations de l'hydrodynamique. Cours du Collège de France, Librarie Scientifique A. Hermann, Paris.

He, Z., Zhou, J., 2003. Comparative study of martensitic transformation behavior of NiAlMn and NiAlMnFe high temperature shape memory alloys. Materials Science and Engineering A360, 183–190.

Hebda, D., White, S., 1995. Effect of training conditions and extended thermal cycling on Nitinol two-way shape memory behavior. Smart Mater. Struct. 4, 298–304.

Horikawa, H., Ichinose, S., Morii, K., Miyazaki, S., Otsuka, K., 1988. Orientation dependence of β_1 to β_1' stressed-induced martensitic transformation in a Cu-Al-Ni alloy. Metall. Trans. A 19, 915–923.

Hsieh, S., Wu, S., 1998. Room - temperature phases observed in Ti53-x Ni47 Zrx high temperature shape memory alloys. Journal of alloys and compounds 266, 276–282.

Huang, M., Gao, X., Brinson, L. C., 2000. A multivariant micromechanical model for SMAs. Part 2. Polycrystal model. Int. J. Plasticity 16 (10–11), 1371–1390.

Huang, M. S., Brinson, L. C., 1998. A multivariant model for single crystal shape memory alloy behavior. J. Mech. Phys. Solids 46 (8), 1379–1409.

Ishida, K., Kainuma, R., Ueno, N., Nishazawa, T., 1991. Ductility enhancement in NiAl (B2)- base alloys by microstructural controls. Metallurgical Transactions 22A, 441.

Jackson, C. M., Wagner, H. J., Wasilewski, R. J., 1972. 55-nitinol—The alloy with a memory: Its physical metallurgy, properties and applications. Tech. Rep. NASA SP-5110, NASA, Technology Utilization Office, Washington, D.C.

Kaufman, L., Cohen, M., 1958. Martensitic transformations. In: Chalmers, B., King, R. (Eds.), Progress in Metal Physics. Vol. 7. Pergamon Press, Oxford, pp. 165–246.

Khachaturyan, A. G., 1983. Theory of Structural Transformations in Solids. John Wiley & Sons.

Kröner, E., 1961. Zur plastischen verformung des vielkristalls. Acta Metallurgica 9, 155–161.

Kröner, E., 1989. Modified Green functions in the theory of heterogeneous and/or anisotropic elastic media. In: Weng, T. (Ed.), Micromechanics and Inhomogeneity. Vol. 2. Springer-Verlag.

Kumar, P., Entchev, P. B., Lagoudas, D. C., November 2003. Thermomechanical characterization of SMA actuators under cyclic loading. In: Proceedings of IMECE'03. ASME International Mechanical Engineering Congress,, Washington D.C., pp. 15–21.

Lagoudas, D. C., Bo, Z., 1999. Thermomechanical modeling of polycrystalline SMAs under cyclic loading, Part II: Material characterization and experimental results for a stable transformation cycle. Int. J. Eng. Sci. 37, 1205–1249.

Lagoudas, D. C., Miller, D. A., Rong, L., Li, C., 2000. Thermomechanical transformation fatigue of SMA actuators. In: Proceedings of the 2000 Conference on Smart Structures and Materials. SPIE, submitted.

Lim, T. J., McDowell, D. L., 1994. Degradation of an NiTi alloy during cyclic loading. In: Proceedings of the 1994 North American Conference on Smart Structures and Materials. SPIE, pp. 153–165.

Lindquist, G., Wayman, C., 1990. Shape memory and transformation behavior of martensitic Ti-Pd-Ni and Ti-Pt-Ni alloys. In: Proc. of the Int. Conf. on Engineering Aspects of Shape Memory Alloys. pp. 58–68.

Lu, L., Lai, M., Lim, A., 1996. Mechanical fatigue of Cu-based shape memory alloy after different heat treatment. Scripta Mater 34 (1), 157–162.

Lu, Z. K., Weng, G. J., 1997. Martensitic transformation and stress-strain relations of shape-memory alloys. J. Mech. Phys. Solids 45 (11/12), 1905–1928.

MacQueron, J. L., Morin, M., Guénin, G., Planes, A., Elgueta, J., Castan, T., 1991. Atomic ordering and martensitic transition in a Cu-Zn-Al shape memory alloy. Journal de Physique IV 1 (9), C4–259–263.

Maki, T., 1999. Shape Memory Materials. Cambridge University Press, Cambridge, Ch. Ferrous Shape Memory Alloys, pp. 117–132.

McCormick, P. G., Liu, Y., 1994. Thermodynamic analysis of the martensitic transformation in TiNi—II. Effect of transformation cycling. Acta Metall. Mater. 42 (7), 2407–2413.

McNichols, J. L., Brookes, P. C., Cory, J., 1981. NiTi fatigue behavior. J. Appl. Phys. 52, 7442–7444.

Melton, K., Mercier, O., 1979a. Fatigue life of CuZnAl alloys. Scripta Met. 13, 73–75.

Melton. K., Mercier, O., 1979b. Fatigue of NiTi thermoelastic martensites. Acta Metallurgica 27, 137–144.

Melton, K. N., 1990. Ni-Ti based shape memory alloys. In: Duerig, T. W., Melton, K. N., Stökel, D., Wayman, C. M. (Eds.), Engineering Aspects of Shape Memory Alloys. pp. 21–35.

Meng, X. L., Tong, Y. X., Lau, K. T., Cai, W., Zhou, L. M., Zhao, L. C., 2002. Effect of Cu addition on phase transformation of Ti-Ni-Hf high-temperature shape memory alloys. Materials letters 57, 452–456.

Miller, D. A., Lagoudas, D. C., 2001. Influence of cold work and heat treatment on shape memory effect and plastic strain development of NiTi. Material Science and Engineering A 308, 161–175.

Miyazaki, S., 1990. In: Duerig, T. W., Melton, K. N., Stökel, D., Wayman, C. M. (Eds.), Engineering Aspects of Shape Memory Alloys. p. 394.

Miyazaki, S., 1999. Medical and dental applications of shape memory alloys. In: Otsuka, K., Wayman, C. M. (Eds.), Shape Memory Alloys. Cambridge University Press, Cambridge, Ch. 12, pp. 267–281.

Miyazaki, S., Imai, T., Igo, Y., Otsuka, K., 1997. Effect of cyclic deformation on the pseudoelasticity characteristics of Ti-Ni alloys. Metallurgical Transactions 42 (7), 115–120.

Miyazaki, S., Kawai, T., Otsuka, K., 1982. Study of fracture in cualni shape memory bicrystals. Journal de physique , 813–818.

Miyazaki, S., Kimura, S., Otsuka, K., Suzuki, Y., 1984. The habit plane and transformation strains associated with the martensitic transformation in Ti-Ni single crystals. Scr. Mett. 18, 883–888.

Miyazaki, S., Mizukoshi, K., Ueki, T., Sakuma, T., Liu, Y., 1999. Fatigue life of Ti-50 at% Ni and Ti-40Ni-10Cu (at%) shape memory alloy wires. Material Science and Engineering A 273–275, 658–663.

Miyazaki, S., Otsuka, K., Wayman, C. M., 1989a. The shape memory mechanism associated with the martensitic transformation in Ti-Ni alloys — I. Self-accomodation. Acta Metallurgica 37 (7), 1873–1884.

Miyazaki, S., Otsuka, K., Wayman, C. M., 1989b. The shape memory mechanism associated with the martensitic transformation in Ti-Ni alloys — II. Variant coalescence and shape recovery. Acta Metallurgica 37 (7), 1885–1890.

Moberly, W., Melton, K., 1990. Engineering Aspects of Shape Memory Alloys. Butterworth-Heinemann Ltd, Ch. Ni-Ti-Cu Shape Memory Alloys, pp. 46–57.

Mori, T., Tanaka, K., 1973. Average stress in matrix and average energy of materials with misfitting inclusions. Acta Metallurgica 21, 571–574.

Morin, M., Trivero, F., 1994. Influence of thermal cycling on the reversible martensitic transformation in a Cu-Al-Ni shape memory alloy. Materials Science and Engineering A196, 177–181.

Murakami, Y., Otsuka, K., Hanada, S., Watanabe, S., 1994. Self-accommodation and morphology of 14M (7R) martensites in a Ni-37.0 at.%Al alloy. Mater. Sci. Eng. A, Struct. Mater., Prop. Microstruct. Process. 189 (1–2), 191–199.

Niclaeys, C., Ben Zineb, T., Arbab-Chirani, S., Patoor, E., 2002. Determination of the interaction energy in the martensitic state. Int. J. Plasticity 18, 1619–1647.

Nishiyama, Z., 1978. Martensitic Transformations. Academic Press, San Diego.

Olander, A., 1932. An electrochemical investigation of solid cadmium-gold alloys. Journal of the American Chemical Society 54, 3819–3833.

Olson, G. B., Cohen, M., 1975. Thermoelastic behavior in martensitic transformations. Scripta Met. 9, 1247–1254.

Olson, G. B., Cohen, M., 1982. Stress assisted isothermal martensitic transformation: Application to TRIP steels. Metall. Trans. A 13A, 1907–1914.

Otsuka, K., 1990. Crystallography of martensitic transformations and lattice invariant shears. Material Science Forum 56–58, 393–404.

Otsuka, K., Sakamoto, H., Shimizu, K., 1979. Successive stress-induced martensitic transformations and associated transformation pseudoelasticity in Cu-Al-Ni alloys. Acta Metallurgica 27, 585–601.

Otsuka, K., Wayman, C., Nakai, K., Sakamoto, H., Shimizu, K., 1976. Superelasticity effects and stress-induced martensitic transformations in Cu-Al-Ni alloy. Acta Metallurgica 24, 207–226.

Otsuka, K., Wayman, C. M., 1999. Shape Memory Materials. Cambridge University Press, Cambridge, Ch. Introduction, pp. 1–26.

Patel, J. R., Cohen, M., 1953. Criterion for the action of applied stress in the martensitic transformation. Acta Metallurgica 1, 531–538.

Patoor, E., Eberhard, A., Berveiller, M., 1988. Thermomechanical behaviour of shape memory alloys. Arch. of Mech. 40 (5-6), 775–794.

Patoor, E., Eberhardt, A., Berveiller, M., 1987. Potentiel pseudoélastique et plasticité de transformation martensitique dans les mono et polycristaux métalliques. Acta Metallurgica 35, 2779–2789.

Patoor, E., Eberhardt, A., Berveiller, M., 1994. Micromechanical modelling of the shape memory behavior. In: Brinson, L. C., Moran, B. (Eds.), Proc. ASME WAM'94: Mechanics of Phase Transformation and Shape Memory Alloys. Vol. AMD189/PVD292. ASME, pp. 23–37.

Patoor, E., Eberhardt, A., Berveiller, M., 1996. Micromechanical modelling of superelasticity in shape memory alloys. Journal de Physique IV 6, C1–277–292.

Perkins, J., 1974. Residual stresses and the origin of reversible (two-way) shape memory effect. Scripta Met. 8, 1469–1476.

Potapov, P., Shelyakov, A., Gulyaev, A., Svistunova, E., Matveeva, N., Hodgson, D., 1997. Effect of Hf on the structure of Ni-Ti martensitic alloys. Materials Letters 32, 247–250.

Raniecki, B., Lexcellent, C., Tanaka, K., 1992. Thermodynamic models of pseudoelastic behaviour of shape memory alloys. Arch. of Mech. 44 (3).

Rodriguez, P., Guénin, G., 1990. Stability of the two way memory effect during thermal cycling of high M^s temperature Cu-Al-Ni alloy. Material Science Forum 56–58 (7), 541–546.

Roytburd, A. L., Pankova, M. N., 1985. Effect of external stresses on habitus orientation and substructure of stress-induced martensite plates in ferrous alloys. Phys. Met. Metall. 59, 131–140.

Saburi, T., 1999. Ti–Ni shape memory alloys. In: Otsuka, K., Wayman, C. M. (Eds.), Shape Memory Materials. Cambridge University Press, Cambridge, Ch. 3, pp. 49–96.

Saburi, T., Nenno, S., 1981. The Shape Memory Effect and Related Phenomena. Pittsburgh, PA, pp. 1455–1479.

Saburi. T., Nishimoto, Y., Nenno, S., Zeniya, M., 1986. Effects of thermomechanical treatment on the shape memory effect and the pseudoelasticity of TI-50.2NI and TI-47.5NI-2.5FE alloys. J. Iron and Steel Inst. 72 (6), 571–578.

Saburi, T., Wayman, C. M., 1979. Crystallographic similarities in shape memory martensites. Acta Metallurgica 27, 979–995.

Saburi, T., Wayman, C. M., Takata, K., Nenno, S., 1980. The shape memory mechanism in 18R martensitic alloys. Acta Metallurgica 28, 15–32.

Sakamoto, H., 1983. Fatigue behavior of monocrystalline Cu-Al-Ni shape memory alloys under various deformation modes. Transactions of the Japan Institute of Metals 24 (10), 665–673.

Shimizu, K., 1985. Aging and thermal cycling effects in shape memory alloys. J. Electron Microsc. 34 (4), 277–288.

Siredey, N., Patoor, E., Berveiller, M., Eberhardt, A., 1999. Constitutive equations for polycrystalline thermoelastic shape memory alloys. Part I. Intragranular interactions and behavior of the grain. Int. J. Solids Struct. 36, 4289–4315.

Stalmans, R., Humbeeck, J. V., Delaey, L., 1992. The two way memory effect in copper-based shape memory alloys—Thermodynamics and mechanisms. Acta Metall. Mater. 40 (11), 2921–2931.

Stoiber, J., Humbeeck, J. V., Gotthardt, R., 1990. Hysteresis effects during martensitic transformation in a Cu-Zn-Al studied by internal friction measurements. Material Science Forum 56–58 (7), 505–510.

Strnadel, B., Ohashi, S., Ohtsuka, H., Miyazaki, S., Ishihara, T., 1995. Effect of mechanical cycling on the pseudoelasticity characteristics of Ti-Ni and Ti-Ni-Cu alloys. Material Science and Engineering A 203, 187–196.

Sun, Q. P., Hwang, K. C., Yu, S. W., 1991. A micromechanics constitutive model of transformation plasticity with shear and dilatation effect. J. Mech. Phys. Solids 9 (4), 507–524.

Sun, Q. P., Xu, T. T., Zhang, X., January 1999. On deformation of A-M interface in single crystal shape memory alloys and some related issues. Journal of Engineering Materials and Technology 121, 38–43.

Sun, Q. P., Zhang, X., Xu, T. T., 1997. Some Recent Advances in Experimental Study of Shape Memory Alloys. Vol. 62. Bochum, Germany, pp. 407–416.

Sure, G., Brown, L., 1985. The fatigue properties of grain refined b-CuAlNi shape memory alloys. Scripta Met. 19, 401–404.

Suzuki, Y., Tamura, H., 1990. In: Duerig, T. W., Melton, K. N., Stökel, D., Wayman, C. M. (Eds.), Engineering Aspects of Shape Memory Alloys. p. 256.

Tadaki, T., 1999. Shape Memory Materials. Cambridge University Press, Cambridge, Ch. Cu based Shape Memory Alloys, pp. 97–116.

Tanaka, K., Nishimura, F., Hayashi, T., Tobushi, H., Lexcellent, C., 1995. Phenomenological analysis on subloops and cyclic behavior in shape memory alloys under mechanical and/or thermal loads. Mechanics of Materials 19, 281–292.

Tautzenberger, P., 1990. Engineering Aspects of Shape Memory Alloys. Butterworth-Heinemann Ltd, Ch. A Comparison of Shape Memory Alloys with Thermostatic Bimetals and Wax Actuators, pp. 207–218.

Thoma, P. E., Boehm, J. J., 1999. Effect of composition on the amount of second phase and transformation temperatures of NixTi90-xHf10 shape memory alloys. Material Science and Engineering A273-275, 385–389.

Tian, Q., Wu, J., 2002. Tensile behavior of Ti50.6Pd30Ni19.4 alloy under different tensile conditions. Material science and engineering A325, 249–254.

Tobushi, H., Hachisuka, T., Hashimoto, T., Yamada, S., 1998. Cyclic deformation and fatigue of a NiTi shape memory alloy wire subjected to rotating bending. Journal of Engineering Materials and Technology 120, 64–70.

Tobushi, H., Hachisuka, T., Yamada, S., Lin, P.-H., 1997. Rotating-bending fatigue of a NiTi shape memory alloy wire. Mech. Mater. 26, 35–42.

Todoroki, T., Tamura, H., 1986. The stress-induced transformation of a Ti-Ni alloy by the pre-load test method. J. Japan Inst. Metals 50, 546–554.

Tong, H., Wayman, C., 1974. Characteristic temperatures and other properties of thermoelastic martensites. Acta Metallurgica 22, 887–896.

Vivet. A., Lexcellent, C., 1998. Micromechanical modeling for tension-compression pseudoelastic behavior of AuCd single crystals. Eur. Phys. J. Appl. Phys. 4 (2), 125–132.

Wang, Y., Zheng, Y.F., Cai, W., Zhao, L., 1999. The tensile behavior of Ti36Ni49Hf15 high temperature shape memory alloy. Scripta Materialia 40, 1327–1331.

Wayman, C. M., 1983. Phase transformations, nondiffusive. In: Cahn, R. W., Haasen, P. (Eds.), Physical Metallurgy. North-Holland Physics Publishing, New York, pp. 1031–1075.

Wechsler, M. S., Liberman, D. S., Read, T. A., 1953. On the theory of the formation of martensite. Trans AIME 197, 1503–1515.

Wollants, P., De Bonte, M., Roos, J., 1979. A thermodynamic analysis of the stress-induced martensitic transformation in a single crystal. Z. Metallkd. 70, 113–117.

Wu, H., 1990. Engineering Aspects of Shape Memory Alloys. Butterworth-Heinemann Ltd, Ch. Cu-Based Shape Memory Alloys, pp. 69–88.

Wu, J., Tian, Q., 2003. The superelasticity of TiPdNi high temperature shape memory alloy. Intermetallics 11, 773–778.

Xu, Y. amd Shimizu, S., Suzuki, Y., Otsuka, K., Ueki, T., Mitose, K., 1996. Recovery and recrystallization processes in Ti-Pd-Ni high temperature shape memory alloys. Acta mater. 45 (4), 1503–1511.